Ion Sensitive Organic Field Effect Transistors

SUPACHAI RITJAREONWATTU

Ion Sensitive Organic Field Effect Transistors

Supachai Ritjareonwattu

Abstract

Ion sensitive organic field-effect transistors (ISOFETs) with a metal–oxide–semiconductor field-effect transistor (MOSFET) architecture have been fabricated by using poly(3-hexylthiophene) (P3HT) and poly(methyl methacrylate) (PMMA) as the semiconductor and dielectric layers, respectively. To avoid any pin-holes in the dielectric layer, the ISOFET was coated by two separate PMMA layers. An Ag/AgCl double-junction reference electrode was used as the gate. The results show that the uncoated ISOFET exhibited transistor behaviour in aqueous solutions. However, these devices possessed a small sensitivity of about 0.5 nA dec^{-1} to H^+, K^+ and Na^+ ions.

Langmuir-Blodgett membranes were then used to improve the ISOFET response to the target ions in solution. By coating the gate dielectric (PMMA) with an LB membrane of pure arachidic acid (AA), the ISOFETs showed a significantly higher sensitivity to H^+ ions of about 3.5 nA pH^{-1}, but no improvement in the pK response (< 0.5 nA dec^{-1}). The compact ionised layers of carboxylic acid head groups were thought to lead to the improvement in the pH sensitivity; however, the layers of long hydrocarbon chains prevented large monovalent ions, such as K^+ and Na^+, from interacting with the ionised carboxylic acid head groups.

ISOFETs coated with an arachidic acid/valinomycin (AA/val) mixture did not show any selectivity to K^+ ions, but exhibited enhanced sensitivities to both K^+ and Na^+ ions. Instead of trapping K^+ ions, the valinomycin molecules in the AA membrane were thought to disrupt the membrane architecture and provide ion-leakage channels. Pure valinomycin-coated ISOFETs also revealed enhancements in both sensitivity and selectivity to K^+ ions over Na^+. This may be due to the fact that the cavity in the valinomycin molecules can accommodate a K^+ ion but not a Na^+ ion.

To study facilitated K^+ transport across the membrane, LB films of AA/val mixture and pure valinomycin were coated on porous supports. The responses of both uncoated and coated membranes were similar. After deposition, collapse of the LB film into the pores may provide leakage channels. This probably led to the observed gradual decrease of the potentials across the membranes.

ION SENSITIVE ORGANIC FIELD EFFECT TRANSISTORS

by

Supachai Ritjareonwattu

Ustinov College

A Thesis submitted in partial fulfillments
of the requirements for the degree of PhD

Centre for Molecular and Nanoscale Electronics
School of Engineering and Computing Sciences
University of Durham

21 November 2011

Contents

List of Figures

List of Tables

Declaration

I hereby declare that the work carried out in this thesis has not been previously submitted for any degree and is not currently being submitted in candidature for any other degree.

Signed …….…….

Candidate

The work in this thesis was carried out by the candidate

Signed …….…….

Director of Studies

Signed …….…….

Candidate

Several of the chapters in this thesis are based on papers that are published. A list of papers and their corresponding chapters is provided in the **Publications**.

Acknowledgement

This doctoral dissertation would not have been possible without the help and support of many people. First of all, I would like to convey my thanks to the Royal Thai Government (for the Strategic Frontier Research Scholarship), which granted me financial support during my study in Durham University.

In particular, I am heartily thankful to my supervisor, Prof. Michael C. Petty, whose encouragement, supervision and support from the preliminary to the concluding level enabled me to develop and shape the concept of this thesis. Also, I would like to express my gratitude to Dr. Christopher Pearson, who was abundantly helpful and offered invaluable assistance, support and guidance.

I would like to convey my grateful thanks to my best friend and colleague, Dr. Youngjun Yun, who gave me technical support and also inspired me to greater efforts. Special thanks to all my friends and colleagues in the Centre for Molecular and Nanoscale Electronics, Durham University.

Last but not least, I wish to express my love and gratitude to my beloved families, for their understanding and overwhelming support through the duration of my study.

Dedicated to my beloved mom and dad

Chapter 1
Introduction

Sensors are electronic devices that can convert various quantities – called measurands – to readable signals. Such devices are able to monitor not only physical but also chemical quantities. The traditional way to measure a chemical quantity required bulky instrumentation and, of course, was a high-cost process. The discovery of ion exchange membranes in the 1930s led to the development of ion-sensitive electrodes (ISEs) [1]. Although ISEs are generally compact and cheaper than the traditional instrumentation, their sensitivity and selectivity remain problematic. In addition, it is impracticable to downscale ISEs for use in integrated circuit (IC) technology.

Following the invention of metal-oxide-semiconductor field effect transistors (MOSFETs) in the 1960s [2], ion sensitive field effect transistors (ISFET) were developed as chemical sensors [3, 4]. ISFETs basically exploited the MOSFET architecture [5]. As a result, chemical sensors became compact and convenient [6]. In the beginning, these devices were fabricated from inorganic materials. These generally require high-cost deposition methods, such as molecular beam epitaxy. In addition, the use of inorganic ion-sensitive layers restricts the range of ions that can be detected.

By using organic materials, more effective ion-sensitive membranes are available for use in ISFET architectures. Moreover, these materials are cheap and require low-cost manufacturing processes [7]. Tremendous advances in chemistry and materials science have let to progress by providing organic semiconductors with high carrier mobilities. Organic field effect transistors (OFETs) therefore offer promising applications in the fields of sensors, large-scale displays and disposal devices [7].

The main objectives of this research are to fabricate organic field-effect transistors which can detect ions in an aqueous solution and to investigate their electrical behaviour. At the moment, the performance of OFETs is significantly lower than that of inorganic devices. Therefore, one key aim is to study the use of Langmuir-Blodgett (LB) membranes to enhance the performance of the OFET

sensors. The background physics of organic thin film transistors is described in Chapter 2. This includes a discussion of the conduction mechanisms in organic semiconductors. The basic concepts of ion-sensitive membranes and ion-sensitive organic field effect transistors are also examined. The experimental techniques used in this research are thermal vapour deposition, photholithography, spin-coating, thermal annealing and Langmuir-Blodgett deposition. All these methods are described in Chapter 3.

Chapter 4 focuses on Langmuir-Blodgett membranes. Arachidic acid, 1,2-dipalmitoyl-sn-glycero-3-phosphatidic acid and valinomycin have been studied. Their isotherms and thin film deposition are described and discussed. To imitate the biological structure of living cells, mixtures of arachidic acid and valinomycin have also been investigated.

Details concerning the OFET fabrication are given in Chapter 5. Two types of transistor, i.e. standard and interdigitated devices, were studied. Their transfer and output characteristics have been investigated, both in air and in deionised water. Some important factors in characterising ion-sensitive organic field effect transistors (ISOFETs) are noted towards the end of this chapter.

Chapter 6 focuses on the hydrogen-ion responses of the ISOFETs. The details of LB deposition onto the ISOFETs are also examined. Both uncoated and coated devices have been characterised in non-buffered solutions. The measurement procedure and the results are also discussed in this chapter.

In Chapter 7, the potassium and sodium responses of the ISOFETs are reported. Some devices were coated with LB membranes of arachidic acid, valinomycin and arachidic/valinomycin mixtures. Similar to Chapter 6, all uncoated and coated ISOFETs are characterised using non-buffered solutions. This chapter also offers models to explain the trapping process of the ion-sensitive membranes.

Chapter 8 gives the results from a preliminary study into the behaviour of Langmuir-Blodgett films deposited onto porous substrates. The details of LB deposition are also described. Some electrical characteristics of LB membranes are reported and discussed.

Conclusions are provided in Chapter 9. Additionally, some suggestions for the further work are given.

References

[1] R. P. Buck and E. Lindner. Tracing the history of selective ion sensors. Anal. Chem., 73(3): 88A – 97A, 2001.

[2] D. Kahng and M. M. Atalla. Silicon-silicon dioxide field induced surface devices. IRE-AIEE Solid- State Device Res. Conf., Carnegie Inst. of Technology, Pittsburgh, PA, 27th-29th October 1960.

[3] J. Janata. Twenty years of ion-selective field-effect transistors. Analyst, 119: 2275 – 2278, 1994.

[4] C. S. Lee, S. K. Kim and M. Kim. Ion-sensitive field-effect transistor for biological sensing. Sensors, 9: 7111 – 7131, 2009.

[5] T. Prodromakis, P. Georgiou, K. Michelakis and C. Toumazou. Effect of mobile ionic-charge pm CMOS based ion-sensitive field-effect transistors (ISFETs). IEEE Int. Symp. Circ. S. : 2165 – 2168, 2009.

[6] U. Guth, W. Vonau and J. Zosel. Recent developments in electrochemical sensor application and technology - a review. Meas. Sci. Technol., 20: 042002-1 – 042002-14, 2009.

[7] G. Hadziioannou and G. G. Malliaras (eds). Semiconducting Polymers: Chemistry, physics and engineering, 2nd edition. Wiley-VCH Verlag GmbH, Weinheim, 2007.

Chapter 2
Organic Thin Film Transistors

2.1 Introduction

In the mid-1920s, the concept of the field effect transistor (FET) was introduced by Lilienfeld [1]. He proposed a method for controlling an electric current between two terminals by applying a voltage at a point between the electrodes. This idea had the potential for commercialising an inexpensive amplifier. It was, however, ignored due to the lack of technology to produce appropriate materials for implementing such a device. Later on, in the late 1940s, the bipolar-junction transistor (BJT) was introduced and led to the rapid expansion of the electronics industry.

Kahng and Atalla developed the first metal-oxide-semiconductor (MOS) field-effect transistor (FET) at Bell Laboratories in 1960 [2]. Their MOSFET device was much slower than the BJT [3]. This technology required significant progress in material preparation to improve the carrier mobility. After a long development period, MOSFETs have become the key basic electronic unit for integrated circuits due to their simple structure [4].

The increase in the cost of inorganic-based FET devices is now making organic transistors an attractive proposition for certain applications. In fact, organic semiconductor materials have been available for many years but have not been used in commercial devices due to their very low carrier mobilities. However, these values are now similar to that found in amorphous silicon, and organic electronic devices have become the focus of research into various applications, such as transistors, display devices, solar cells and sensors [5]. Despite their relatively low mobilities, organic materials have significant advantages over inorganic crystalline compounds. These include low manufacturing costs, mechanical flexibility and the ability to make large-area devices. This chapter focuses on the physics background of organic field-effect transistors. Some general aspects of organic materials and FET devices will first be introduced.

2.2 Organic Semiconductors

Organic compounds are carbon-based materials. However, not all carbon-containing molecules are organic. A few carbon-containing molecules are classified as inorganic. These include carbides, carbonates, simple oxides of carbon and cyanides. Traditionally, urea and oxalic acid do not include a carbon in their molecules, but are classified as organic. Organic materials are generally electrically insulating, but some have a conductivity in between those of a conductor and an insulator. Such compounds are classified as organic semiconductors.

Organic semiconductive materials can take various forms, such as small molecules and polymers. Small organic molecules with semiconductor character are generally polycyclic aromatic compounds (comprised of benzene rings), such as pentacene (Figure 2.1a), anthracene (Figure 2.1b) and rubrene (Figure 2.1c). Polymeric organic semiconductors are comparatively large molecules, such as poly(3-hexylthiophene) (Figure 2.1d), poly(p-phenylene vinylene) (Figure 2.1e), and polyacetylene (Figure 2.1f).

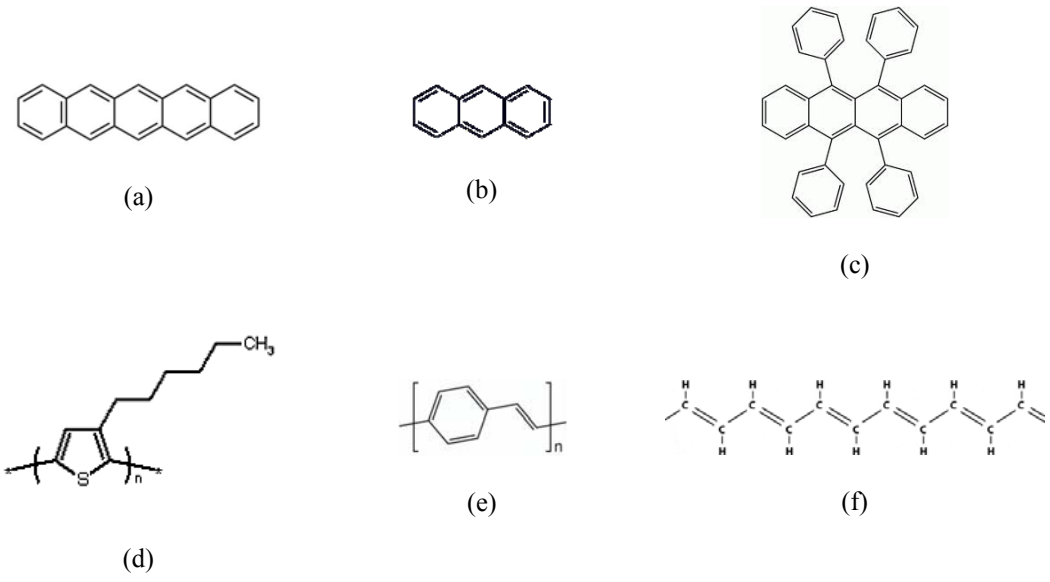

Figure 2.1 Chemical structure of some organic semiconductors. (a) Pentacene. (b) Anthracene. (c) Rubrene. (d) Poly (3-hexylthiophene). (e) Poly(p-phenylene vinylene). (f) Polyacetylene.

Carbon is an element with electron configuration $1s^2$ $2s^2$ $2p^2$. When interacting with other atoms, the 2s orbital can hybridise with the 2p orbital in a number of ways, i.e. sp^3, sp^2 and sp hybridisations. In sp^3 hybridisation, only σ-

bonds are formed between the carbon and the other atoms. In contrast, carbon atoms with sp^2 and sp hybridisations have p orbitals (left over) to form π-bonding in the molecules, as shown in Figure 2.2. σ bonds are strong and the electrons are located between the pair of the atoms. In contrast, electrons associated with the π bond can diffuse throughout the molecule. Most organic semiconductors (or conjugated organic materials) include sp^2 hybridised carbon atoms.

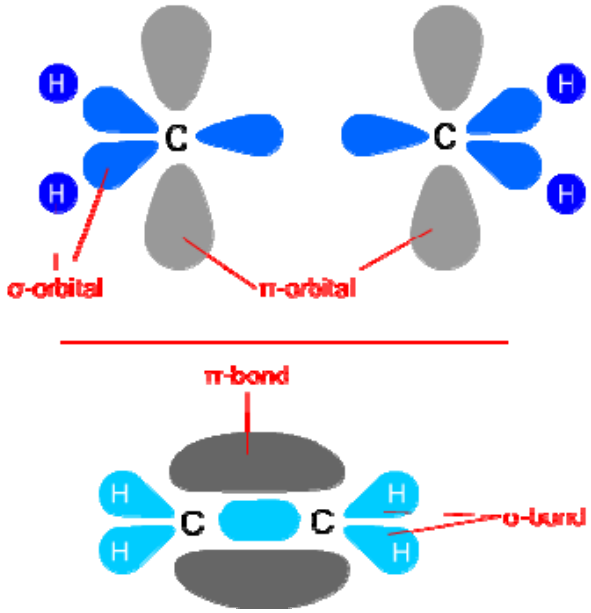

Figure 2.2 Schematic diagrams of σ and π bonds formed between carbon atoms.

Molecular Orbitals

Molecular orbital theory is used to account for the energy distribution of electrons in a molecule. In this theory, electrons do not belong to any individual atom or fixed in any bond, but are shared with the whole molecule. Therefore, each nucleus in a molecule has an influence on the behaviour of the assembly of electrons. Atomic orbitals in each constituent atom are combined linearly to derive the molecular orbitals. A set of molecular orbitals is then used to represent an electron configuration. The molecular orbitals are basically divided into three main groups, namely bonding orbitals, anti-bonding orbitals and non-bonding orbitals:

(a) A bonding orbital represents a wave function of an electron that has a high probability of being located between the nuclei. If an electron is in this orbital, it will tend to hold the nuclei together.

(b) An anti-bonding orbital represents a wave function of an electron that has a high probability of not being located between the nuclei. By contrast with a bonding orbital, the bond will be weakened if an electron is in this anti-bonding orbital.

(c) A non-bonding orbital represents a wave function of an inner electron which tends to associate with only one nucleus. Therefore, this type of a molecular orbital does not contribute to the bonds in the molecule.

This section will focus on only bonding and anti-bonding molecular orbitals because these contribute to the electrical conductivity of the material. Assuming a system has two identical atoms, A and B, the system will possess two identical valence orbitals when the atoms are far away from each other. When atom A comes closer to atom B, the nucleus of A will have an influence not only on its electrons but also on the electrons of B, and vice versa. In this fashion, the electrons are shared between the whole system, but not any individual atom. Therefore, the two valence orbitals will split into two molecular orbitals, bonding and anti-bonding orbitals, as shown in Figure 2.3a. In the case of four atoms in the system, four identical valence orbitals are split into four different molecular orbitals (Figure 2.3b). In a similar way, four molecular orbitals can be divided into bonding and anti-bonding groups. The highest occupied molecular orbital (HOMO) and the lowest unoccupied molecular orbital (LUMO) are shown in Figure 2.3. The energy difference between the HOMO and LUMO levels is the HOMO-LUMO gap, or band gap.

Assuming an organic semiconductor molecule has N carbon atoms, all the valence orbitals will form molecular orbitals, half of which are bonding orbitals and the other half are anti-bonding orbitals. If the system has only one molecule, the energy states of the electrons are discrete in the bonding and anti-bonding regimes. When a system has many organic molecules, the gap between two adjacent energy states becomes smaller in both regimes. As shown in Figure 2.4, the energy states will become continuous if the system has a large number of the molecules. Anti-bonding energy states form a conduction band, while bonding energy states form a valence band.

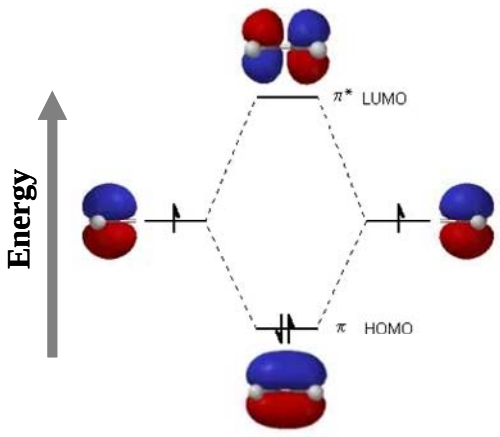

(a)

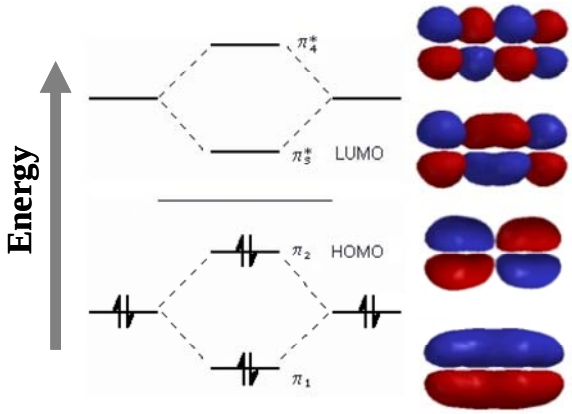

(b)

Figure 2.3 (a) Molecular orbitals of two identical atoms. (b) Molecular orbitals of four identical atoms.

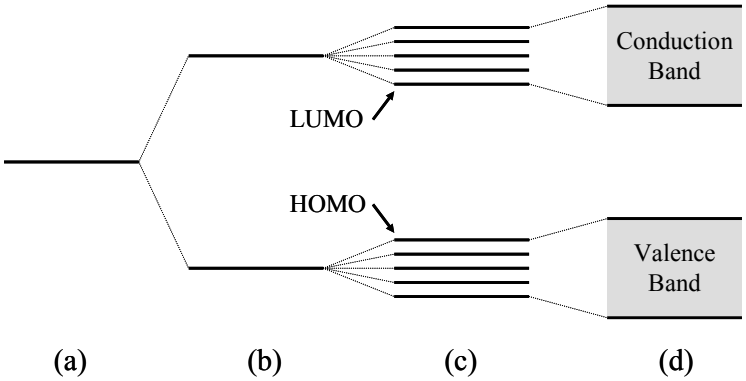

Figure 2.4 Energy diagram of carbon atoms: (a) A single carbon atom. (b) A molecule with two carbon atoms. (c) A large molecule of many carbon atoms. (d) Bulk material.

Charge Transport in Organic Semiconductors

In a polycrystalline organic semiconductor, the π-bonding orbitals overlap mainly with the π-orbitals in the same molecule. This overlapping with the orbitals of adjacent molecules is, however, limited due to the disordered structure of the material. Therefore, the π electrons cannot move freely to an adjacent molecule due to the presence of potential barriers between the molecules. In a bulk material, π electrons can move from one molecule to the other molecules using hopping or related mechanisms. In the hopping process, a phonon is absorbed by the π electron in the valence band. However, only phonons with sufficient energy can excite the π electron to energy states in the higher anti-bonding energy state in the conduction band. As noted above, anti-bonding (π^*) electrons have a low probability of being confined in a molecule. These electrons are therefore likely to hop to adjacent molecules.

In practice, a π-conjugated system in each organic semiconductor molecule is generally disrupted by kinks, twists and/or other defects in its molecule. The π electrons therefore require an intramolecular hopping process during charge transport. This intramolecular hopping is also phonon-assisted. Both inter- and intramolecular processes depend on various parameters, such as temperature, band gap and external electric field. After absorbing a phonon, the π electron is, in reality, not delocalised completely. The excited π electrons, however, interact with the surrounding molecules and lead to the formation of polarons. These quasiparticles have a relatively low velocity and thus a low mobility.

p-Type and n-Type Organic Semiconductors

When π electrons in a π-conjugated semiconductor absorb phonons, they will leave energy states in the valence band unoccupied (vacant). The excited π electrons will occupy energy states in the conduction band. The number of vacant states (free holes) is equal to the number of occupied states (free electrons). In practice, the numbers of the holes and the electrons are not identical. In a similar fashion to inorganic semiconductors, organic semiconductors can be categorised into two groups based on the nature of the charge carriers. These are p-type and n-type

semiconductors, which have holes and electrons as the majority carriers, respectively.

P-type organic semiconductors generally possess high HOMO levels, resulting from the overlap of the π bonding molecular orbitals. Therefore, these materials tend to donate π electrons to the electron traps or the localised states. The donated electrons are localised (trapped) and cannot move freely in the bulk material. The number of holes in the semiconductor is therefore higher than the number of free electrons, and the majority carriers are holes in valence band. Acenes and oligomers are typical p-type organic semiconductors. Many organic materials have p-type characteristics, but only a few organic semiconductors have a hole mobility comparable to that of amorphous silicon (~ 1 $cm^2 V^{-1} s^{-1}$ [5]). However, many p-type materials have the advantages of being compatible with solution-process techniques, such as spin-coating and ink-jet printing.

Poly (3-hexylthiophene) was used as a p-type semiconductor in this research since its solution is stable in chloroform and can be deposited using spin-coating or casting. Organic FETs may be fabricated by depositing poly(methyl methacrylate) (PMMA) as a dielectric on top of P3HT [6]. PMMA is cheap and also compatible with the solution processing.

N-type semiconductors generally have low HOMO levels. In these materials, unoccupied energy states in the conduction band tend to accept electrons from localised states in the HOMO-LUMO gap. This electron-accepting process provides free electrons in the conduction band. Therefore, the majority carriers in these materials are electrons. N-type semiconductors have not attracted as much interest as p-type materials [7]. This may be because many of these materials are not very stable in air. Relatively few stable organic semiconductors are available, such as the fullerene C_{60} and its derivatives. However, some of these materials cannot be fabricated by solution-process methods, but require molecular-beam techniques to fabricate devices with high carrier mobilities. Such relatively high-cost processing method makes these organic materials lose key advantages over amorphous silicon.

2.3 Organic Field Effect Transistors

An organic field-effect transistor (OFET) is a device in which the semiconductor layer is an organic material. In a similar fashion to typical thin film FET devices, an OFET has three terminals: a gate, a drain and a source. Various techniques can be used to fabricate OFETs: for example, vacuum evaporation, solution-casting or spin-coating. With these methods, OFETs can be built up on substrates, such as silicon wafers, glass, metals and plastics. Such OFETs have been used to realise low-cost devices, large-area electronic products, flexible electronic devices and biodegradable electronics. For example, flexible flat panel displays can be manufactured using polymeric substrates and organic semiconductors [8].

Inorganic dielectric materials are not very well suited to flexible devices because of their relative fragility. This problem can be circumvented by using an organic insulator. In addition, the manufacturing cost can be reduced by using an organic dielectric. OFETs using both organic semiconductor and dielectric layers have attracted the highest interest in recent years.

Organic materials are generally comprised of large molecules with various functional groups. This results in properties that are dependent on certain physical and/or chemical factors, such as temperature [9], light [10], gas [11] and pH [12]. Therefore, the OFETs can also be exploited as sensors. In this research, OFETs were employed to detect monovalent ions in aqueous solutions.

2.3.1 OFET Structure

Various configurations can be used to fabricate organic transistors. The common components of the FET structure are a semiconductor layer, a dielectric (or insulator) layer and a conductor (to form the three terminals). The structure of a typical field-effect transistor is shown in Figure 2.5.

Organic field-effect transistors may be built up using different methods. By using an organic single crystal grown by vapour phase epitaxy (VPE), OFETs with high carrier mobilities can be achieved.

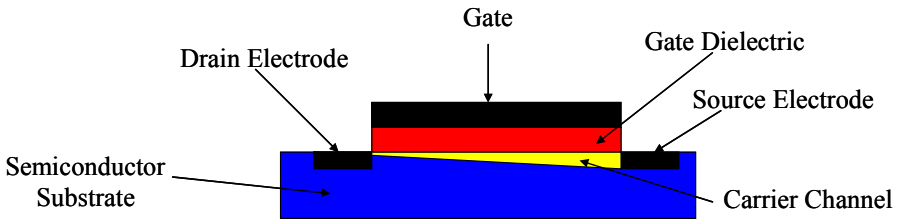

Figure 2.5 Schematic diagram of a typical field-effect transistor.

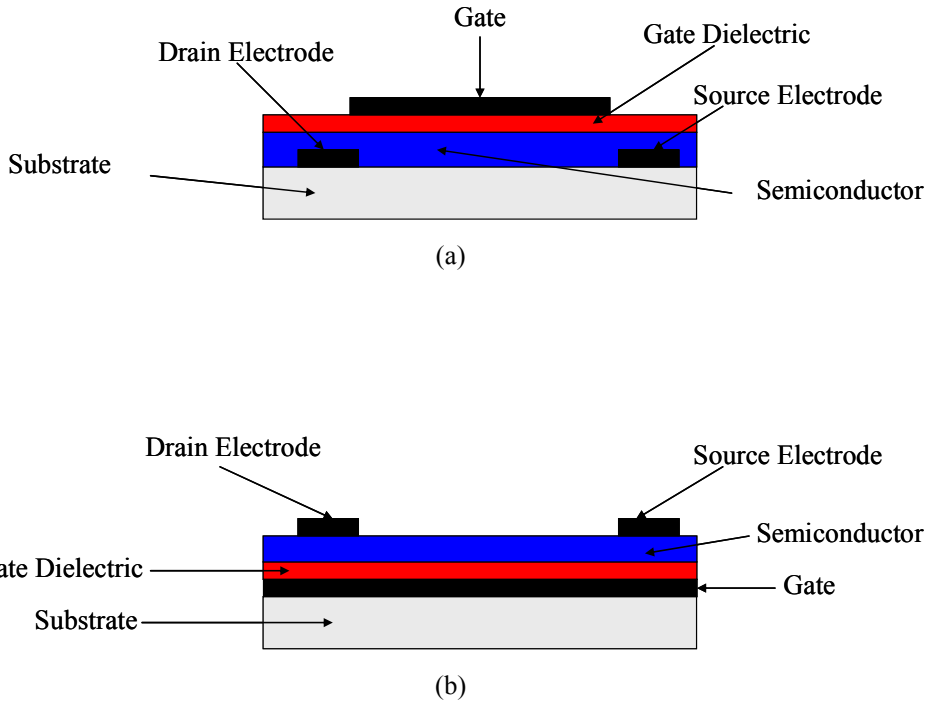

Figure 2.6 Schematic diagrams of thin-film transistors: (a) Top-gate structure. (b) Bottom-gate structure.

The performance of these single crystal OFETs is superior to those of thin-film devices [13]. However, sophisticated techniques are needed for the crystal growth process. Although it is possible to use these methods in the laboratory, it is impractical for industry to adopt them due to their low yield and high manufacturing costs.

In the operation of organic FETs, carriers are accumulated to form a channel in the surface layer of the semiconductor material. All the remaining material is used as a substrate to support the device. The manufacturing cost of the FET can therefore be reduced by depositing only the required amount of semiconductor material on a cheaper substrate.

In the past few years, not only has the quality of organic materials improved, but deposition techniques have been developed to build up reliable thin-film devices. This type of field-effect transistor is comprised of thin films of a semiconductor active layer, a dielectric layer, and metallic contacts. Two distinct configurations of this device are the top-gate structure and the bottom-gate structure, as shown in Figure 2.6. All the thin-film layers are deposited on a supporting substrate, such as glass or plastic material.

In this research, the top-gate architecture was used because this is compatible with the Langmuir-Blodgett (LB) technique, which was used to deposit a selective layer on top of the gate dielectric.

2.3.2 Electrical Behaviour

In this research, the devices were p-type OFETs because P3HT was used as the semiconductor. Therefore, this section focuses only on the operation of p-type OFETs. When operating a p-type field-effect transistor, it is generally connected as shown in Figure 2.7. V_{ds} is the voltage applied across the source and the drain while V_{gs} is the voltage between the gate and the source, which is held at zero potential. I_d is the current which flows into the device via the drain terminal.

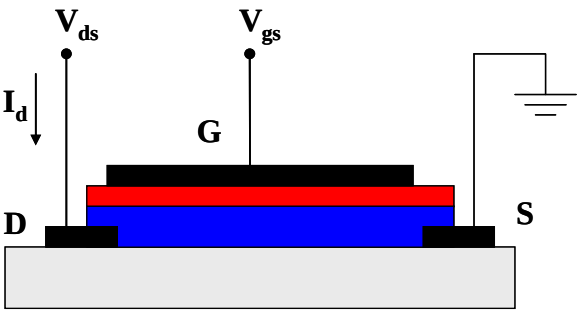

Figure 2.7 A circuit for biasing a thin – film transistor.

The drain current is a function of both V_{gs} and V_{ds}. For $V_{gs} = 0$ V, theoretically there is no drain current. In this case, the device is in the off mode since there is no carrier channel formed in the semiconductor layer. When $V_{gs} < 0$, free holes will accumulate at the interface between the insulator and the semiconductor [14]. This forms the channel between the source and drain. Charges can then flow through the device. The drain current depends on the voltage between the source and drain.

If $|V_{ds}| < |V_{gs}|$ (in the case of p – type devices), the drain current can be derived from Ohm's law [15]

$$V_{ds} = I_d R = I_d \frac{L}{\sigma A} = I_d \frac{L}{\sigma t W} \qquad (2.1)$$

where L is channel length, A is the cross-section area (A = tW, where t is the thickness of the channel and W is the channel width), and σ is conductivity of the semiconductor layer. The latter is given by

$$\sigma = \frac{J}{E} = J\frac{\mu}{\nu_d} \quad ; \quad \nu_d = \mu E \qquad (2.2)$$

$$J = e\, n_{av} \nu_d \qquad (2.3)$$

where J is the current density, E is the electric field, μ is the carrier mobility, ν_d is the drift velocity of the free carriers, e is the charge of free electrons, and n_{av} is the average carrier density in the channel.

By substituting Equations 2.2 and 2.3 into Equation 2.1,

$$I_d = \frac{W}{L} (n_{av} e\, t)\, \mu\, V_{ds} \tag{2.4}$$

For low V_{ds} and $V_{gs} < 0$, the FET device is operated in the accumulation regime. Therefore, the average value of the induced charge (q_{ind}) at the interface between the insulator and the semiconductor is

$$q_{ind,\,av} = n_{av} e\, t = C_i (V_{gs} - V_T - \frac{V_{ds}}{2}) \tag{2.5}$$

where the threshold voltage, V_T, is the gate voltage required to induce a carrier channel at the insulator/semiconductor interface [16]. By substituting Equation 2.5 into Equation 2.4, the drain current in the linear regime [16] is

$$I_{d,\,lin} = \frac{W}{L} C_i (V_{gs} - V_T - \frac{V_{ds}}{2})\, \mu\, V_{ds} \tag{2.6}$$

As V_{ds} increases, the conductivity of the channel decreases since the gate-drain voltage become smaller. At the onset of the saturation regime, the channel is 'pinched-off'. In this mode, the drain current becomes constant and independent of V_{ds}. By sustituting $V_{ds} = V_{gs} - V_T$, the drain current [16] is

$$I_{d,\,sat} = \frac{W}{2L} C_i\, \mu_{sat}\, (V_{gs} - V_T)^2 \tag{2.7}$$

From Equations 2.6 and 2.7, OFETs can therefore be characterised by either scanning V_{ds} while keeping V_{gs} constant (referred to as output characteristics), or scanning V_{gs} while keeping V_{ds} constant (referred to as transfer characteristics).

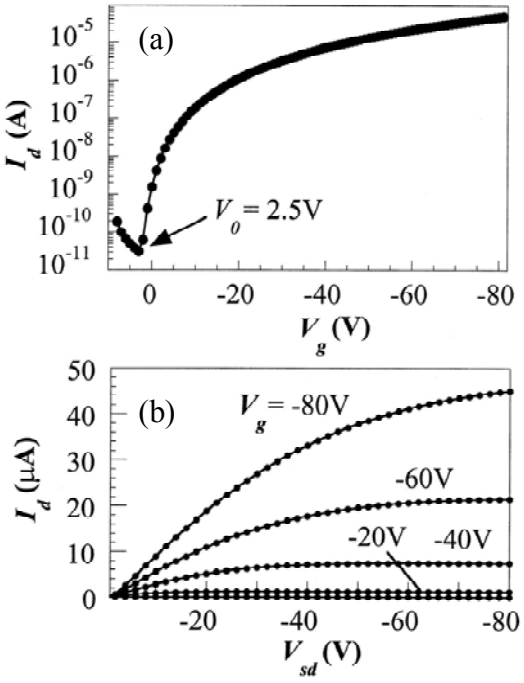

Figure 2.8 (a) Transfer characteristics in the saturation regime. (b) Output characteristics of a typical P3HT FET (L = 75 μm, W = 1500 μm) [17].

Figures 2.8a and 2.8b show typical transfer and output characteristics of an OFET [17]. The field effect mobility of the devices can be calculated using the above equations. The transconductance (g_m) and conductance (g_d) can be derived from Equation 2.6

$$g_m = \left.\frac{\partial I_d}{\partial V_{gs}}\right|_{V_{ds}} = \frac{W}{L} C_i \mu_{lin} V_{ds} \qquad (2.8a)$$

$$g_d = \left.\frac{\partial I_d}{\partial V_{ds}}\right|_{V_{gs}} = \frac{W}{L} C_i \mu_{lin} \left(V_{gs} - V_T\right) \qquad (2.8b)$$

when $|V_{gs} - V_T| >> |V_{ds}|$ [18]. Either g_m or g_d can be used to calculate the mobility by using the Equation 2.9:

$$\frac{\partial g_m}{\partial V_{ds}} = \frac{\partial g_d}{\partial V_{gs}} = \frac{W}{L} C_i \mu_{lin} \qquad (2.9)$$

2.4 Ion Selective Membranes

Ion selective membranes are active layers which sense changes in ion concentration. The selection of the active membrane is a key to producing high-performance ISOFETs. These membranes are generally in direct contact with the test solutions. Their wettability, semi-permeability, and ion selectivity are important parameters in their selection.

Ion-selective membranes can be categorised into two major groups: a membrane with fixed charged sites and a membrane containing ionophores. Membranes in the first category have functional groups fixed within them; examples are $-SO_3^-$, $-COO^-$ or $-NR_3^+$. These groups are bound in the membrane by covalent bonds or by strong ionic bonds. When the membrane is in contact with the test solution, some of the targets ions will be attracted to the functional groups. Consequently, the trapped ions in the membrane cannot diffuse freely, but are fixed at active sites.

Ionophores are lipid-soluble molecules that can transport certain ions across a membrane. Structurally, an ionophore molecule has a hydrophobic outer surface, while the interior is hydrophilic. Apart from ionophores, the membranes in this second category are comprised of lipids which have two main parts: a hydrophilic head and a hydrophobic tail. Hydrophilic heads generally point out towards water, while the hydrophobic tails point in to the membrane. With this structure, ions cannot penetrate directly across the membrane. However, the ionophores can interact with some ions at the outer surface of the membrane and then transport them through the membrane. There are two main types of ionophores:

(a) Ion carriers: These molecules trap particular ions and shield their charge from their surroundings. In this way, they can facilitate ion transport across the hydrophobic layer of the lipid membrane.
(b) Ion channels: These molecules provide a hydrophilic channel through the lipid membrane. Certain ions can then move across the membrane without interacting with the hydrophobic layer.

Most of the membranes in the first group are glass membranes used in conventional ion-sensitive electrodes [19]. The techniques for depositing these

membranes on substrates are generally high-temperature processes, such as chemical vapour deposition. In contrast, membranes in the second group can be deposited using low-temperature processes, such as the LB technique. The ion-sensitive membranes in this research were membranes with mobile sites.

This research focuses on the use of ion carriers to fabricate an ion-sensitive membrane. When the ions are trapped in the membrane, they form complexes with the ion carriers. In practice, these ion-carrier complexes cannot dissolve in any lipid solvent, but only the lipids with dielectric constant below 35. Such lipid solvents are also called mediators. If the permittivity is above this limit, the membranes cannot keep their shape in water because the lipid mediators will dissolve. Some ionophores and their target ions are shown in Table 2.1.

Table 2.1 Ionophores and the target ions

Ionophore	Type	Target Ions
Amphotericin [20]	Channel	Na^+, K^+
Crown ether [21]	Carrier	Na^+, K^+
Gramicidin [22]	Channel	H^+, Na^+, K^+
Nystatin [23]	Channel	Li^+, Na^+, K^+
Valinomycin [24]	Carrier	K^+

2.5 Ion Sensitive Field Effect Transistors

In 1970, Bergveld [25] introduced the first ion sensitive field effect transistor (ISFET) which is a device sensitive to the ions in a solution. Over the past decades, ISFET devices have been developed for measuring various molecules [26], such as inorganic salts [27], enzymes [28] and glucose [29]. The structure of the ISFET is adapted from that of MOSFET, as shown in Figure 2.9. However, a reference electrode is used as the gate. By removing the gate electrode from the structure, the outer layer of the device is in contact with the solution and can interact with the ions in the solution. In this way, the gate voltage at the ISFET outer layer depends on the ionic concentration.

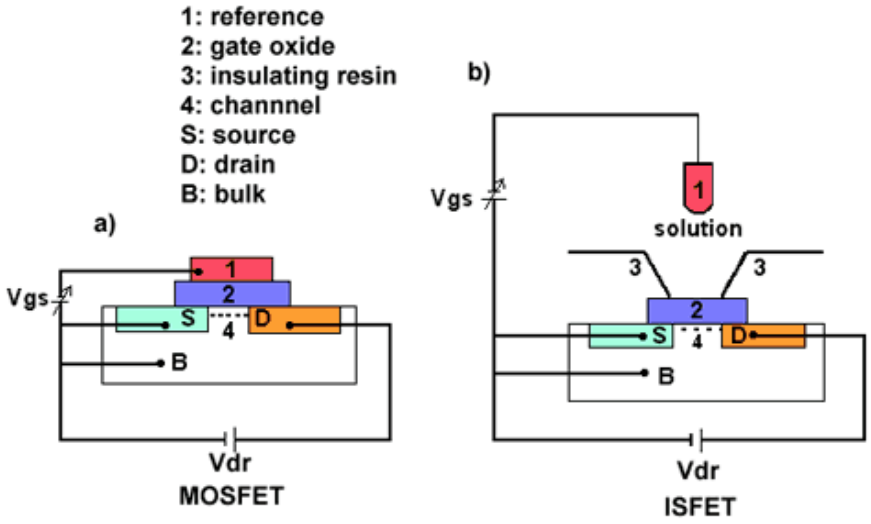

Figure 2.9 Schematic diagram of (a) a MOSFET. (b) An ISFET.

At equilibrium (no current flows through a membrane), a potential across the membrane of an ISFET is known as the Nernst potential (E_{Nernst}). This can be written

$$E_{Nernst} = E^0 + \frac{RT}{Z} \ln a_{ion} \qquad (2.10)$$

$$E_{Nernst} = E^0 + \frac{RT}{Z} \ln [ion] \qquad (2.11)$$

where E^0 is the standard reduction potential (compared to the standard half cell of hydrogen), Z is the total charge in each ion, T is the temperature of the solution, R is the gas constant (1.987 cal $K^{-1}mol^{-1}$), and a_{ion} is the ion activity of ions. However, in practice, the ion activity approximates to the ion concentration. Therefore, Equation 2.10 can be rearranged as Equation 2.11.

Equation 2.11 shows that the potential across the membrane depends on the ion concentration. When changing the ion concentration, V_T will therefore change accordingly. The Nernst potential can be included into Equation 2.6 using an effective threshold voltage ($V_{T, eff}$).

$$V_{T, eff} = V_T - E_{Nernst} = V_T - E^0 - \frac{RT}{Z} \ln [ion] \qquad (2.12)$$

When substituting $V_{T,\,eff}$ in Equation 2.6, the drain current of the ISFET can be rewritten

$$I_d = \frac{W}{L} C_i \left(\left(V_{gs} + E^0 + \frac{RT}{Z} \ln[ion] - V_T \right) - \frac{V_{ds}}{2} \right) \mu V_{ds} \qquad (2.13)$$

$$I_d = \frac{W}{L} C_i \left(\left(V_G^* - V_T^* \right) - \frac{V_{ds}}{2} \right) \mu V_{ds} \qquad (2.14)$$

where

$$V_G^* = V_{gs} + \frac{RT}{Z} \ln[ion] \qquad (2.15a)$$

$$V_T^* = V_T - E^0 \qquad (2.15b)$$

where V_G^* is an corresponding gate voltage and V_T^* is the corresponding threshold voltage when operating in a solution.

The drain current of the ISFET is in a similar form to that of the MOSFET. However, a change of the ion concentration leads to a variation of the gate voltage of the ISFET through Equation 2.15a.

Figure 2.10 shows typical charge and potential distributions across the ISOFET structure. The Nernst potential from Equation 2.11 is induced across the ion-sensitive membrane. When the activity (concentration) of the solution increases, the charge distribution will vary correspondingly. This induces the change of the charge at the dielectric/semiconductor interface. The redistribution of the charge across the device structure will lead to the change of the potential distribution across the ISOFET. As a consequence, the drain current will vary based on the concentration of the solution. However, the distribution of the potential across the ISOFET depends on the properties of the materials and also the interaction between the ions and the membrane [30].

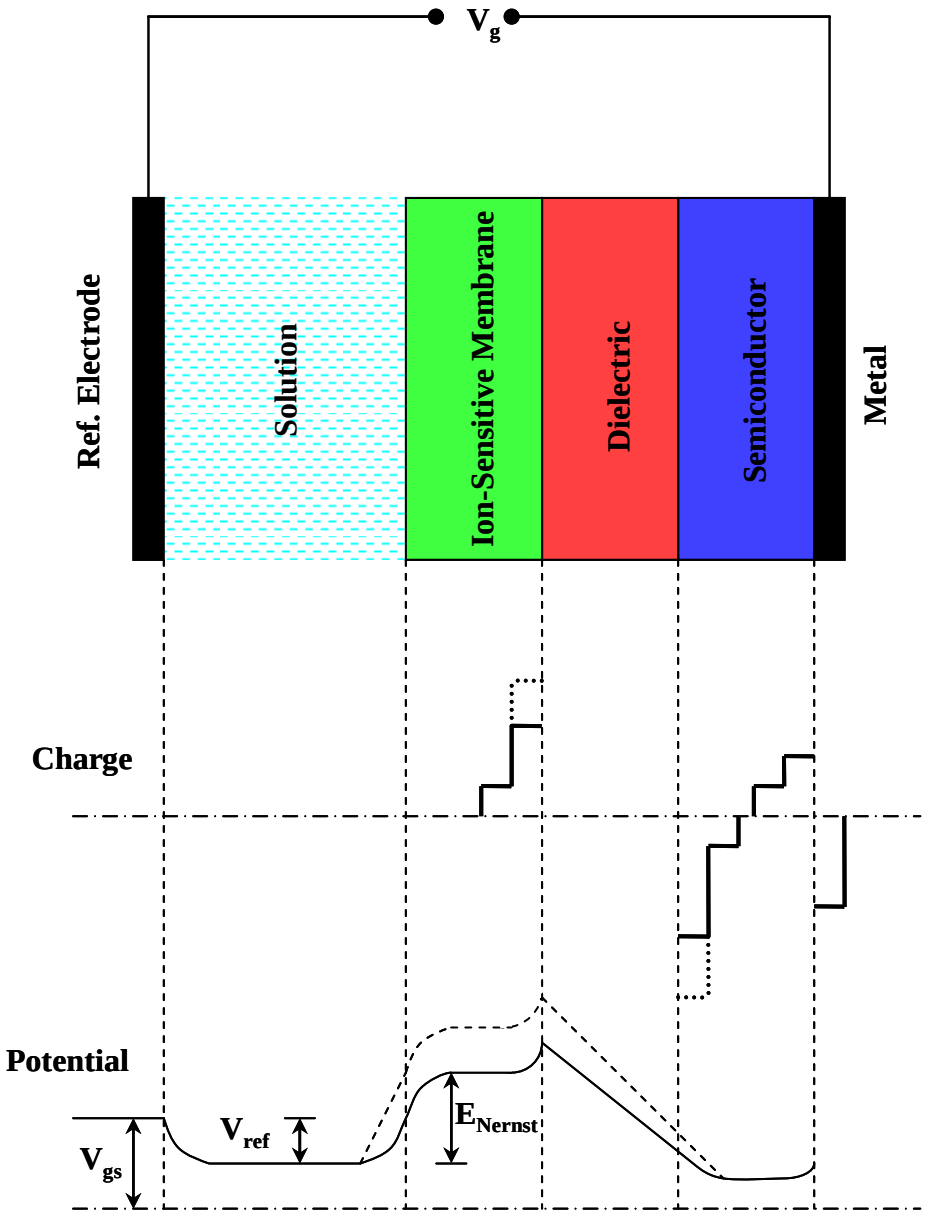

Figure 2.10 Charge and potential distributions across the ISOFET structure; dashed line represents the distributions when the activity (concentration) of the solution changes [30].

Ion Sensitive Organic Field Effect Transistors

In this research, ion sensitive devices were fabricated using organic materials as both the semiconductor and dielectric. Therefore, this section will focus on an ion sensitive organic field effect transistor (ISOFET). In the similar fashion to ISFETs, ISOFETs have electrical properties which depend on ion concentrations in solution.

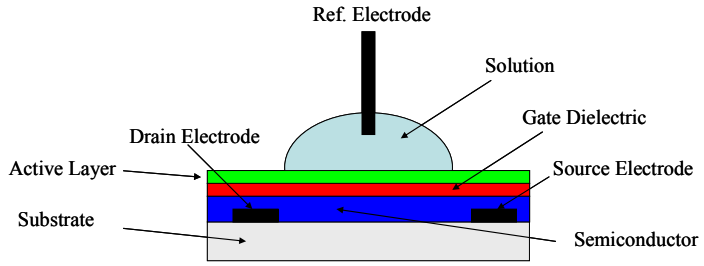

Figure 2.11 Schematic diagram of an ion sensitive organic field effect transistor with a top-gate configuration.

The structure of an ISOFET is similar to that of an organic field effect transistor. However, ISOFETs have an active layer (or ion-selective layer) in their structure for detecting target ions in solution. A typical diagram of an ISOFET is shown in Figure 2.11. Some organic materials that are used as the dielectric have a polar moeity in their molecules which can interact with the ions in solution. For example, polyvinyl chloride (PVC) has chloride atoms. This polymer can therefore interact with positive ions in the solution. Most organic dielectrics are, however, not sensitive to particular ions and/or have low sensitivity. An ion-selective membrane is an essential part for enhancing the ion sensitivity of the OFETs. For example, the pH response can be improved significantly by depositing a stearic acid LB film on top of the gate dielectric [31]. Some ion-sensitive devices are also made by combining ion-sensitive molecules with the dielectric layer [32].

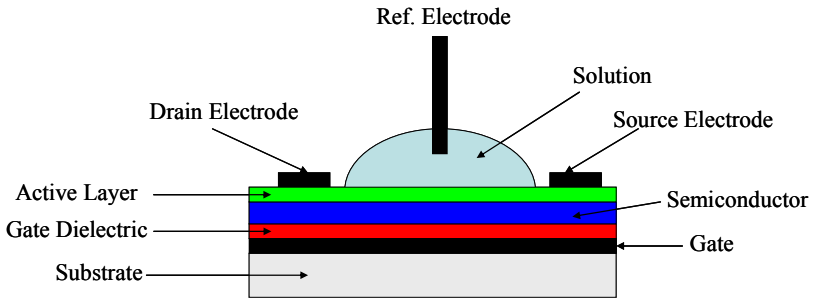

Figure 2.12 Schematic diagram of an ion sensitive organic field effect transistor with the bottom-gate structure.

As shown in Figure 2.11, the ISOFET is in direct contact with a test solution. A reference electrode forms as the gate electrode. An alternative device architecture

is depicted in Figure 2.12. With this structure, the reference electrode is not necessary part for operating the device since the gate electrode is beneath the dielectric layer [12, 33]. Attempts to exploit this structure in this research were unsuccessful because it is not compatible with the LB technique. For example, it was found that the dielectric and the semiconductor layers were both removed from the substrate during the LB deposition of an ion-sensitive membrane.

The top-gate structure shown in Figure 2.11 was therefore used in this study. The semiconductor layer in this structure was deposited directly on a glass substrate. By making the substrate hydrophobic, the semiconductor could be attached firmly to the substrate.

2.6 Reference Electrodes

An electrode with a stable electric potential is required for the operation of organic field-effect transistors, as shown in the Figure 2.11. As noted above, this reference electrode forms the gate. Its fixed potential results from the constant reaction rate of a redox process. Fixed concentrations (buffered or saturated) of each of the reactants in the reference electrode are used to keep the reaction rate constant.

Various types of reference electrodes are currently available. These include the standard hydrogen electrode (SHE, $E^0 = 0.000$ V), the saturated calomel electrode (SCE, $E^0 = +0.244$ V saturated), the copper-copper (II) sulfate electrode ($E^0 = +0.314$ V) and the silver/silver chloride electrode (Ag/AgCl, $E^0 = +0.197$ V saturated). The structure of a Ag/AgCl reference electrode is depicted in Figure 2.13. By contrast with SHE or SCE electrodes, a Ag/AgCl electrode does not require any preparation before use. In addition, this kind of a reference electrode is compact due to its simple structure.

The overall reaction of a silver chloride electrode can be written

$$Ag^0_{(s)} + Cl^- \leftrightarrow AgCl_{(s)} + e^- \qquad (2.16)$$

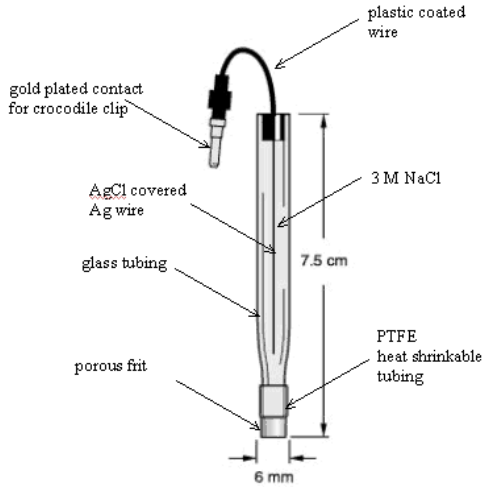

Figure 2.13 A structure of a silver/silver chloride reference electrode.

Therefore, the Nernst potential is

$$E = E^0 - \frac{RT}{F} \ln a_{Cl^-} \qquad (2.17)$$

The activity of chloride ion (a_{Cl^-}) is dependent on the concentration of the chloride ions in the solution. The corresponding Nernst equation for the Ag/AgCl reference electrode is

$$E = E^0 + 0.059 \log \frac{1}{[Cl^-]} \qquad (2.18)$$

The activities of the Ag wire and AgCl are unity and, therefore, to a good first approximation, only the chloride ion concentration determines the E value.

Minor drift in case of Ag/AgCl electrodes usually comes from a change in the concentration of Cl^- ions. This electrode is not suitable for use in a basic solution. When the electrode is in a solution with $[OH^-]$ above 0.1 M, silver oxide (Ag_2O) and/or silver hydroxide (AgOH) will form at the surface of the silver wire in the electrode. This will lead to a mixed $Ag/AgCl/Ag_2O$ potential, and hence its potential will depend on the pH. In using Ag/AgCl electrodes, basic solutions (pH > 7) should be avoided in order to keep the electrode potential stable and constant.

2.7 Conclusions

Organic thin-film transistors have some advantages over inorganic-based devices. This is due to the fact that organic semiconductors and organic dielectrics are cheap and require low-cost manufacturing process compared to silicon devices. Thin film transistor devices have various applications, such as flexible displays, solar cells and chemical sensors.

By adapting a structure of MOSFETs, an organic field-effect device can be used as an ion-sensitive device. The gate electrode is removed to expose the dielectric layer to a solution. In operating this device, a reference electrode is used as the gate. However, organic dielectrics have low sensitivity and low selectivity to target ions in an aqueous solution. By depositing an appropriate ion-sensitive membrane on top of the gate dielectric, ion-sensitive organic FETs are therefore able to detect target ions in a solution.

References

[1] J. E. Lilienfeld. Method and apparatus for controlling electric currents. U.S. Patent, 1,745,175, Application filed October 22 1925.

[2] D. Kahng and M. M. Atalla. Silicon – silicon dioxide field induced surface devices. IRE-AIEE Solid- State Device Res. Conf., Carnegie Inst. of Technology, Pittsburgh, PA, 27th-29th October 1960.

[3] R. G. Arns. Early history of the metal – oxide – semiconductor field – effect transistor. Eng. Sci. Educ. J., : 233 – 240, 1998.

[4] C. T. Sah. Evolution of the MOS transistor – From conception to VLSI. P. IEEE, 76(10): 1280 – 1326, 1988.

[5] T. Tiedje, J. M. Cebulka, D. L. Morel and B. Abeles. Evidence for exponential band tails in amorphous silicon hydride. Phys. Rev. Lett., 46(21): 142 – 1428, 1981.

[6] H. Klauk. Organic Electronics. Wiley – VCH Verlag GmbH, Weinheim, 2006.

[7] Y. Yamashita. Organic semiconductors for organic field – effect transistors. Sci. Technol. Adv. Mater., 10: 1 – 9, 2009.

[8] G. P. Crawford. Flexible Flat Panel Display Technology. John Wiley & Sons, Chichester, UK, 2005.

[9] T. Someya, Y. Kato, T. Sekitani, S. Iba, Y. Noguchi, Y. Murase, H. Kawaguchi, and T. Sakurai. Conformable, flexible, large-area networks of pressure and thermal sensors with organic transistor active matrixes. P. Natl. Acad. Sci. USA., 102(35): 12321 – 12325, 2005.

[10] R. A. Street, M. Mulato, R. Lau, J. Ho, J. Graham, Z. Popovic, and J. Hor. Image capture array with an organic light sensor. Appl. Phys. Lett., 78(26): 4193 – 4195, 2001.

[11] A. Das, R. Dost, T. Richardson, M. Grell, J. Morrison, and M. Turner. A nitrogen dioxide sensor based on an organic transistor constructed from amorphous semiconducting polymers. Adv. Mater., 19: 4018 – 4023, 2007.

[12] J. T. Mabeck, and G. G. Malliaras. Chemical and biological sensors based on organic thing – film transistors. Anal. Bioanal. Chem., 384: 343 – 353, 2006.

[13] V. Podzorov, S. E. Sysoev, E. Loginova, V. M. Pudalov, and M. E. Gershenson. Single – crystal organic field effect transistors with the hole mobility ~ 8 cm^2/V s. Appl. Phys. Lett., 83(17): 3504 – 3506, 2003.

[14] G. Hadziioannou and G. G. Malliaras. Semiconducting Polymers: Physics and Engineering. Wiley – VCH Verlag GmbH, Weinheim, 2007.

[15] G. Horowitz. Organic field-effect transistors. Adv. Mater., 10(5): 365 – 377, 1998.

[16] J. P. Colinge. Conduction mechanisms in thin-film accumulation-mode SOI p-channel MOSFETs. IEEE T. Electron Dev., 37(3): 718 – 723, 1990.

[17] H. Sirringhaus, N. Tessler, and R. H. Friend. Integrated optoelectronic devices based on conjugated polymers. Science, 280(5370): 1741 – 1744, 1998.

[18] C. R. Newman, C. D. Frisbie, D. A. S. Filho, J.L. Bredas, P. C. Ewbank, and K. R. Mann. Introduction to organic thin film transistors and design of n – channel organic semiconductors. Chem. Mater., 16: 4436 – 4451, 2004.

[19] M. J. Madau and S. R. Morrison. Chemical sensing with solid state devices. Academic Press, London, 1989.

[20] M. Baginski, J. Czub and K. Sternal. Interaction of amphotericin B and its selected derivatives with membranes: molecular modeling studies. Chem. Rec., 6: 320 – 332, 2006.

[21] C. J. Pedersen. Cyclic polyethers and their complexes with metal salts. J. Am. Chem. Soc., 89(10): 2495 – 2496, 1967.

[22] D. W. Urry, M. C. Goodall, J. D. Glickson and D. F. Mayers. The gramicidin A transmembrane channel: characteristics of head-to-head dimerized $\pi_{(L,D)}$ helices. Proc. Nat. Acac. Sci., 68(8): 1907 – 1911, 1971.

[23] N. Akaike and N. Harata. Nystatin perforated patch recording and its applications to analyses of intracellular mechanisms. Jpn. J. Physiol., 44: 433 – 473, 1994.

[24] T. E. Andreoli, M. Tieffenberg and D. C. Tosteson. The effect of valinomycin on the ionic permeability of thin lipid membranes. J. Gen. Physiol., 50: 2527 – 2545, 1967.

[25] P. Bergveld. Development of an ion-sensitive solid-state device for neurophysiological measurements. IEEE Trans. Biomed. Eng., BME-17: 70 – 71, 1970.

[26] P. Bergveld. Thirty years of ISFETOLOGY: what happened in the past 30 years and what may happen in the next 30 years. Sensor Actuat. B-Chem., 88(1): 1 – 20, 2003.

[27] S. D. Moss, C. C. Johnson and J. Janata. Hydrogen, calcium, and potassium ion-sensitive FET transducers: a preliminary report. IEEE Trans. Biomed. Eng., BME-25(1): 49 – 54, 1978.

[28] B. H. van der Schoot and P. Bergveld. ISFET based enzyme sensors. Biosensors, 3(3): 161 – 186, 1987 – 1988.

[29] V. Volotovskya, A. P. Soldatkinb, A. A. Shul'gac, V. K. Rossokhatya, V. I. Strikhaa and A. V. El'skayab. Glucose-sensitive ion-sensitive field-effect transistor-based biosensor with additional positively charged membrane: dynamic range extension and reduction of buffer concentration influence on the sensor response. Anal. Chim. Acta, 322(1-2): 77 – 81, 1996.

[30] P. W. Cheung, D. G. Fleming, W. H. Ko and M. R. Neuman (eds). Theory, design, and biomedical applications of solid-state chemical sensors. CRC Press, Florida, 1978.

[31] T. Osa. Potentiometric response of lipid modified ISFET. Appl. Biochem Biotech., 41: 35 – 40, 1993.

[32] E. J. Fogt, D. F. Untereker, M. S. Norenberg and M.E. Meyerhoff. Response of ion - selective field effect transistors to carbon dioxide and organic acids. Anal. Chem., 57: 1995 – 1998, 1985.

[33] M. J. Spijkman, J. J. Brondijk, T. C. T. Geuns, E. C. P. Smits, T. Cramer, F. Zerbetto, P. Stoliar, F. Biscarini, P. W. M. Blom and D. M. de Leeuw. Dual-gate organic field-effect transistors as potentiometric sensors in aqueous solution. Adv. Funct. Mater., 20: 898 – 905, 2010.

Chapter 3
Experimental Techniques

3.1 Physical Vapour Deposition

Physical vapor deposition (PVD) is a technique that is used to coat a thin film onto a surface under a vacuum environment. All PVD techniques use physical processes to vaporise a material and then condense the vapour onto a substrate. There is no chemical reaction associated with PVD, only a phase transition. Physical vapour deposition techniques are generally categorised into two main methods: thermal vapour deposition and sputtering. Thermal vapour deposition is used in this research; this was employed for depositing metal layers onto glass substrates. In practice, there are a variety of PVD techniques based on thermal evaporation sources, such as filaments and electron-beam systems. In this section, the focus is on thermal vapour deposition, which uses a filament as the thermal source.

Thermal Vapour Deposition

Thermal vapour deposition is often used to deposit metal films. It requires a vacuum environment to allow the gaseous molecules of the source material to move directly to a substrate without colliding with the background gaseous molecules. In addition, these molecules and the source material have a high temperature, and hence are very reactive to oxygen. Under a vacuum, unwanted oxidation reactions are minimised.

A schematic diagram of thermal vapour deposition is shown in Figure 3.1. The evaporation process is undertaken in a glass bell jar or similar vacuum vessel. The solid source material is placed on a filament. A crystal microbalance detector is placed at the same distance from the source as the substrate. This is used for monitoring the thickness of the deposited film. A high vacuum is created using the combination of a rotary pump and a diffusion pump. The air in the bell jar is evacuated until the pressure is below 10^{-6} mbar. The mean free path of the residual gas molecules, λ, can then be calculated using kinetic theory.

$$\lambda = \frac{k_B T}{P\pi d^2 \sqrt{2}} \qquad (3.1)$$

where d is the diameter of gaseous molecules, T is the temperature, P is the gas pressure, and k_B is Boltzmann's constant.

From Equation 3.1, the mean free path of the molecules of the gas in the chamber is greater than 500 cm when the pressure is below 10^{-5} mbar and the temperature is 300 K. Since the distance between a filament and a substrate is about 30 cm, the vaporised molecules will travel to the substrate without a collision with other molecules.

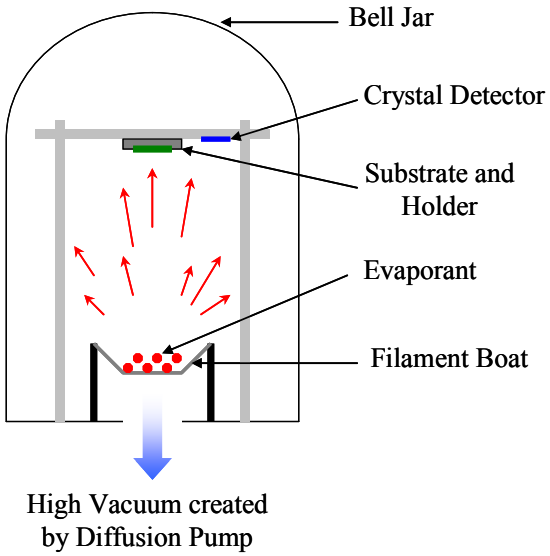

Figure 3.1 Schematic diagram of thermal vapour deposition.

In this research, an Edwards Auto306 evaporator was used to deposit a chromium/gold layer on a glass substrate. The chamber was first pumped using an Edwards RV12 rotary pump until the pressure reached about 10^{-2} mbar. An Edwards EXT255H diffusion pump was then used to evacuate the system to a pressure of less than 10^{-5} mbar. A crystal detector, as a microbalance, was used to monitor thickness of the evaporised film.

Shadow Mask Deposition

Shadow mask deposition is a method that selectively coats a material onto a substrate through a shadow mask. A schematic diagram of this process is shown in Figure 3.2.

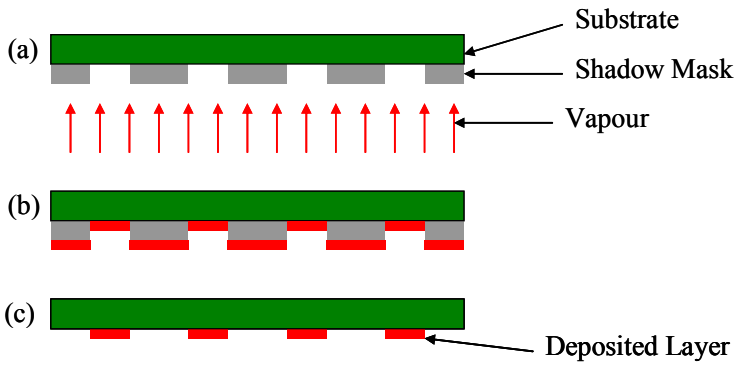

Figure 3.2 (a) Schematic diagram of the shadow mask deposition. (b) Thin film deposited on the masked substrate. (c) Thin film on the substrate after removing the mask.

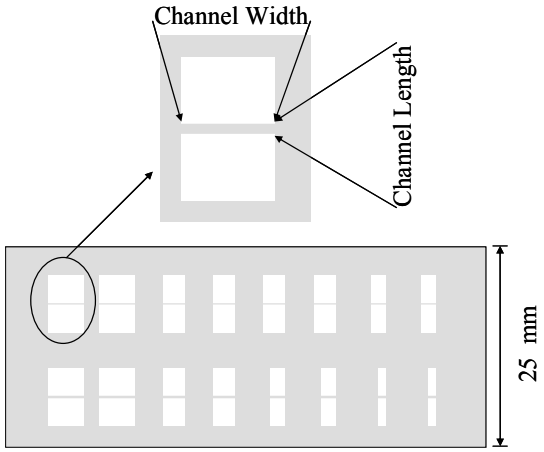

Figure 3.3 A diagram of the shadow mask used for depositing the source and drain electrodes in this research.

Table 3.1 The channel widths and channel lengths of the shadow mask.

Channel Length (μm)	Channel Width (μm)	W/L ratio	Channel Length (μm)	Channel Width (μm)	W/L ratio
50	4000	80	200	4000	20
50	4000	80	200	4000	20
50	2000	40	200	2000	10
50	2000	40	200	2000	10
50	1000	20	100	2000	20
50	1000	20	100	2000	20
50	500	10	100	1000	10
50	500	10	100	1000	10

The shadow mask is placed in contact with the substrate and then the source material is evaporated. Some of this material is coated on the substrate, but some is also coated on the mask, as shown in Figure 3.2b. When removing the mask, a deposited layer on a substrate has the same pattern as that of the mask, as depicted in Figure 3.2c.

The shadow mask used in the research is shown in Figure 3.3. The channel length (L) is the gap between the electrodes and the channel width (W) is the width of the electrodes. This method was used to fabricate the non-interdigitated pattern of source/drain electrodes; the various electrode dimensions are listed in Table 3.1. Before depositing the chromium and gold layers, each metal had an in-situ cleaning for 30 seconds by heating it to the evaporation temperature while the main shutter was closed. In this way, the surface of the source material was cleaned.

3.2 Photolithography

Photolithography (or "optical lithography") is a process to transfer a pattern onto a substrate. This method uses light (generally ultra-violet (UV) light) to transfer a geometric pattern from a mask to a light-sensitive photoresist (or simply resist) on the substrate. The process of photolithography is depicted in Figure 3.4a. In this research, photolithography was used to transfer an interdigitated electrode pattern on to glass substrates. A typical interdigitated pattern is shown in Figure 3.4b.

The samples are first coated with photoresist. There are two types of photoresist, positive and negative. A negative resist is comprised of monomers which are polymerised under exposure to UV light. As shown in Figure 3.4, the unexposed area of the resist remains soluble and is then removed after the exposure by the developer. The area that is in direct contact with the etching solution is removed, while the polymerised resist protects the area underneath from the etching process. After removing the photoresist, a complementary pattern to that on the mask is obtained on the substrate.

By contrast, a positive resist is a light-sensitive polymer. The area exposed to the UV light becomes soluble in a developer. By removing this area, an identical pattern to that on the mask is transferred to the substrate.

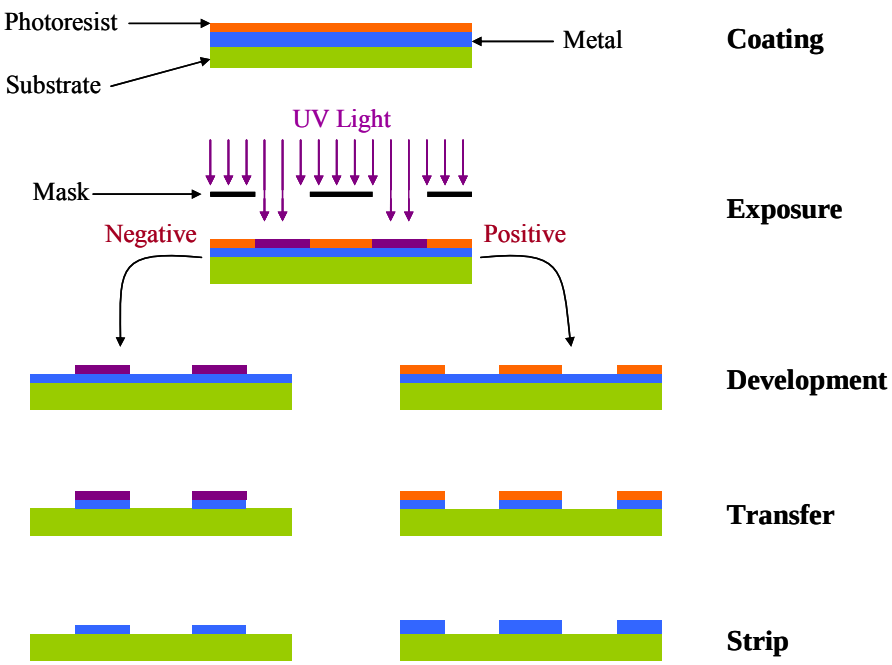

(a)

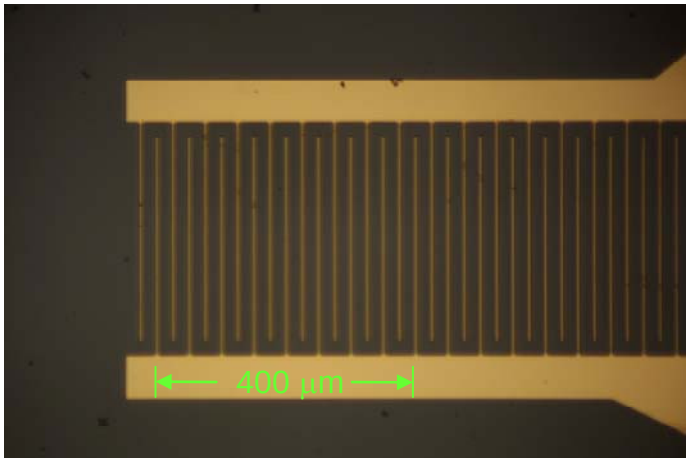

(b)

Figure 3.4 (a) Photolithographic process of transferring a pattern onto a substrate. (b) Typical interdigitated pattern.

In this research, the surface of hydrophobic glass substrates was first coated with chromium and gold. The chromium layer was required to improve the adhesion between the gold layer and the glass substrate. Following this, Microposit S1813 positive resist was spin-coated on the gold layer. Before exposure, the resist-coated samples were baked on a hot plate at 95 °C for 5 min. The samples were masked by the interdigitated patterned mask and then exposed to UV light for 5 seconds. The samples were developed using Microposit 351B developer (aqueous sodium hydroxide) (351B developer : DI water is 1 : 4) for 30 seconds. The samples were then rinsed with DI water and dried using filtered N_2. Before etching the metal layers, the samples were baked at 120 °C for 5 min. After rinsing with DI water, the resist was removed using the Microposit 1112A resist remover (ethyleneglycol n-butyl ether).

3.3 Spin – Coating

Spin-coating is a solution process to deposit a thin film on a flat substrate. Figure 3.5 shows a diagram of the process. After dissolving a source material in an appropriate solvent, an excess amount of the resulting solution is placed on a substrate. The substrate is then rotated at a high speed. The uniformity and the thickness of coated layers depend on the spinning speed. With a suitable speed, the solution is spread uniformly and covers the whole surface of the substrate. This technique is generally used to produce thin films of polymer, such as photoresist [1], PMMA [2] and P3HT [3], onto various substrates, e.g. silicon wafers, glass and plastics. The spin speed depends on the solution concentration.

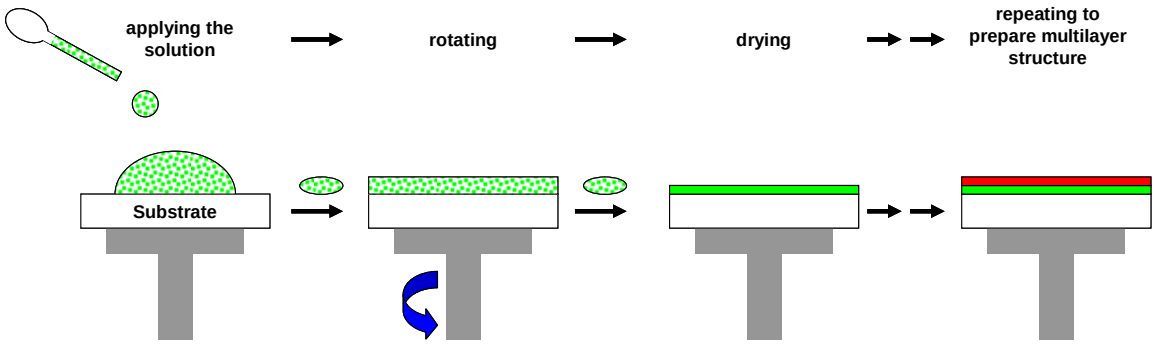

Figure 3.5 Schematic diagram of the spin-coating process.

Following film deposition, the spin-coated layer is left, generally in air, to evaporate the solvent. In some cases, the samples need a particular treatment, such as vacuum drying at a controlled temperature. By repeating the spin-coating process, a multilayer structure may be obtained. However, it is essential that the solvent used in the next spin - coating should not dissolve the previously coated film.

3.4 Thermal Annealing

Thermal annealing is a process of heat treatment that is used to modify both the mechanical and electrical properties of materials, such as strength, hardness and electrical conductivity. Samples are heated to a particular temperature and maintained at that temperature for a period of time to recrystallise the lattice, to reduce dangling bonds and also to relieve internal stresses. In addition, some polymers require an appropriate heat treatment for polymerisation.

When organic materials are processed at elevated temperatures, they may become more reactive. A vacuum oven is therefore required to prevent the oxidation reaction between the organic materials and molecules of water and oxygen gas. In addition, the required temperature for evaporating the solvent is lower when the samples are kept in vacuum.

In this study, the main purposes of employing vacuum annealing were to evaporate the solvent from the organic layers, and to enhance the properties of the dielectric layer. A vacuum oven OV-11 (Jeio Tech) was used to anneal the samples after each spin-coating step. The vacuum was kept below 1 mbar during the thermal annealing.

3.5 Langmuir-Blodgett Deposition

The Langmuir-Blodgett (LB) technique is a simple method for transferring organic monolayers onto substrates such as glass, metallised glass and silicon. Various organic materials, such as fatty acids and phospholipids, can be arranged into monolayers and then deposited onto substrates by this method. The molecules are generally comprised of two main parts, namely hydrophobic and hydrophilic sections, as shown in Figure 3.6. When a fatty acid is placed on a water surface, its

hydrophobic part is oriented towards the air. In contrast, the hydrophilic part of the molecule is in contact with the subphase (water).

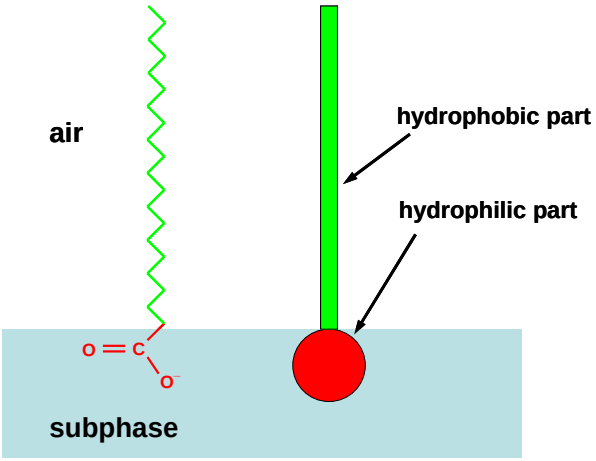

Figure 3.6 Amphiphilic molecule (fatty acid) on the surface of water (subphase).

When a solution of fatty acid is dropped onto the water (Figure 3.7a), the amphipathic (or amphiphilic) molecules try to align themselves (Figure 3.7b). At the same time, solvent molecules evaporate from the floating film (Figure 3.7c). An expanded monomolecular film is then formed on the subphase (Figure 3.7d). However, the amphipathic molecules are loosely attached to each other. To produce a crystalline film, a barrier is moved to compress and force the molecules closer to each other. The condensed floating monolayer is therefore in the form of a two-dimensional crystal (Figure 3.7e).

π - A Isotherms

A surface pressure (π) - area (A) isotherm is a plot of surface pressure against molecular area when the temperature is fixed. Generally, this is simply referred to as an isotherm. In essence, an appropriate pressure for film deposition is obtained from the isotherms since they provide information about phase changes of a floating monolayer of a particular material on a subphase. A typical isotherm is shown in Figure 3.8.

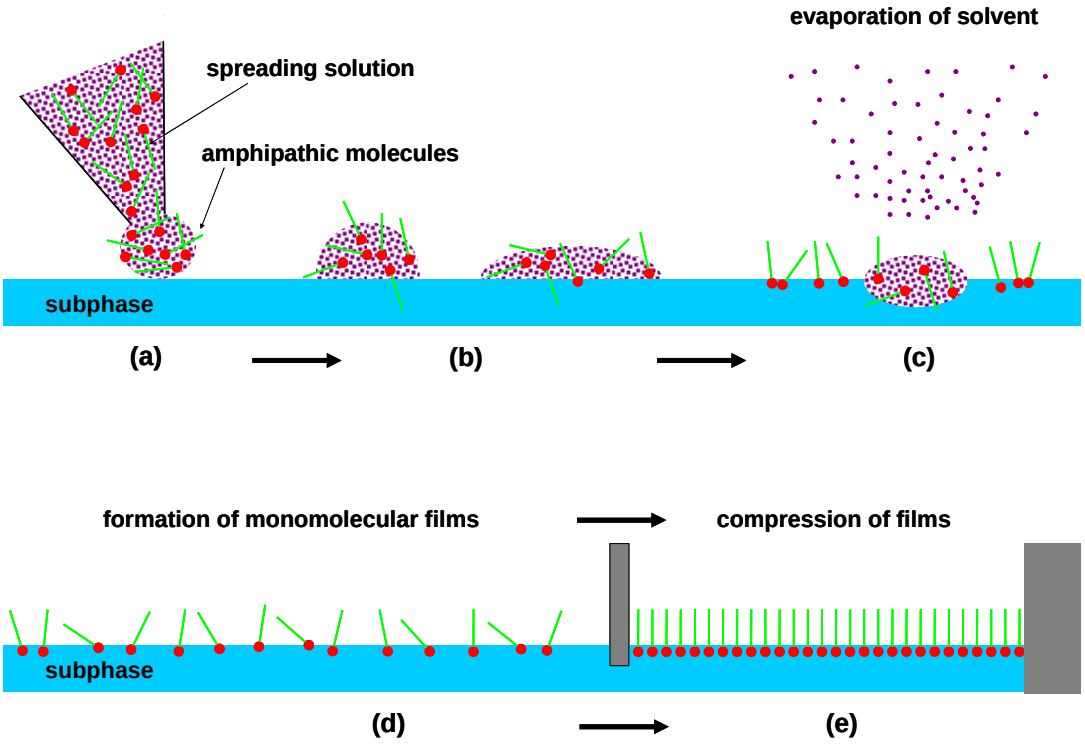

Figure 3.7 Formation of monomolecular film : (a) organic solution dropped onto the subphase, (b) organic molecules spread on the subphase, (c) solvent molecules evaporate, (d) expanded monomolecular films formed on the subphase, (e) condensed film on the subphase.

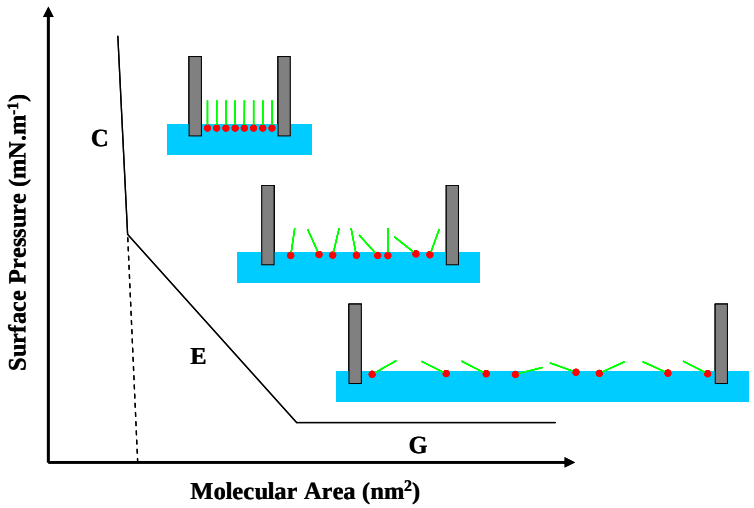

Figure 3.8 A typical isotherm showing surface pressure versus molecular area.

When a floating layer is compressed, the phase transition basically occurs in the two-dimensional layer. This two-dimensional phase change is analogous to that of the three dimensions of a bulk material. As shown in Figure 3.8, molecules are initially in gas phase (G). In this phase, molecules have no or very slight interactions between molecules.

When reducing the area of the floating layer, the molecules move closer and start to interact with each other. However, the interaction in this phase is weak because the molecules are still distant from their neighbours. This leads to a gradual increase of the surface pressure. In this phase, the molecules show thermodynamic behaviour similar to that in a (3-dimensional) liquid phase. This is generally called the expanded phase (E).

If the decrease of the trough area continues, the interaction between molecules finally becomes strong. The area reaches a limiting value and the surface pressure increases sharply. This is similar to a three-dimensional solid phase. This phase of the floating monolayer is known as the condensed phase (C). The rising pressure seen in the isotherm marks the onset of the closed packed structure of the floating monolayer.

Film Deposition

After the condensed monolayer of the amphipathic molecules is formed on the subphase (Figure 3.9a), a substrate is lowered into the subphase. When this is removed, a monolayer is transferred to the substrate (Figure 3.9b). If the substrate is again lowered into the subphase, a further monolayer is deposited (Figure 3.9c). By moving the substrate up and down, a multilayer molecular film is built up on the substrate (Figure 3.9d). The thickness of the film is therefore dependent on the number of dips into the subphase.

Three types of LB membranes are shown in Figure 3.10. A Y-type LB film can be deposited easily on substrates by moving the substrates in and out of the subphase. In case of Y-type deposition, the multilayer architecture will possess a hydrophobic surface (Figure 3.10b) if the deposition process is ended in air. In contrast, if the process finishes in the subphase, a hydrophilic surface (Figure 3.10a) will be obtained.

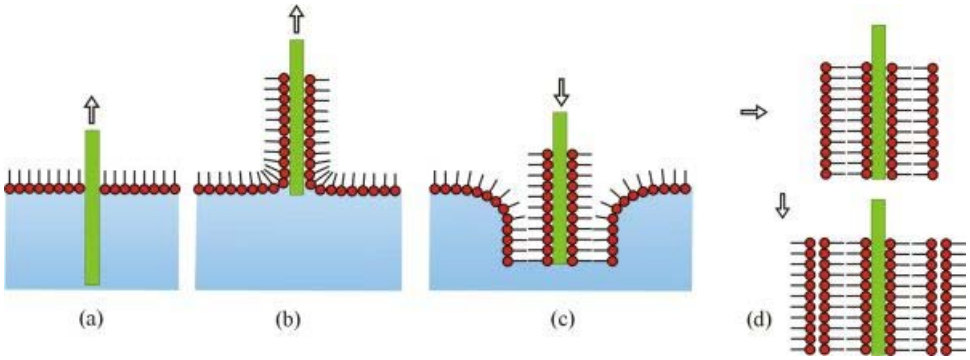

Figure 3.9 Y-type deposition of monomolecular film onto a substrate : (a) Moving the substrate out of the subphase. (b) Monomolecular layer attached onto the substrate while moving out the subphase. (c) A further monomolecular layer is deposited onto the substrate while moving the substrate down into the subphase. (d) A multilayer film is deposited on the substrate by repeatedly moving the substrate up and down.

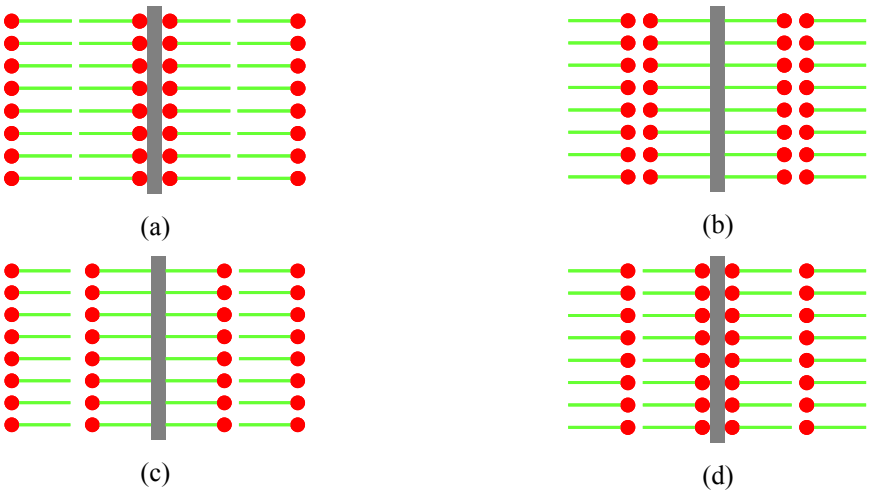

Figure 3.10 (a) Y-type deposition on hydrophilic surface. (b) Y-type deposition on hydrophobic surface. (c) X-type deposition. (d) Z-type deposition.

In the Y-type deposition mode, the floating layer is transferred on both the downstroke and the upstroke. In the X-type deposition mode, the monolayer is, in contrast, transferred onto a substrate only on the downstroke. A typical structure of X-type LB films is depicted in Figure 3.10c. However, in the Z-type deposition mode, the monolayer is transferred only on the upstroke. Figure 3.10d shows a typical Z-type LB film. In essence, certain conditions are required to obtain an X-type or Z-type film; for example, high pH values can favour X-type deposition of fatty acid materials.

To improve film quality, a metal salt, such as $CdCl_2$, is added to the water. Since the metal ions bind to the hydrophilic parts, the molecules are then attached to the neighboring molecules. As a result, a monomolecular layer of cadmium arachidate is formed. This film is more stable and the quality of deposited film on the substrate is improved [4].

A transfer ratio, or deposition ratio (τ), is used to characterise the quality of film transfer. This is the ratio between the decreased area of monolayer film on the subphase and the deposited area of the solid substrate, i.e.,

$$\tau = \frac{A_L}{A_S} \tag{3.2}$$

where A_L is the decrease in monolayer area while a substrate is dipped trough the subphase at the constant pressure and A_S is the deposited area on the substrate. If the film is of high quality, the transfer ratio should be within the range of 0.95 to 1.05 [4].

In this research, the LB technique was used to build up artificial membranes on a substrate. The LB membranes were used as an ion-selective layer. The hydrophobic substrates were first moved into the subphase and then pulled out of the subphase.

3.6 Conclusions

The background concepts to the experimental techniques used in this research have been presented. Although various PVD techniques could be used to deposit a metal layer onto substrates, only thermal vapour deposition has been described in detail. This method has been used to deposit both chromium and gold layers on glass substrates. The shadow mask technique for transferring a standard pattern of source/drain electrodes onto substrates has been introduced. The photolithographic method for transferring an interdigitated pattern of source/drain electrodes has also been explained. Spin-coating was used for depositing semiconductor and dielectric layers. The process of vacuum annealing is also described. This was used for evaporating the solvent from the organic layers and enhancing the properties of the spin-coated layers. Finally, the LB technique for fabricating a well-ordered membrane on substrates has been outlined.

References

[1] Y. Jin, Z. Rang, M. I. Nathan, P. P. Ruden, C. R. Newman and C.D. Frisbie. Pentacene organic field-effect transistor on metal substrate with spin-coated smoothing layer. Appl. Phys. Lett., 85(19): 4406 – 4408, 2004.

[2] N. Benson, M. Schidleja, C. Melzer, R. Schmechel and H. Seggern. Complementary organic field effect transistors by ultraviolet dielectric interface modification. Appl. Phys. Lett., 89: 182105, 2006.

[3] J. F. Chang, B. Sun, D. W. Breiby, M. M. Nielsen, T. I. Solling, M. Giles, I. McCulloch and H. Sirringhaus. Enhanced mobility of poly(3-hexylthiophene) transistors by spin-coating from high-boiling-point solvents. Chem. Mater., 16: 4772 – 4776, 2004.

[4] M. C. Petty. Langmuir-Blodgett films: an introduction. Cambridge University Press, 1996.

Chapter 4

Langmuir-Blodgett Membranes

4.1 Materials

In this research, an artificial membrane is fabricated to imitate the membranes found in human cells. The hydrocarbon chain in naturally occurring lipids and phospholipids in cell membranes contains generally between 16 to 20 carbon atoms. Arachidonic acid, one of the major constituents [1], contains 20 carbons in the normal hydrocarbon chain, with 4 double bonds. This fatty acid plays a significant role in maintaining the fluidity of the cell membrane [2] because the double bonds prevent the molecules of the fatty acids from packing together tightly. In normal circumstances, all the constituents will be held in the form of a stable cell membrane because the cytoskeleton forms scaffolding which supports all the fatty acids and lipids. On the other hand, no supporting microstructure is imbedded in the artificial membrane. Therefore, any double bond in a fatty acid molecule can lead to a weak attractive force between the molecules. In this research, arachidic acid (AA), instead of arachidonic acid, was used to avoid the double bonds in the fatty acid molecules. With an unbranched saturated hydrocarbon chain, AA molecules can form a close-packed floating monolayer on a subphase. As a result, an artificial AA membrane can be transferred onto a substrate more efficiently and effectively than a membrane of arachidonic acid. Arachidic acid was therefore selected as the basic constituent of the artificial membranes in this research.

The 16-carbon phospholipids are one of the most common constituents in cell membranes. Although both saturated and unsaturated fatty acids are generally found in cell membranes throughout the human body, fatty acids with a saturated hydrocarbon chain are more inert than unsaturated fatty acids and not reactive to water (H_2O) or oxygen (O_2) molecules. This makes 1,2-dipalmitoyl-sn-glycero-3-phosphatidic acid (DPPA) suitable for this research because this phospholipid is comprised of two palmitoyl groups, in the form of a 16-carbon saturated hydrocarbon chain. This kind of fatty acid can be exposed to an aqueous environment without undergoing any chemical reactions with oxygen or water. Furthermore, this

molecule has its hydrocarbon chains of the same length, similar to the main constituents in cell membranes.

An ion channel or ionophore is required to sensitise a layer to potassium ions. Although many ionophores have been studied and characterised, valinomycin [3-11] shows a high sensitivity and potential for detecting potassium ions in an aqueous solution. Following incorporation in an active layer, such as PVC [12], photoresist [13] or lacquer [14], valinomycin can detect potassium ions in saline solution with a low interference from sodium or other ions. However, there is little work on the incorporation of this molecule in an active layer of an ion-sensitive organic field effect transistor.

In this chapter, the main objective is to study the characteristics of Langmuir-Blodgett (LB) membranes of the materials noted above. The substrate is a single-crystal silicon wafer.

Arachidic Acid

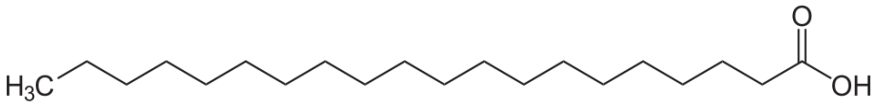

Figure 4.1 Chemical structure of arachidic acid.

Arachidic acid, or eicosanoic acid, is a saturated fatty acid comprised of a long chain hydrocarbon with only single bonds, as shown in Figure 4.1. Its chemical formula is $C_{19}H_{39}COOH$ and its molecular weight is 312.5 g mol^{-1}. Arachidic acid (anhydrous; Sigma grade, ≥ 99%) was obtained from Sigma Chemicals. This material can be completely dissolved by chloroform under normal conditions, but it is insoluble in water. Because the molecular structure of arachidic acid is that of a single hydrocarbon chain, its cross-sectional area per molecule is around 0.19 nm^2.

In this work, AA is used as a basic component in creating the LB film. However, the hydrocarbon chain is not long enough to provide the strong Van der Waals force to hold the crystalline film stable on a subphase. Therefore, $CdCl_2$ is added to a subphase to improve a stability of the floating crystalline layer [15]. The reaction between AA and cadmium chloride is

$$2C_{19}H_{39}COOH + CdCl_2 \rightarrow Cd(C_{19}H_{39}COO)_2 + 2HCl \qquad (4.1)$$

Since each cadmium ion (Cd^{2+}) binds with two arachidate groups, a monolayer of cadmium arachidate (CdAA) is more rigid than the corresponding monolayer of AA on the surface of a subphase.

1,2-Dipalmitoyl-*sn*-Glycero-3-Phosphatidic Acid

1,2-Dipalmitoyl-sn-glycero-3-phosphatidic acid (DPPA) is a phospholipid with two saturated hydrocarbon chains, as shown in Figure 4.2. The empirical formula of this material is in its sodium salt form, $C_{35}H_{68}O_8P{\bullet}Na$; its molecular weight is 670.87. Normally, this material is in the form of a white powder. 1,2-Dipalmitoyl-sn-glycero-3-phosphatidic acid (TLC grade, ≥ 98%) was obtained from Fluka Chemicals.

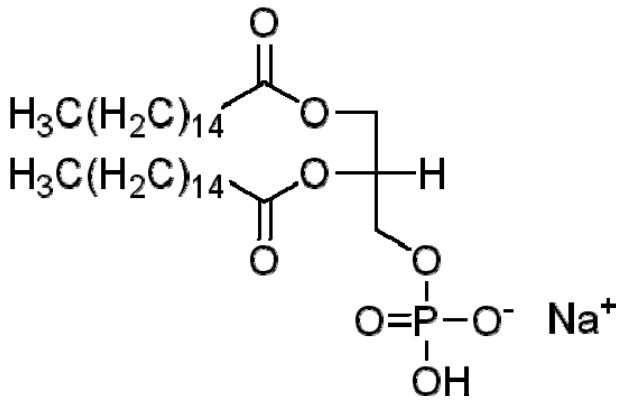

Figure 4.2 Chemical structure of 1,2-Dipalmitoyl-*sn*-glycero-3-phosphatidic acid.

1,2-Dipalmitoyl-sn-glycero-3-phosphatidic acid can be completely dissolved by warm chloroform. However, when the solution is cooled, some molecules of DPPA can precipitate out of the solution due to its low solubility at room temperature. Therefore, the solution must be warmed to make DPPA completely dissolve before using it in the experiment.

Valinomycin

Valinomycin is a dodecadepsipeptide because it is comprised of twelve amino acids. As shown in Figure 4.3, these amino acids are connected in a circle. Generally, its molecular weight is 1111.32 and its empirical formula is $C_{54}H_{90}N_6O_{18}$. This material is normally dissolved by non-polar solvents [7] at room temperature. However, chloroform is used as the solvent in this research due to its low boiling point. Valinomycin (TLC grade, ≥ 98%) was obtained from Fluka Chemicals.

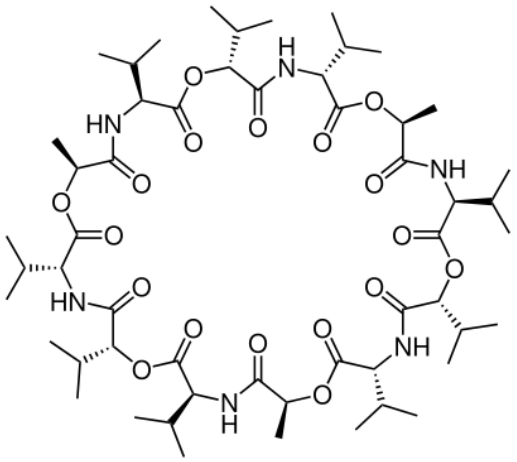

Figure 4.3 Chemical structure of valinomycin.

A valinomycin molecule is normally arranged so that its twelve carbonyl groups (hydrophilic groups) are inside the molecule. The methyl groups and isopropyl groups (hydrophobic groups) are pointed outwards. The shape of the valinomycin molecule is very flexible because of its sheer size. As a result, the molecular structure is not locked into the form depicted in Figure 4.3. Thus, this molecule can be dissolved in a polar solvent by exposing the hydrophilic groups to the solvent molecules; however, it can also be dissolved in a non-polar solvent by exposing the hydrophobic groups to the solvent molecules.

The twelve carbonyl groups from the amino acids are arranged to form an ion compartment or ionophore that is specific to potassium ions. The molecule traps K^+ within this cavity and transports K^+ across the membrane. When K^+ is trapped inside valinomycin, a potassium-ion complex is formed; the shape and size of valinomycin is changed slightly from that shown in Figure 4.3. Within the membrane environment, this change is sufficient to free this ion complex from the neighbouring

molecules. This complex is a hydrophobic macromolecule; it can move through LB membrane because its exterior is made up from the methyl and isopropyl groups. Consequently, the complex moves across the membrane and the K^+ ion is released from valinomycin on the other side. In this way, valinomycin functions as a K^+ carrier [3].

Silicon Substrates

Silicon wafers were used as a substrate for supporting the LB films. In this work, a p-type Si wafer was cut into 1 x 3 cm^2 pieces, as shown in Figure 4.4. To remove all particles and contamination from the surface of the substrate, the silicon was immersed in a series of solvents and left in an ultrasonic bath for 15 minutes. The substrates were rinsed by analytical-grade solvents and dried by filtered nitrogen gas. By using isopropanol, acetone, 2% Decon solution and DI water in sequence, both polar and non-polar contaminations are removed from the surface. The wafers were finally treated using 2% dimethyldichlorosilane to provide hydrophobic surfaces.

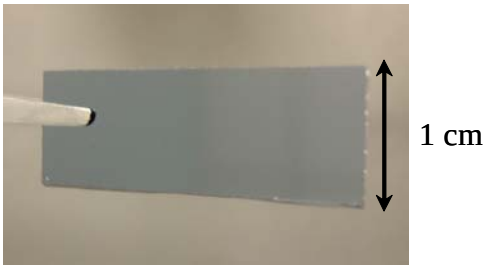

Figure 4.4 A silicon substrate.

4.2 Pressure - Area Isotherms

Langmuir-Blodgett films are normally deposited at a pressure within the condensed phase. The purpose of these experiments was to investigate the surface pressure - area isotherms of materials that were used in this work, namely AA, DPPA and valinomycin. In addition, a mixture of fatty acid and valinomycin was studied to find the optimum condition for pressure control during film deposition.

The LB trough was cleaned by using isopropanol and deionised (DI) water respectively, before carrying out the experiments. The LB trough was filled with DI water (subphase). To improve the quality of the deposited film, the surface of a subphase was cleaned until the difference between the maximum and minimum pressures was less than 0.5 mN m^{-1}. This was done by compressing the surface of a subphase without spreading any fatty acid. Since the aqueous subphase was exposed to the air, carbon dioxide (CO_2) dissolved into the DI water. As the result, the pH of the subphase was around 5.5. All the experiments were undertaken in the cleanroom at 293 K.

After preparing the LB equipment, a solution of the appropriate material was dispersed via a syringe onto the subphase. The solution was left on the subphase for 10 minutes, to allow for solvent evaporation.

Arachidic Acid

To measure an isotherm, 30 μl of a solution of arachidic acid (conc. = 1.02 mg ml^{-1}; in chloroform) was spread on the surface of a subphase. About 10 minutes was allowed for the chloroform to evaporate until the surface pressure reached a stable value. The monolayer was then compressed at a rate of 2.0 ± 0.1 cm^2 s^{-1} (the barrier speed was approximately 1 mm s^{-1}) and the isotherm was recorded as shown in Figure 4.5a. The observable transition of the arachidic acid monolayer from the gaseous phase into the expanded phase occurred at a molecular area of about 0.25 ± 0.01 nm^2. A condensed or solid phase of AA was noticeable when the surface pressure exceeded about 25 mN m^{-1}. Similarly, Pezron et al [16] reported that the film entered into an expanded phase when the molecular area was lower than 0.25 nm^2, and the phase transition into the solid condensed state was observed at a surface pressure of about 26 mN m^{-1}. When the graph in the condensed region was extended to intercept the x axis, it is evident that the area per arachidic acid molecule is approximately 0.21 ± 0.01 nm^2. This interpolation method was also used in subsequent work. The result shows that the molecular area of AA is similar to the theoretical value noted in Section 4.1. At a given surface pressure, the reproducibility of AA on DI-water subphase was better than 0.01 nm^2.

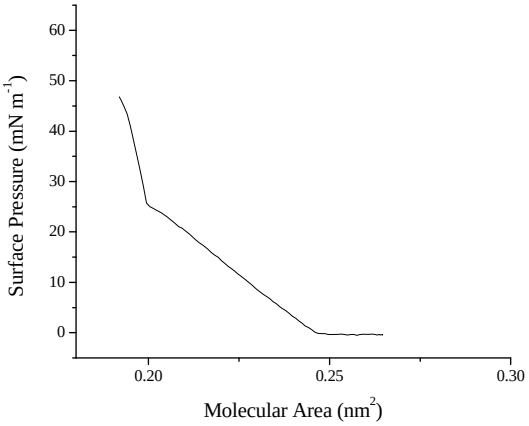

(a)

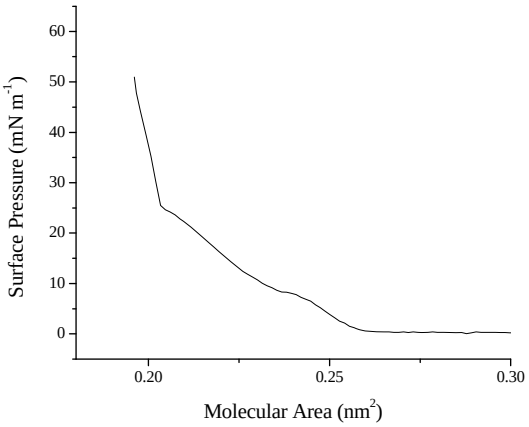

(b)

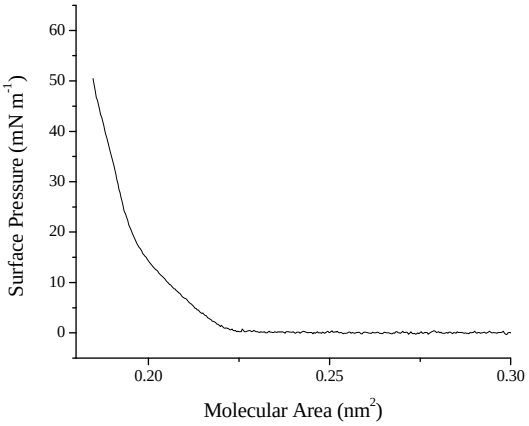

(c)

Figure 4.5 Isotherms of arachidic acid at 293 K, pH 5.5, measurement using subphase as : (a) DI water. (b) 1 mg ml^{-1} KCl solution. (c) 0.1 mg ml^{-1} $CdCl_2$ in DI water.

Using potassium chloride (KCl) solution at a concentration of about 1 mg ml^{-1} as a subphase, 20 μl of the solution of AA (conc. = 1.02 mg ml^{-1}; in chloroform) was spread on the subphase. After allowing 10 minutes for evaporation of the solvent, the isotherm of AA was measured and plotted as in Figure 4.5b. It is evident that the transitions from the gaseous phase to the expanded phase and from the expanded phase to the condensed phase occur at the same surface pressures as those for the monolayer on the DI water subphase. With the molecular area of 0.21 ± 0.01 nm^2 in case of the KCl subphase, the presence of the K^+ ions did not have an observable effect on the molecular area in the condensed phase of the AA. Similarly, the reproducibility of AA isotherms on KCl solution subphase at a specific surface pressure was better than 0.01 nm^2.

Pezron et al [16] showed that the presence of the monovalent salt did not have an effect on the isotherm of arachidic acid at a pH of 5.6. In contrast, Goddard et al [17] reported that the effect of the alkaline ions on the isotherms of pure AA could be observable at a pH above 12, when the carboxylic groups of the fatty acid were fully ionised. In this study, a small repeatable bump occurs at a surface pressure of about 10 mN m^{-1}. This agrees with that reported by Goddard [17]. The bump occurring in Figure 4.5b may therefore be the effect of potassium monovalent ions (K^+) on AA molecules on the aqueous subphase. However, this small bump may also result from other contamination, such as fatty acid or ions. Further work is needed to clarify this.

Figure 4.5c shows the isotherm of arachidic acid on cadmium chloride solution at a concentration of 0.1 mg ml^{-1}. The molecular area of cadmium arachidate is approximately 0.20 ± 0.01 nm^2; this is slightly smaller than that of AA. Unlike the isotherm of AA, the expanded phase is not observed in the isotherm of CdAA. In this case, when cadmium chloride is added to the subphase, each cadmium ion is bound to two COO^- groups of AA to form cadmium arachidate (CdAA), an organic salt. Consequently, each arachidic acid molecule is attached to another more tightly than in the case of AA. As noted in previous work [18, 19], Cd^{2+} is a suitable divalent ion to improve the stability of a monomolecular layer of AA. Adding divalent ions into subphase can improve the transfer ratio of the LB film. In this work, arachidic acid and cadmium arachidate were both transferred onto substrates at a surface pressure of 32 mN m^{-1}.

1,2-Dipalmitoyl-sn-Glycero-3-Phosphatidic Acid

1,2-dipalmitoyl-sn-glycero-3-phosphatidic acid was dissolved in chloroform at a concentration of 0.5 mg ml^{-1}. 200 μl of the solution was spread on the surface of an aqueous subphase. The isotherm of DPPA was shown in Figure 4.6a. This was found to be similar to that of cadmium arachidate. However, the molecular area of DPPA, approximately 0.07 ± 0.01 nm^2, is far less than the theoretical value, about 0.38 nm^2 (due to the two hydrocarbon chains in the DPPA molecule). The result suggests an error in the concentration of the DPPA solution. As noted in datasheet of the Matreya Company, DPPA can be completely dissolved in warm chloroform. However, a dramatic decrease in the solubility of DPPA at room temperature led to the precipitation of DPPA in the solution. This makes the concentration of the DPPA solution uncertain. DPPA could be dissolved completely without any precipitation at room temperature, if the concentration was more diluted, less than 0.1 mg ml^{-1}.

The solubility of DPPA could be increased by using an ethanol:hexane mixture or an ethanol:chloroform mixture. In the case of using the ethanol:hexane (1:4) mixture, the molecular area was about 0.52 nm^2. However, the isotherm has a large hysteresis loop as shown in Figure 4.6b. Both the hysteresis and the very large molecular area probably result from the remains of solvent in the monolayer due to its low evaporation rate.

In case of using the ethanol:chloroform mixture (1 : 9) as the solvent, DPPA was dissolved at a concentration of about 0.91 mg ml^{-1}. The DPPA isotherm is shown in Figure 4.6c. Similar to the isotherm of CdAA, no phase transition is observed in the isotherm of DPPA. This agrees with the work of Minones et al, who experimented in forming a monolayer using a DPPA solution with a concentration of about 0.46 mg ml^{-1} [20]. However, the result in this study shows that the molecular area is about 0.23 nm^2, one half of the theoretical value. This may be because the DPPA did not dissolve completely in such solvent.

As shown in Figure 4.6c, it is difficult to indicate the transition pressure between the expanded phase and the condensed phase. The slope in the expanded phase is clearly different from that in the condensed phase. The transition pressure can then be approximated using the interception point between the slopes of the expanded and condensed phases. In this work, an ethanol:chloroform mixture was used to dissolve DPPA since the addition of ethanol increased the DPPA solubility.

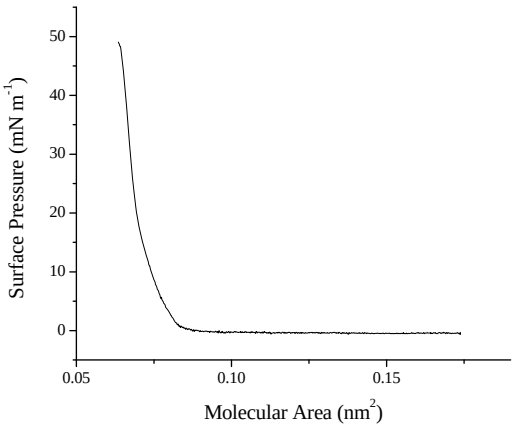

(a)

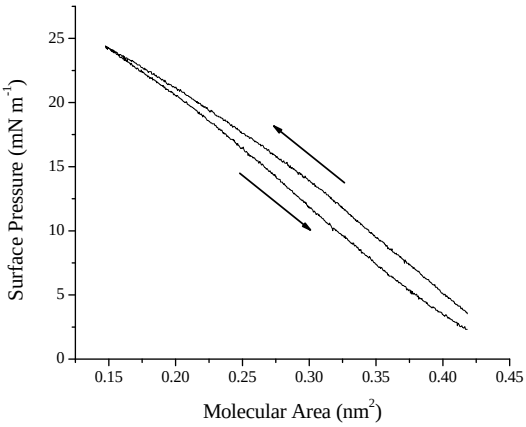

(b)

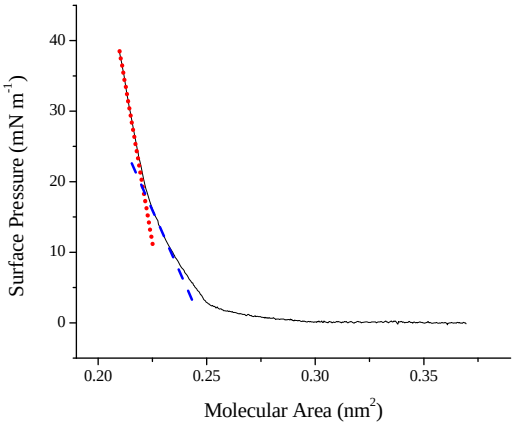

(c)

Figure 4.6 Isotherms of DPPA at 293 K, pH 5.5 : (a) Using pure chloroform as a solvent (conc. = 0.5 mg ml^{-1}). (b) Using an ethanol : hexane mixture (1 : 4) as a solvent (conc. = 0.83 mg ml^{-1}). (c) Using an ethanol : chloroform mixture (1 : 9) as a solvent (conc. = 0.91 mg ml^{-1}).

In Figure 4.6c, the slope of the isotherm is -504.5 pN nm^{-3} (in the expanded phase) when the surface pressure is between 2 mN m^{-1} and 18 mN m^{-1}. On the other hand, the slope becomes -1585.8 pN nm^{-3} (in the condensed phase) when the pressure is more than 22 mN m^{-1}. Therefore, the interception point between the slopes is approximately 20 mN m^{-1}. Minones reported that the surface pressure at which the monolayer of DPPA (spread on water at pH 6 and 293 K) changed from the expanded phase to the condensed phase was approximately 24 mN m^{-1} [20]. The difference between these values may be the result from the differences in the temperature and the pH of the subphase. Based on the result in Figure 4.6c, monolayers of DPPA were deposited onto substrates at surface pressure of about 22 mN m^{-1}, at a temperature of 298 K and a pH value of about 5.5.

Pure Valinomycin

Birdi [21] noted that the valinomycin isotherm on the aqueous subphase is independent of the compression speed if a valinomycin concentration on the subphase surface is low. In contrast, the behaviour depends significantly on the compression rate of the barriers when a high-concentration solution of valinomycin is spread on a subphase. In this study, when spreading valinomycin solution on a subphase, the valinomycin concentration was initially low. By compressing the trough barriers, the valinomycin concentration increased while the molecular area reduced gradually. Nature (or phase) of the floating film will therefore depend on the compression. Hence, the compression speed is likely to have an influence on the LB deposition. Birdi [21]reported that the compression speed will become a key factor in film deposition when the molecular area approaches 2 nm^2 (high valinomycin concentration). With a proper compression rate, the monolayer of valinomycin could therefore be deposited on a substrate.

To obtain an isotherm of pure valinomycin, 10 μl of valinomycin solution (conc. = 0.96 mg ml^{-1}; in chloroform) was spread onto the aqueous subphases, DI water and KCl solution. The floating film was then left for about 10 minutes to evaporate the solvent. In this study, the floating layer of valinomycin was compressed at two speeds, 0.1 and 0.8 mm s^{-1}. Figure 4.7 shows the isotherms obtained from the two different speeds.

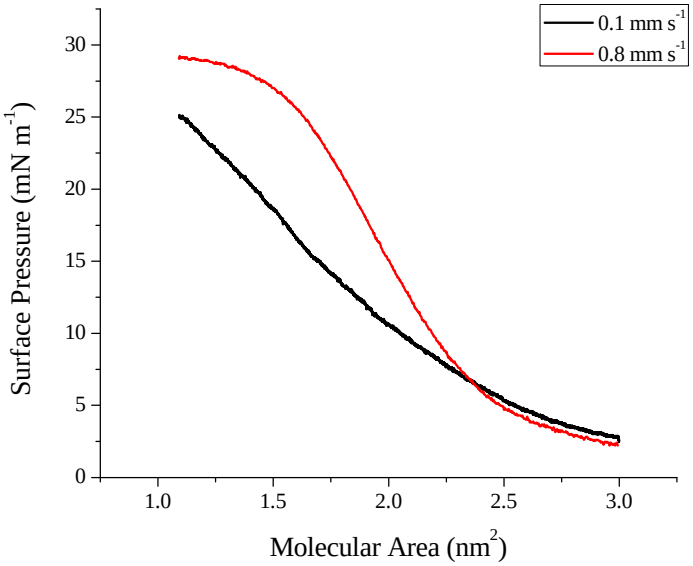

Figure 4.7 Isotherms of valinomycin at 293 K, pH 5.5, with compression speeds of 0.1 mm s^{-1} (black) and 0.8 mm s^{-1} (red).

In case of the 0.1 mm s^{-1} compression speed (black line), the phase change is unclear. This leads to a problem in defining the onset of the condensed phase of valinomycin. In addition, the result suggests that the floating layer may probably not enter the condensed phase at the slow speed. Instead, the molecules may pile up and form a multimolecular layer of valinomycin [22]. In contrast, a constant-pressure plateau region, at about 30 mN m^{-1}, is evident for the isotherm (red line) when the barriers were moved at speed of 0.8 mm s^{-1}. Baoukina et al suggested that the coexistence of the liquid-expanded (LE) and the liquid-condensed (LC) phases is a relevant factor behind the presence of the constant-pressure plateau on isotherms [23]. The plateau region may therefore indicate the presence of the liquid-condensed phase.

When using the compression speed of 0.8 mm s^{-1}, the isotherm of pure valinomycin does not reveal any condensed phase, as in case of arachidic acid or cadmium arachidate, since the LB trough has an insufficient area to show the entire isotherm. Although valinomycin molecules in the plateau region do not form a close-packed structure as in the condensed phase, the floating layer in this region is more compact than that in the expanded phase. However, it is impractical to transfer a floating layer in the plateau region. In this work, the floating layer was therefore

transferred onto substrates at the surface pressure at 25 mN m^{-1} and a compression speed at 0.8 mm s^{-1}. At this pressure, valinomycin has the most compact layer before entering into the plateau region.

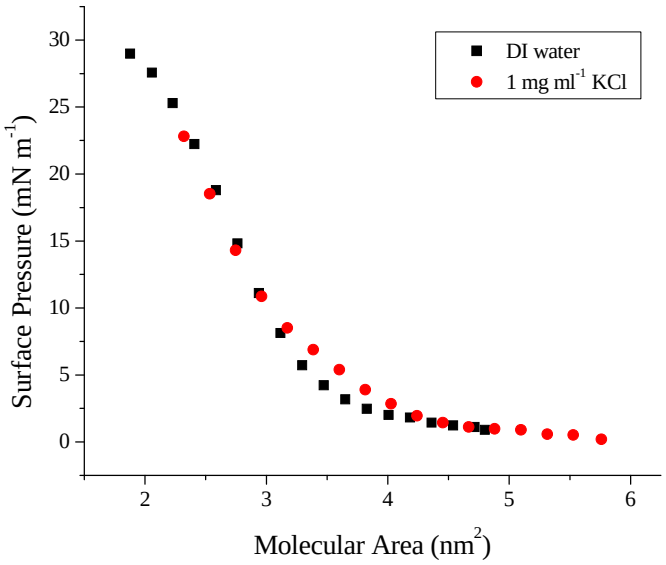

Figure 4.8 The isotherms of valinomycin at 293 K, with compression speeds of 0.8 mm s^{-1}, pH 5.5; using DI water (●) and 1 mg ml^{-1} KCl (■) as a subphase, respectively.

Because valinomycin molecules are sensitive to potassium ions in solution, an experiment using a KCl subphase was undertaken. A KCl solution concentration of 1 mg $ml^{-1}$was used as a subphase. As shown in Figure 4.8, the effect of potassium ions in the subphase on an isotherm of valinomycin is not obvious at this low concentration. Caspers et al [9], as well as Kemp and Wenner [11], reported similar results showing that the influence of the potassium ions in the subphase was not apparent for concentrations below about 7 mg ml^{-1} (<1 M); however, the condensed phase showed two distinct sections when the concentration was higher than 1 M. In Figure 4.8, the molecular area is approximately 3.60 nm^2, similar to that reported by Kemp and Wenner [11], when using DI water as a subphase. In case of using 1 mg ml^{-1} KCl as a subphase, the molecular area is approximately 3.50 nm^2, which is similar to the result reported by Ries and Swift [24]. When a molecule of valinomycin interacts with K^+ and forms a valinomycin-K^+ complex, its size is slightly reduced compared to uncomplexed valinomycin. This may be a reason why

the molecular area in case of 1 mg ml^{-1} KCl is slightly smaller than that in case of DI water. Overall, these experiment suggests that K^+ ions in the subphase do not have a significant effect on forming a monolayer of valinomycin on a subphase. However, to avoid any influence of residual K^+ in the measurement, the deposition of valinomycin monolayer was undertaken on DI water.

Arachidic Acid/Valinomycin Mixtures

In section 3.2.3, valinomycin was shown to form a floating layer on an aqueous subphase; however, the isotherm of valinomycin suggests that the valinomycin monolayer is not stabilised fully on the subphase due to the flexibility of valinomycin molecules. Pathirana and Neely [6] have suggested that interactions between molecules of valinomycin and fatty acid in a monolayer could help the valinomycin molecules to form a valinomycin-K^+ complex when in contact with a potassium-containing solution. Thus, this subsection concerns isotherms of the mixtures of valinomycin and AA.

The valinomycin and the arachidic acid solutions were prepared separately at a concentration of 1 mg ml^{-1}. Then, a mixed solution with 1 %w/w of valinomycin was made by adding 10 μl of the valinomycin solution into 990 μl of the arachidic acid solution. The solution with 5 %w/w of valinomycin was made by adding 50 μl of the valinomycin solution into 950 μl of the arachidic acid solution.

In these experiments, the mixed solution of about 20 μl was spread over the subphase surface. Isotherms of the solutions with 1% and 5% of valinomycin by weight were measured on subphases of both DI water and KCl solutions. Since a valinomycin molecule has a different molecular weight from that of an AA molecule, an interpolated molecular weight (MW_i) is required for calibrating an isotherm. By using a linear interpolation, a MW_i is calculated from Equation 4.2.

$$MW_i = \sum_k \frac{a_k \times (MW_k)}{100} \qquad (4.2)$$

where a_k is a concentration (% w/w) of molecule k in the mixture and MW_k is a molecular weight of molecule k.

In these experiments, the interpolated MW could be calculated as shown in Table 4.1.

Table 4.1 The interpolated molecular weight of a mixture between valinomycin and AA

% w/w Valinomycin	% w/w AA	Interpolated Molecular Weight
1	99	320.5
5	95	352.4

By using the average molecular weight of the mixture, the isotherms of the AA/val mixtures on a DI water subphase are plotted and shown in Figure 4.9a. Both isotherms of the AA/val mixtures on an aqueous subphase are similar to that of pure AA. This may be due to the low content of valinomycin in the floating layer. However, the isotherms of the 1% and 5% w/w valinomycin mixtures have characteristics inherited from valinomycin molecules when the surface pressure is below 30 mN m^{-1}. Since valinomycin has a molecular weight of approximately 1111, three times greater than that of arachidic acid, this makes the Van der Waals forces between valinomycin and AA molecules much greater than the forces between molecules of arachidic acid. Therefore, valinomycin molecules dominate the characteristics in the expanded phase of the isotherm.

When the surface pressure is above 30 mN m^{-1}, the isotherms show that both 1% and 5% mixtures are in the condensed phase region, a characteristic inherited from arachidic acid. This may be because only arachidic acid, not valinomycin, can form a close-packed structure when using this LB system with the small trough area. Both isotherms of the mixtures, however, have small differences from that of pure arachidic acid, perhaps due to experimental errors. In this work, the floating monolayers with 1 % and 5 % w/w valinomycin were transferred onto a substrate at a surface pressure slightly less than 30 mN m^{-1}.

Figure 4.9b shows the isotherms of the 1% and 5% AA/val mixtures when using a 1 mg ml^{-1} KCl subphase. With the KCl subphase, the isotherms in the expanded phase are different from those on the DI water (Figure 4.9a). Small 'bumps' occur at a surface pressure of approximately 8 mN m^{-1}.

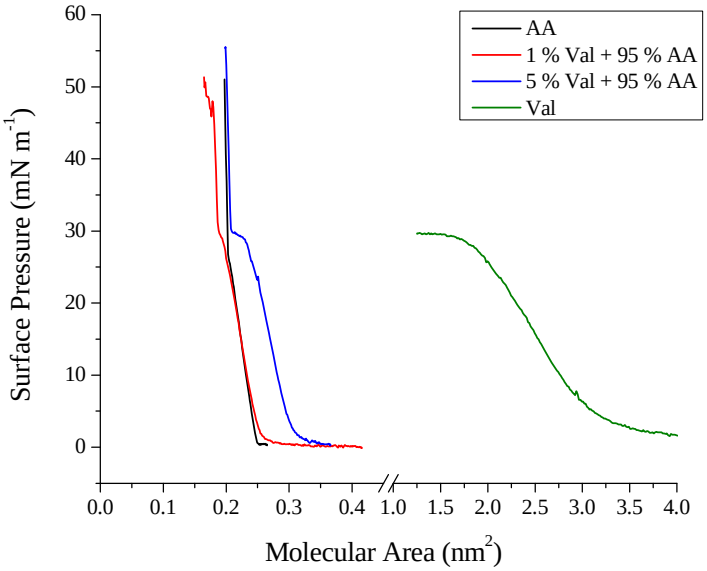

(a)

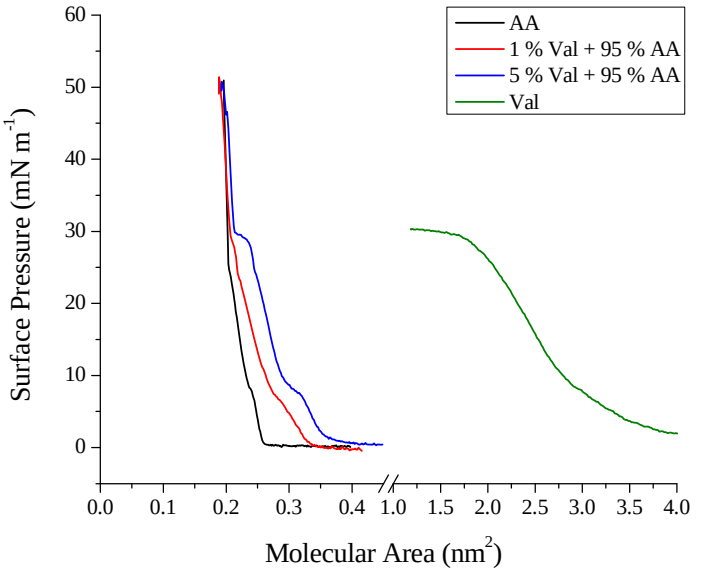

(b)

Figure 4.9 Isotherms of mixtures of 1% and 5% valinomycin in AA compared to those of pure AA and pure valinomycin at 293 K, with compression speeds of about 0.1 mm s^{-1}, pH 5.5, (a) DI water subphase. (b) 1 mg ml^{-1} KCl solution subphase.

By using a 0.75 mg ml^{-1} KCl solution as a subphase, Goddard et al reported that similar bumps for pure AA were evident at approximately 12 mN m^{-1} when the pH of a subphase was above 12 [17]. Additionally, Goddard et al also showed that the pH of a KCl solution subphase has a significant influence on the size of these bumps [17]. Since an AA floating layer does not ionise completely on a weak basic solution, the size of these bumps becomes smaller when decreasing pH of a KCl solution subphase below 12. The experimental results in this study therefore suggest that the presence of small bumps is due to the interaction of K^+ ions and the arachidic acid molecules.

Although there is no evidence of the influence of K^+ on the valinomycin isotherm in this study, the presence of valinomycin in the floating layer seems to have an effect on the isotherm of the AA/val mixtures on the KCl subphase. When increasing the amount of valinomycin in the mixture, the bump becomes larger. This may indicate that the valinomycin molecules can assist the dissociation of arachidic acid on the KCl subphase. Each valinomycin molecule is comprised of six amines, as shown in Figure 4.3. Generally, amines are bases although they are significantly weaker than alkali metal hydroxides. The pH around the valinomycin molecules is therefore increased. The surroundings of the arachidic acid become more basic when increasing the amount of valinomycin. This increase of the local pH may influence the bump on the arachidic acid isotherm and hence, result in the increase in size of the bump.

In Figure 4.9b, the effect of the potassium ions disappears from the isotherms of the arachidic acid/valinomycin mixture, when the surface pressure increases above 30 mN m^{-1}. Therefore, the isotherms of the mixtures on the KCl subphase converge to that of pure arachidic acid. This shows that the valinomycin molecules did not form any K^+-valinomycin complex on the 1 mg ml^{-1} KCl subphase. Kemp and Wenner [11] showed that pure valinomycin monolayers can, however, form complexes on highly concentrated (3M or > 200 mg ml^{-1}) KCl solutions. Although the molecular area of valinomycin is significantly larger than that of arachidic acid, there is no apparent effect on the isotherms of the AA/val mixtures. Similar to the case of pure arachidic acid, the molecular areas of both mixtures are about 0.20 nm^2. There are two possible explanations. First, valinomycin molecules may still be embedded in the floating layer; however, their shape is changed significantly in the condensed phase, and/or their alignment is altered from a horizontal alignment to a

vertical alignment. Second, some valinomycin molecules may be expelled from the floating layer and pile up on top of the arachidic acid monolayer.

The isotherms of the mixture in Figure 4.9b show that a floating layer on the KCl solution may be more condensed than that on the DI water in Figure 4.9a. This suggests that KCl solutions are probably suitable for transferring the monolayers of the AA/val mixtures onto substrates. However, the main goal of this work is to fabricate an organic-based device for detecting K^+ ions. To avoid effects from residual K^+ ions in the subphase, DI water was used as the subphase in this work.

4.3 LB Film Deposition

Even though one of the primary objectives of this research is to deposit an active LB layer onto an ISFET, a p-Si wafer with a hydrophobic surface was used as a basic substrate in pilot experiments. Therefore, this section will focus on transferring a floating layer on a subphase to a Si substrate using the LB technique. To deposit high-quality LB films, it is necessary to control three main parameters: drying time; dipping speed; and dipping pressure. As noted above, a suitable pressure to deposit the LB film is within the condensed phase because the floating film has a dense structure in this phase.

In the case of a hydrophobic surface, a monomolecular layer is transferred from the subphase surface in the first downwards movement. The next layer is coated onto the substrate when it is moved upwards. A dip, defined as a downward and upward movement of the substrate, causes the substrate be coated with two layers of a floating monolayer. Normally, the front and back surfaces of the substrate are in contact with the monomolecular layer during dipping into the subphase. As a result, the dipping area of substrate is four times the area of the dipping surface of the substrate.

After applying the solution to the subphase, the chloroform solvent was left to evaporate completely from the water surface (approximately 10 minutes). The barriers were then controlled to maintain a constant surface pressure. Before dipping the Si substrate into the subphase, the compressed monolayers of AA, CdAA and valinomycin on the subphase were left approximately 10 minutes to stabilise the film at the control pressure. However, the DPPA monolayer was left on the subphase for

at least 2 hours before film deposition as suggested by Lukes et al [4]. In all depositions, the temperature was 293 K and the pH was 5.0.

Arachidic acid

The surface pressure for depositing arachidic film should be greater than 25 mN m^{-1} to ensure that the deposition occurs in the condensed phase. Therefore, the surface pressure in these deposition experiments was set at 32 mN m^{-1}.

To transfer a monolayer of AA onto silicon, it was dipped 10 mm into the subphase. Figure 4.10 shows that every dip of the Si wafer into the subphase causes a steady decrease in the monolayer area. The ten short steps in this graph indicate that there are ten successive dips into the subphase. The reduction in area is about 4.7 cm^2 per dip. Since the Si wafer is 1 cm wide, the dipping area of Si wafer is approximately 1 cm^2. This suggests that the LB film of AA is deposited on both sides of the Si wafer and it is coated during both the downward and upward movements.

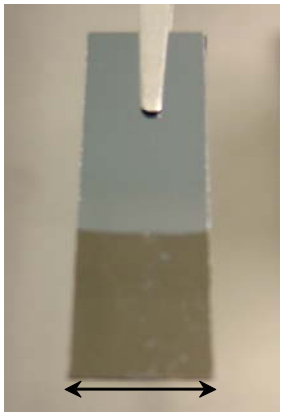

(a)

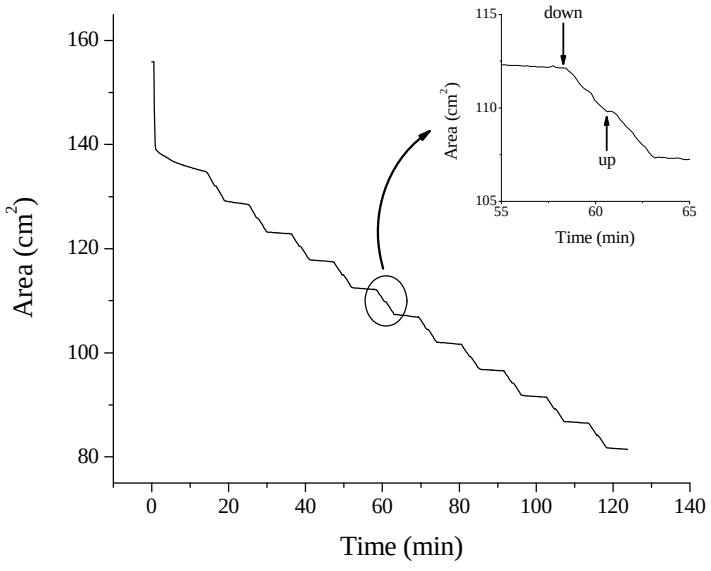

(b)

Figure 4.10 (a) Arachidic acid film on a Si wafer. (b) Dipping profile for depositing arachidic acid film onto a Si wafer.

The experimental result shows that the transfer ratio is 1.2, in contrast to the theoretical value of 1. This agrees with the conclusion of Claesson [18] that it is difficult to transfer compact monolayers of AA onto substrates using the LB technique. Due to the effects of ionic repulsion among hydrophilic groups, it is also difficult to keep the monolayer of AA stable at an exact surface pressure [18, 25]. However, a LB film could be transferred onto a hydrophobic surface of a substrate by using an appropriate dipping speed. In this research, the LB layers were transferred successfully onto a Si wafer at a dipping speed of about 0.08 mm s^{-1}.

Cadmium arachidate

To enhance the quality of the arachidic acid LB film, 10 mg of cadmium chloride ($CdCl_2$) was added to the subphase (DI water). Consequently, CdAA, an organic salt, formed on the water surface, as indicated by Equation 4.1. Similar to arachidic acid, the Si wafer was dipped about 10 mm into the subphase. The ten steps on the graph in Figure 4.11 are similar to the arachidic-acid dipping profile. This shows that 20 monomolecular layers of Cd arachidate are deposited onto the Si wafer.

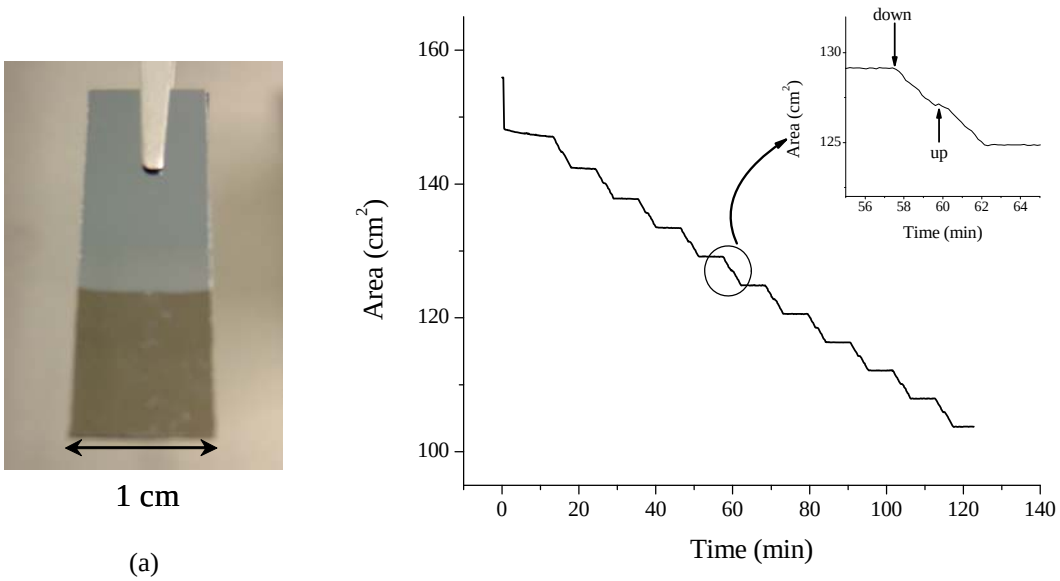

Figure 4.11 (a) Cadmium arachidate film on a Si wafer. (b) Dipping profile for depositing cadmium arachidate film onto a Si wafer

The dipping profile gives an average transfer ratio of approximately 1.00 ± 0.05. This value is much closer to the theoretical value than in the case of AA. This suggests that the arachidic acid monolayer incorporated with Cd^{2+} ions can form a compact structure when compared to pure arachidic acid without Cd^{2+} ions, as indicated by the isotherm in Figure 4.5a.

1,2-Dipalmitoyl-sn-glycero-3-phosphatidic acid

Lohner et al showed that it was quite difficult to transfer 1,2-Dipalmitoyl-sn-glycero-3-phosphatidic acid monolayers onto Si wafers using the LB technique without the addition of calcium ions in the subphase [26]. However, this research attempted to avoid effects from residual ions on an ion-sensitive device. Therefore, the floating monolayer was transferred onto a substrate by using DI water as a subphase. Howarth suggested that the monomolecular layer of DPPA needs a long stabilising time before dipping the Si wafer into the subphase [22]. In this study, the floating DPPA monolayer was controlled at a constant surface pressure for approximately two hours.

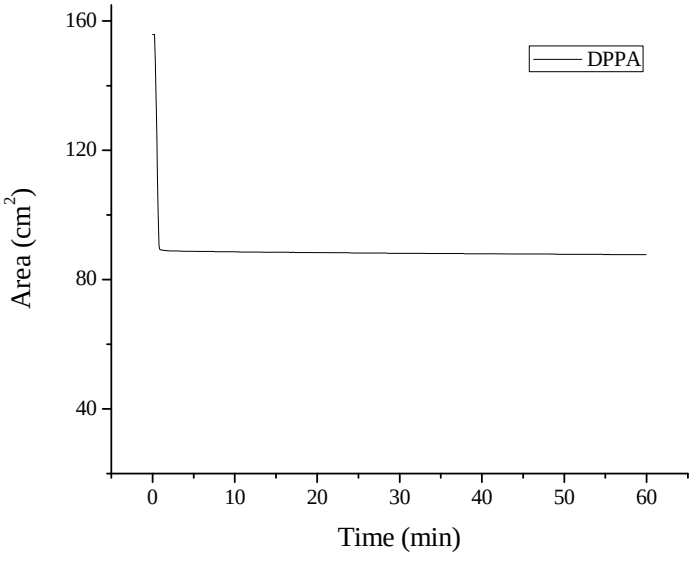

Figure 4.12 A profile of the pressure control of a DPPA monolayer at constant pressure of 25 mN m^{-1}, 297 K.

By keeping the surface pressure constant at 25 mN m^{-1}, a pressure-control profile of the DPPA floating layer is depicted in Figure 4.12. This curve shows that

a monolayer of DPPA exhibited good stability on a pure water subphase. Since DPPA is in the form of an organic salt ($C_{35}H_{68}O_8PNa$), its head group was ionised (to give the phosphate ions, PO_3^-) when spread onto subphase (DI water). Each DPPA molecule was tightly held together and formed a compact monomolecular layer on the subphase as a result of hydrogen bonding.

Figure 4.12 shows that DPPA molecules can form a stable monolayer on a subphase. However, the floating layer was not transferred successfully to the silicon substrates, as shown in Figure 4.13. The deposited layer in the previous dip peeled off during the next excursion into the subphase. Although the transfer ratio is about 0.51 for the first dip, it decreases to about 0.07 for the last dip. The average transfer ratio was about 0.35. This shows that the amount of the DPPA monolayer transferred onto the Si decreases while the dipping progresses. This suggests that the DPPA monolayer did not firmly attach to the Si wafer as this was moved through the surface of subphase. Unlike AA or CdAA molecules, both palmitoyl groups of DPPA molecules are not aligned parallel, but form an angle of about 145° [27]. Although the pamitoyl hydrocarbon chains are hydrophobic, these groups are not upright like alkane groups in AA or CdAA molecules. Therefore, the compressed monolayer of DPPA might not be able to form a tightly packed monolayer. This structure probably trapped some water molecules in the floating layer. This may be the reason why the deposited layer peeled off the surface of the Si wafer when the Si was repeatedly dipped into the subphase [18]. Additionally, in Figure 4.13a, it is evident that the deposited film has the poor optical quality.

To improve the quality of the DPPA LB film, 10 layers of AA or CdAA were first coated onto a Si wafer by dipping a 15 mm length into the subphase; then 10 layers of DPPA were deposited onto this treated Si wafer. Monolayers of DPPA could be transferred effectively onto this fatty-acid coated Si wafer as shown in Figure 4.14a and 4.14b. For deposition onto the AA layer, the transfer ratio of DPPA was 0.95 ± 0.05. In contrast, the transfer ratio was 1.00 ± 0.05 in the case of deposition onto a cadmium arachidate layer.

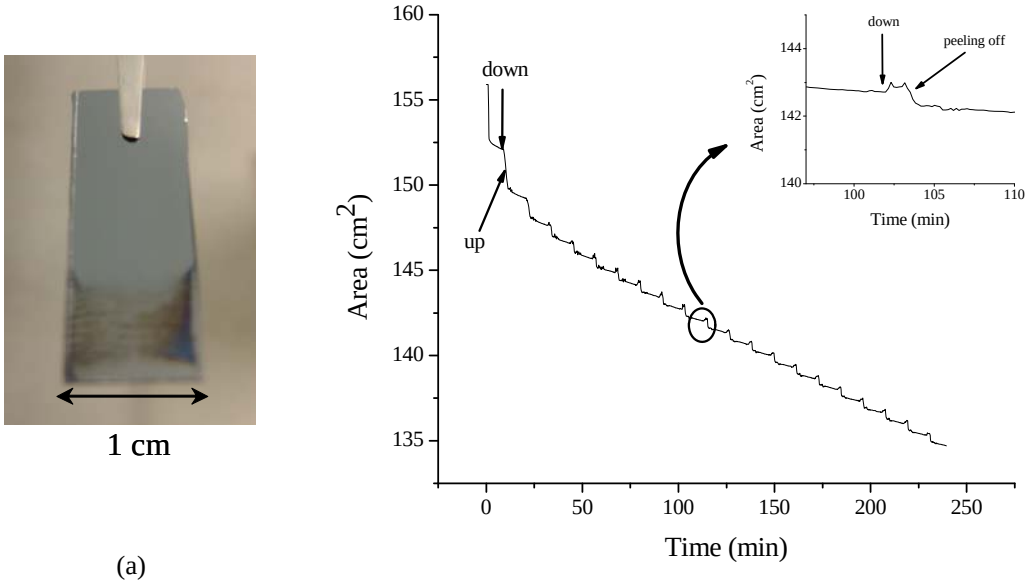

(a) (b)

Figure 4.13 (a) DPPA film on Si wafer, 20 dips. (b) Dipping profile of a DPPA film onto Si wafer.

(a) (b)

Figure 4.14 (a) DPPA film on arachidic acid/Si wafer, 5 dips of DPPA on 10 AA layers. (b) DPPA film on Cd arachidate/Si wafer, 5 dips of DPPA on 10 CdAA layers.

Pure Valinomycin

Valinomycin molecules could be formed into a floating layer at the air-water interface, as described in previous section. However, the doughnut-like shape of valinomycin molecules makes it difficult to deposit a high-quality LB valinomycin film onto a substrate. Due to weak interactions between the valinomycin molecules on the subphase, a relatively small external force on the surface of a subphase can break the fragile floating film. This is a reason why the stability of a floating valinomycin monolayer depends markedly on the surface pressure [22], although it was not very dependent on the pH and ionic concentration.

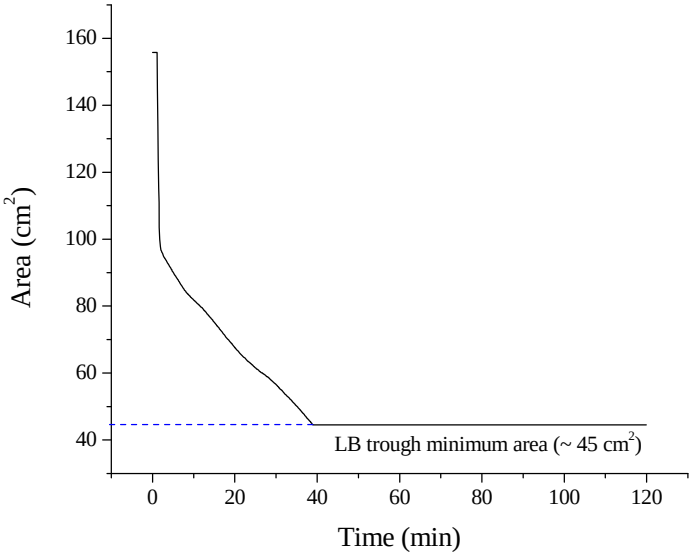

Figure 4.15 Pressure-control profiles of valinomycin; constant surface pressure of 15 mN m^{-1}

Howarth reported that the area decayed dramatically when the surface pressure was controlled at 30 mN m^{-1}; however, the area decayed only slowly when the pressure was kept below 23 mN m^{-1} [22]. Therefore, it is possible to deposit a floating monolayer of valinomycin onto a substrate at a pressure below 23 mN m^{-1} [22]. However, an attempt to repeat the results of Howarth was not successful; the area of the valinomycin monolayer still decayed, even though the pressure was held at 15 mN m^{-1}, as shown in Figure 4.15. After compression for about 40 min, the area was constant at a value of about 45 cm^2 since it reached the minimum area of the trough.

In this study, although a valinomycin monolayer could not be stabilised on an aqueous subphase, an attempt to transfer such a floating monolayer onto silicon was undertaken at a constant surface pressure (15 mN m^{-1}) without the film stabilisation on the subphase after the surface pressure reached such pressure. Figure 4.16 shows the dipping profile of valinomycin onto a Si wafer. The result shows that the area of the trough decreased continuously during the deposition until it reached the minimum area (approximately 45 cm^2). The small bumps on the curve correspond to movements of the substrate into and out of the subphase. Moreover, the slope of the curve was steeper during moving the substrate into the subphase. This reveals that some valinomycin molecules were transferred onto the silicon. When pulling the substrate upwards, the curve decreased less steeply. This indicates that some valinomycin came out of the substrate surface. Howarth et al have reported the same problem which occurred in transferring valinomycin onto both hydrophobic and hydrophilic silicon substrates [5, 22].

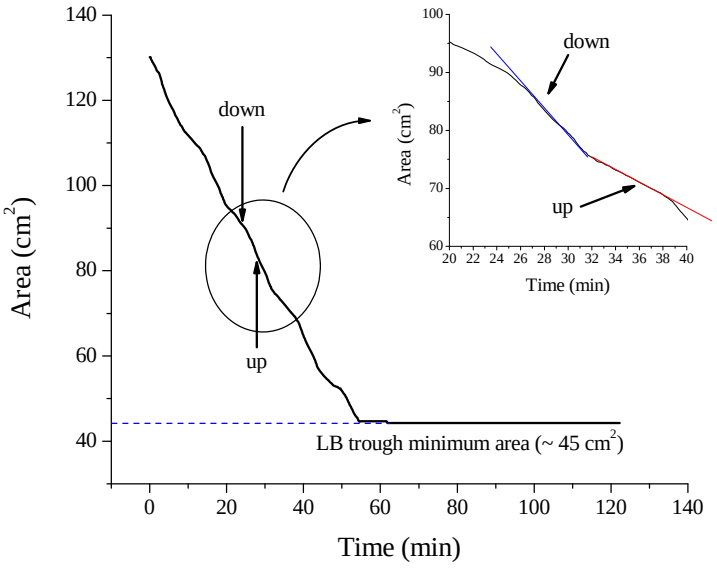

Figure 4.16 Dipping profile of a valinomycin film deposited on a Si wafer

4.4 Conclusions

The LB membranes in this study were deposited to imitate cell membranes in living cells. Therefore, arachidic acid and 1,2-dipalmitoyl-*sn*-glycero-2-phosphatidic acid were studied. Since the LB membranes were also used as ion-sensitive membranes in the following chapters, valinomycin and its mixture with AA were investigated. Their isotherms and deposition on Si wafer were studied. The results show that arachidic acid can form a compact monolayer on an aqueous subphase. However, with a small amount of $CdCl_2$ in the subphase, the molecules of cadmium arachidate form a more stable floating monolayer. In case of DPPA molecules, the isotherm shows that their floating layer has a compact architecture on DI water. In contrast, the valinomycin isotherms show that valinomycin formed a loosely packed structure.

Arachidic acid LB films were built-up successfully on Si wafers. Despite its condensed isotherm, DPPA films were of poor optical quality when they were transferred directly to the surface of the substrates. Improved film quality was achieved by coating the substrate surface with a several layers of the AA film before the DPPA deposition. It was difficult to deposit valinomycin on silicon wafers. This is because of the low stability of the valinomycin monolayer on aqueous subphase.

References

[1] B. Perret, H. J. Chap and L. Douste-Blazy. Asymmetric distribution of arachidonic acid in the plasma membrane of human platelets: A determination using purified phospholipases and a rapid method for membrane isolation. BBA-Biomembranes, 556: 434 – 446, 1979.

[2] R. Beck, S. Bertolino, S. E. Abbot, P. I. Aaronson and S. V. Smirnov. Modulation of arachidonic acid release and membrane fluidity by albumin in vascular smooth muscle and endothelial cells. Circ. Res., 83: 923 – 931, 1998.

[3] O. Shirai, Y. Yoshida and S. Kihara. Voltammetric study on ion transport across a bilayer lipid membrane in the presence of a hydrophobic ion or an ionophore. Analytical and Bioanlytical chemistry, 386(3): 494-505, 2006.

[4] P. J. Lukes, M. C. Petty and J. Yarwood. An infrared study of the incorporation of ion channel forming peptides into Langmuir-Blodgett films of phosphatidic acid. Langmuir, 8(12): 3043-3050, 1992.

[5] V. A. Howarth, M. C. Petty, G. H. Davies and J. Yarwood. The deposition and characterisation of multilayers of the ionophore valinomycin. Thin Solid Films, 160(1): 483-489, June 1988.

[6] S. Pathirana and W. C. Neely. Interaction of valinomycin and stearic acid in monolayers. Langmuir, 8(8): 1984-1987, 1992.

[7] H. R. Ries. Effect of the spreading solvent on monolayers of valinomycin. Langmuir, 6(4): 883-885, 1990.

[8] J. B. Peng, B. M. Abraham, P. Dutta, J. B. Ketterson and H. F. Gibbard. Langmuir-Blodgett deposition of a ring-shaped molecule (valinomycin). Langmuir, 3(1): 104-106, 1987.

[9] J. Caspers, M. Landuyt-Caufriez, M. Deleers and J. M. Ruysschaert. The effect of surface charge density on valinomycin-K+ complex formation in model membranes. Biochimica et Biophysica – Biomembranes, 554(1): 23-28, 1979.

[10] S. Y. Zaitsev, V. P. Vereschetin, V. P. Zubov, W. Zeiss and D. Mobius. Comparative study of the mixed monolayers of valinomycin with dioctadecyldimethylammonium bromide and dipalmitoylphosphatidylethanolamine. Colloids and Surfaces A: Physicochemical and Engineering Aspects, 121(1): 37-46, 1997.

[11] G. Kemp and C. E. Wenner. Interaction of valinomycin with cations at the air-water interface. Biochimica et Biophysica – Biomembranes, 282: 1-7, 1972.

[12] J. Gallardo, S. Alegret, R. Munoz, M. De-Roman, L. Leija, P. R. Hernandes and M. del Valle. An electronic tongue using potentiometric all-solid-state PVC-membrane sensors for the simultaneous quantification of ammonium and potassium ions in water. Analytical and Bioanalytical Chemistry, 337(2): 248-256, 2003.

[13] C. C. Wen, I. Lauks and J. N. Zemel. Valinomycin-doped photoresist layers for potassium ion sensing. Thin Solid Films, 70(2): 333-340, 1980.

[14] S. Wakida, M. Yamane, K. Hiiro, T. Kihara, Y. Ujihira and T. Sugano. Potassium Ion-Selective Field Effect Transistor with Urushi as the Membrane Matrix. Analytical Science, 4: 501-504, 1988.

[15] X. Du and Y. Liang. Improved thermal stability of Langmuir-Blodgett films through an intermolecular hydrogen bond and metal complex. Journal of Chemical Physics, 120(1): 379-383, 2004.

[16] E. Pezron, P. M. Claesson, J. M. Berg and D. Vollhardt. Stability of arachidic acid monolayers on aqueous salt solutions. Journal of Colloid and Interface Science, 138(1): 245-254, 1990.

[17] E. D. Goddard, O. Kao and H. C. Kung. Monolayer properties of fatty acids IV influence of cation at high pH. Journal of Colloid and Interface Science, 24: 297 – 309, 1967.

[18] P. M. Claesson and J. M. Berg. The stability of carboxylic acid Langmuir-Blodgett films as studied by the surface force technique. Thin Solid Films, 176: 157-164, 1989.

19] D. K. Schwartz, J. Garnaes, R. Viswanathan and J. A. N. Zasadzinski. Surface order and stability of Langmuir-Blodgett films. Science, 257: 508-511, July 1992.

[20] J. Minones, Jr., J. M. Rodriguez Patino, J. Minones, P. Dynarowicz-Latka and C. Carrera. Structural and topographical characteristics of dipalmitoyl phosphatidic acid in Langmuir monolayers. Journal of Colloid and Interface Science, 249: 388-397, 2002.

[21] K. S. Birdi. Lipid and biopolymer monolayers at liquid interfaces. Plenum press, 1989.

[22] V. A. Howarth. A study of Langmuir-Blodgett films of valinomycin. Ph.D. thesis, University of Durham, 1989.

[23] S. Baoukina, L. Monticelli, S. J. Marrink and D. P. Tieleman. Pressure-area isotherm of a lipid monolayer from molecular dynamics simulations. Langmuir, 23: 12617 – 12623, 2007.

[24] H. E. Ries and H. S. Swift. Monolayers of valinomycin and its equimolar mixture with cholesterol and with steric acid. Journal of Colloid and Interface Science, 64(1): 111 – 119, 1978.

[25] Y. Oishi, Y. Takashima, K. Suehiro and T. Kajiyama. Effect of ionic repulsion among hydrophilic groups on aggregation structure of fatty acid monolayer on the water surface. Langmuir, 13: 2527-2532, 1997.

[26] K. Lohner, O. V. Konovalov, I. I. Samoilenko, I. V. Myagkov, V. I. Troitzky and T. I. Berzina. Preparation and structural analysis of Langmuir-Blodgett films of acidic and zwitterionic phospholipids. Thin Solid Films, 288: 262-267, 1996.

[27] D. Marsh and T. Pali. Lipid conformation in crystalline bilayers and in crystals of transmembrane proteins. Chemistry and Physics of Lipids, 141: 48 – 65, 2006.

Chapter 5

Ion Sensitive Organic Field Effect Transistors

5.1 Structure and Deposition Techniques

5.1.1 ISOFET Structure

The drain current flowing through the ISOFET is dependent on the gate voltage or the accumulated charge on the gate surface. By removing the gate electrode and modifying the insulator surface to respond to target ions, a device with an open gate area is able to detect ions in solution.

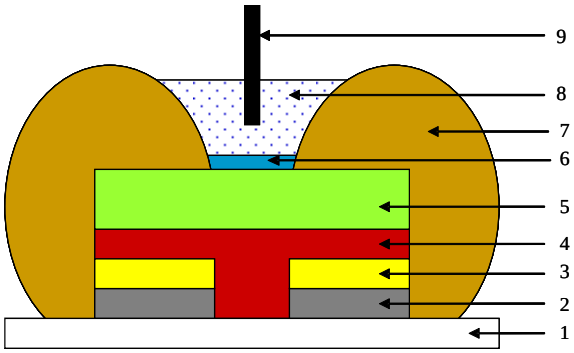

Figure 5.1 Structure of an ISOFET. 1 Hydrophobic glass. 2 Chromium. 3 Gold. 4 P3HT. 5 PMMA. 6 LB film. 7 Epoxy resin. 8 Electrolyte solution. 9 Reference (gate) electrode.

A bottom-gate structure is often used for organic FETs, but in this study a top-gate structure was necessary to provide open access to the gate dielectric. As illustrated in Figure 5.1, the substrate was a glass slide which was cleaned and rendered hydrophobic. Thermal evaporation was then used to define the source and drain electrodes. A chromium (Cr) layer was first evaporated to increase the adhesion between the gold and the hydrophobic glass [1]. A gold (Au) layer was then deposited on top of the Cr. Patterned Cr and Au layers were used as the source and drain electrodes. In this work, two configurations of electrodes were used: a standard pattern and an interdigitated pattern, as depicted in Figures 5.2a and 5.2b, respectively. The shadow mask technique was used to transfer the standard pattern on to the substrate. In contrast, photolithography was used to define the interdigitated electrodes. Full details on the photolithography are described in Section 3.2.

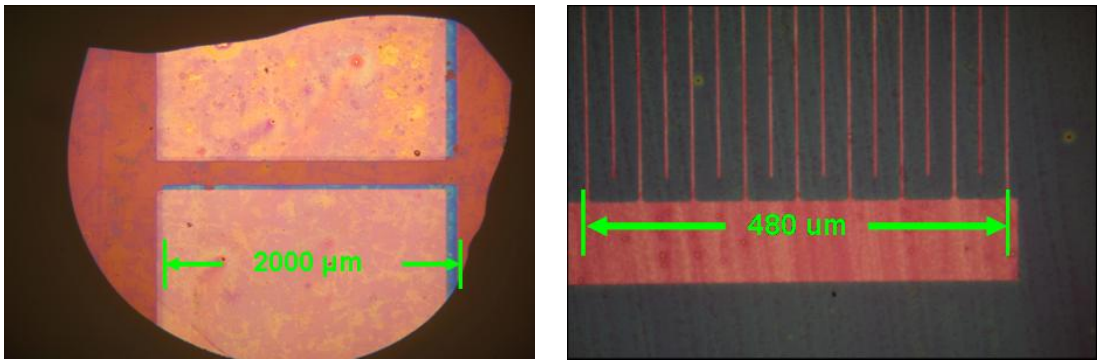

(a) (b)

Figure 5.2 Patterns of source and drain electrodes. (a) Standard pattern. (b) Interdigitated pattern.

Poly(3-hexylthiophene) (P3HT) was used as the semiconductive material. After defining the electrodes, this layer was deposited on top of the metal layer. Poly(methyl methacrylate) (PMMA) was used as the gate dielectric. Langmuir-Blodgett films were then deposited on top of this dielectric layer for some devices. Finally, the devices were encapsulated, by hand, using an epoxy resin.

As shown in Figure 5.1, the ISOFET configuration requires a reference electrode for operation. This electrode functions as the gate. Both the ISOFET and the electrode were operated in an aqueous solution, providing a connection between the reference electrode and the transistor.

5.1.2 Materials

Hybrid organic/inorganic architectures have been used as chemical sensors. For example, Bartic et al [2] reported that the polythiophene-based transistors were fabricated by using P3HT as the semiconductive layer and Ta_2O_5 as the gate layer. These hybrid P3HT/Ta_2O_5 thin-film transistors were able to detect not only charged but also uncharged molecules in an aqueous solution. By operating at low voltages, these transistor devices were stable in aqueous solutions. P3HT can easily be deposited on a substrate using a solution-process technique, such as spin coating [2].

In this work, P3HT was therefore selected as the semiconductor layer. Poly(methyl methacrylate) was used as the gate insulator because this material exhibits low leakage currents and can be used to produce devices with a high carrier

mobility and minimal hysteresis [3]. The ISOFET device should be able to detect the concentration of ions in an aqueous solution because the ions adsorbed on the surface of the dielectric layer are proportional to their concentration in the solution.

Poly(3-hexylthiophene)

Unsubstituted polythiophenes (PT) are based on a cycloalkene group, as depicted in Figure 5.3. By adding or removing the electrons from the conjugated π-orbitals, electrons can flow through the polymer chain. The sulphur (S) atom in the cycloalkene provides PT molecules with a weak hydrophobicity. Therefore, PT molecules are not soluble in normal non-polar solvents.

Poly(3-hexylthiophene) is a polymer of substituted thiophenes, as shown in Figure 5.3b. The addition of the alkyl chain increases the hydrophobicity of the polymer. P3HT can therefore dissolve in basic nonpolar solvents, such as tetrahydrofuran (THF) or chloroform [2,4,5].

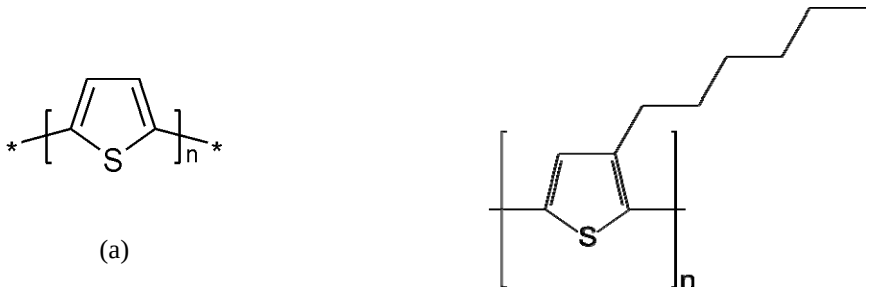

(a) (b)

Figure 5.3 Structure formulas : (a) Unsubstituted polythiophenes. (b) Poly(3-hexylthiophene).

Poly(3-hexylthiophene) (molecular weight 25,000 – 35,000, ≥ 98.0%) was purchased from Sigma-Aldrich and dissolved in chloroform in a glass vial to a concentration of 10 mg ml^{-1}. The vials were sealed by thermoplastic (Parafilm M) to protect the solution from moisture. These were also wrapped in aluminum foil to shield the solution from light and kept on a magnetic stirrer overnight before use.

Poly(methyl methacrylate)

Poly(methyl methacrylate), a transparent thermoplastic, is synthesised using a methyl methacrylate monomer. Its chemical structure is shown in Figure 5.4. PMMA is a safe alternative compared to other polymers, such as polycarbonate, because this material does not possess the toxic bisphenol-A subunit. Poly(methyl methacrylate) does not have the extreme impact strength of some engineered polymers, but its strength is higher than glass or polystyrene. Apart from its moderate physical properties, this material is a preferable choice for the gate dielectric of an organic FET because of its superior electrical properties. Furthermore, the cost of PMMA is low and it requires only simple processing (e.g. spin – coating) to form high-quality thin films.

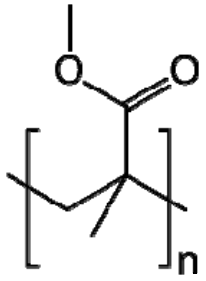

Figure 5.4 Structural formula of PMMA

The glass transition temperature of PMMA, normally varies from 85 to 165 °C. For a polymer with the molecular weight of about 10^5, the glass transition temperature is approximately 105 °C [6]. Kuo et al [7] reported that the T_g of PMMA was approximately 100 °C. However, Zulfikar et al [8] found that the T_g temperature of PMMA depended on the molecular weight (MW); for example, T_g for about 116 °C for a MW of approximately 350,000. In this study, PMMA films were hence annealed at about 135 °C. By annealing PMMA above the glass transition temperature, the rubbery viscous amorphous material can be changed to a brittle glassy amorphous polymer.

Poly(methyl methacrylate) (molecular weight 93,000) was purchased from Sigma-Aldrich. It was dissolved in anisole (methoxybenzene) to a concentration of 42 mg ml^{-1}. The resulting solutions were sealed using Parafilm M and kept on a magnetic stirrer overnight before use.

5.1.3 Device Fabrication

Metal Deposition

In this research, thermal vapour deposition was used to deposit a metal film onto the substrates. Further background details are described in Section 3.1. A hydrophobic slide glass was used as a substrate. Before vacuum evaporation, the substrate was heated on a hot plate to remove any moisture adsorbed on its surface. The vacuum system was evacuated until the pressure was below $< 10^{-5}$ mbar. By thermally evaporating Cr (≈ 20 nm) and then Au (≈ 20 nm) through a shadow mask (Figure 3.3), a standard pattern of the source and drain electrodes was transferred onto the substrate: the channel width, W, and length, L, were 2,000 μm and 50 μm, respectively.

To transfer the interdigitated pattern onto the substrate, Cr and Au were evaporated on the surface of the substrate directly without any mask and subsequently patterned using photolithography. The positive-type photoresist was used to pattern the source and drain electrodes. The full details of the photolithography process are provided in Section 3.2. After removing the excess metal layer, the substrate was patterned with the interdigitated electrodes; the channel width, W, and length, L, were 22,000 μm and 25 μm, respectively.

Spin Coating

The background to spin coating is given in Section 3.3. Before spin coating, the metallised substrates were baked on a hot plate at 120 ºC for 10 min. The P3HT (thickness about 55 nm) was deposited at a spin speed of 5000 rpm for 45 s. To avoid the oxidation of P3HT during annealing, the samples were baked at a low temperature (25 ºC) in a vacuum oven for 10 min to remove any residual solvent.

Following this, spin coating was used to deposit two separate layers of PMMA. This technique was used to avoid any pin-holes in the gate dielectric. Each layer of PMMA was coated on the substrate using a two-step process: spinning at 500 rpm for 10 s followed by 3000 rpm for 50 s. To minimise the effect of pin-holes, the first PMMA layer was heated above its glass transition temperature (T_g) to provide an increase in density. After coating the first layer of PMMA, the sample

was thus kept in the vacuum oven at 135 ºC for 60 min. Subsequently, the second layer of PMMA was coated using the same two-step process and the resulting structure was baked in the vacuum oven at 135 ºC for 120 min. The samples were left to cool in vacuum oven overnight. The overall thickness of both PMMA layers was approximately 130 nm.

Encapsulation

An Araldite epoxy resin (molecular weight < 700) was used to encapsulate the final device by hand. The ratio of the resin to the hardener was 1 : 1. After mixing for 45 s, the resin was ready for encapsulation. The devices were sealed by opening an active area (approximately 3 mm x 4 mm) to allow the electrolyte solution to come into direct contact with only the gate insulator. The encapsulated devices were left in air to set the resin for an hour before the second encapsulation. This double encapsulation was used to avoid any unwanted electrochemical reactions at the electrodes due to pinholes formed during the hardening of the resin.

.

5.2 Electrical Characteristics

Carbon dioxide can dissolve in DI water and have a significant influence on its pH. Therefore, the pH of the solution (DI water) was monitored using a Philips PW9420 pH meter. The pH was measured before and after the measurements. If the pHs differed by more than 0.5, the experiments were repeated until the pH values were approximately constant (pH difference < 0.5). In this way, the H^+ ion concentration in the solution could be assumed to be constant. The electrical characteristics of the ISOFET were recorded using an HP 4140B picoammeter/voltage source.

Before the electrical measurements, both the gate electrode and the pH electrode were rinsed using DI water. All the measurements were undertaken at room temperature and with the devices in the dark.

5.2.1 Gate Electrodes

Gold wires and standard silver/silver chloride (Ag/AgCl) reference electrodes were used to probe the built-in potential in the solution. As shown in Figure 5.5, the potential obtained from gold wires decreased significantly after measuring for a few minutes (because of their polarised characteristics). Although Ag/AgCl reference electrodes are nonpolarised, the potential from the single junction Ag/AgCl reference electrodes decreased slightly during monitoring the potential in DI water. During the measurement of the potential in the dilute solution, some ions leak from the electrodes and contaminate the measuring solution. As a consequence, a small change is evident while measuring the potential. However, by using double junction Ag/AgCl reference electrodes, a stable response was obtained while measuring the potential in DI water, as shown in Figure 5.5. Thus, a double junction Ag/AgCl reference electrode was used in this work.

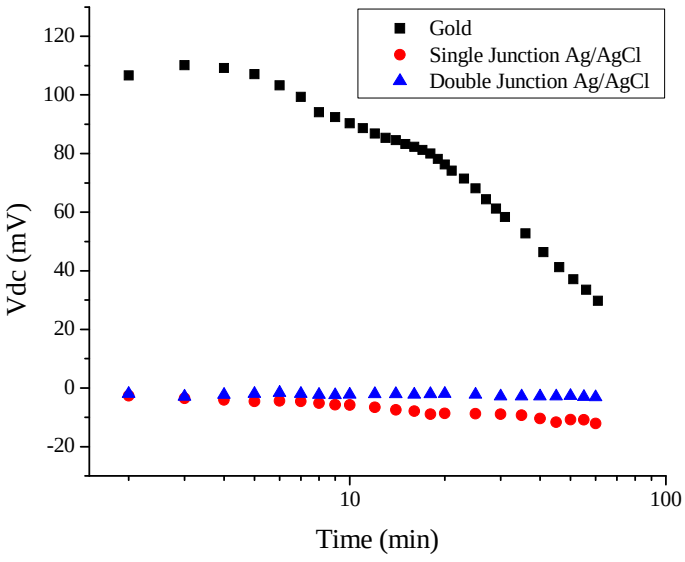

Figure 5.5 Potentials across the different gate electrodes, gold wires, single junction Ag/AgCl and double junction Ag/AgCl, in DI water.

5.2.2 Reference FET Characteristics

To characterise the standard (non-interdigitated) reference FET, an aluminum (Al) gate electrode was evaporated on top of the dielectric layer after fabricating the ISOFET on the hydrophobic glass substrate. The output and transfer characteristics of the devices with standard source-drain electrodes were tested in air in the measurement chamber (in the dark) using an HP 4140B picoammeter/voltage source. The results are shown in Figure 5.6a and 5.6b. The transistor is turned off when applying V_{gs} with a magnitude below 10 V; the leakage current was less than 15 nA. As shown in the Figure 5.6a, the drain current (I_d) reaches the saturation region if the magnitude of the V_{gs} is greater than 20 V and the magnitude of V_{ds} is above 15 V.

The transfer characteristics in Figure 5.6b reveal some hysteresis. This suggests that charge could not move freely through the P3HT layer but was trapped in localised states. By extrapolating the result reported by Huang et al [9], the dielectric constant (ε_r) of PMMA with 150 nm thickness is approximately 2.5 at 1 MHz. By determining the threshold voltage using graph $(I_d)^{1/2}$ versus V_{gs}, the electron mobility was calculated by using Equation 2.7; a value of V_T of approximately 10 V and a field-effect mobility of about 4.5 x 10^{-3} cm^2 V^{-1} s^{-1} were obtained.

5.2.3 I–V Characteristics of the Standard ISOFETs in DI Water

Transfer Characteristics

The ISOFETs with the standard (non-interdigitated) pattern of source and drain electrodes were characterised in DI water using the HP 4140B picoammeter/voltage source. To monitor the ISOFET behaviour in solution, an Ag/AgCl reference electrode was used as the gate electrode, instead of the Al gate electrode as in the previous section. The drain current was monitored by scanning V_{gs} over the range 1 V $\rightarrow$ -1 V $\rightarrow$ 1 V and applying V_{ds} of 0 V.

The transfer graphs for different V_{ds} values are shown in Figure 5.7. By applying constant V_{ds} = 0 V, the transfer curve in Figure 5.7a reveals that the transistor was in the cut-off mode. This small drain current shows the level of the leakage current from the gate to the drain electrode.

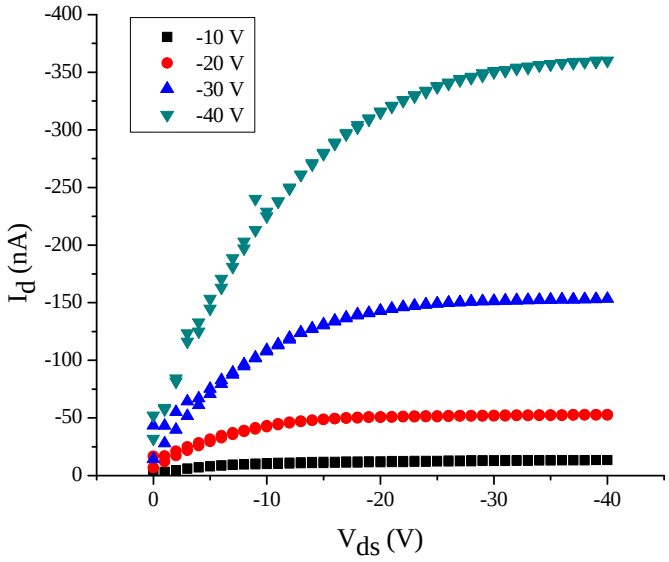

(a)

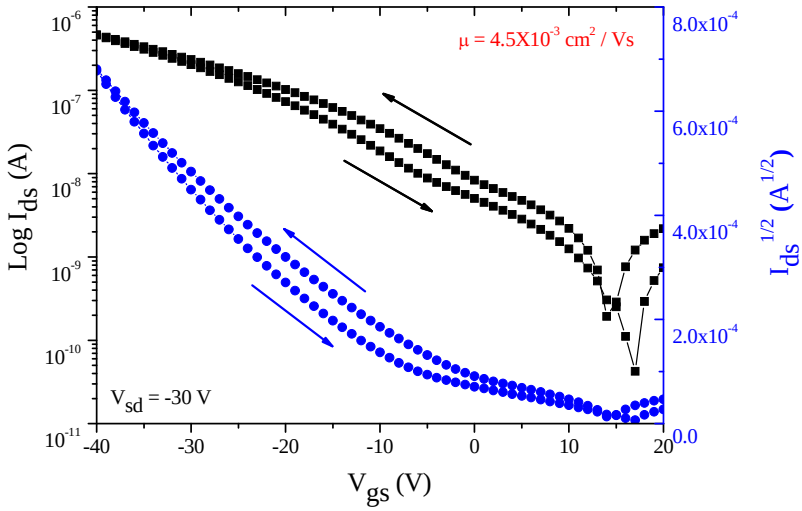

(b)

Figure 5.6 Output and transfer characteristics of the reference FET with an standard pattern of source and drain electrodes and an aluminum layer as the gate electrode. This device was measured in air within the chamber (without light). (a) Output characteristics. (b) Transfer characteristics.

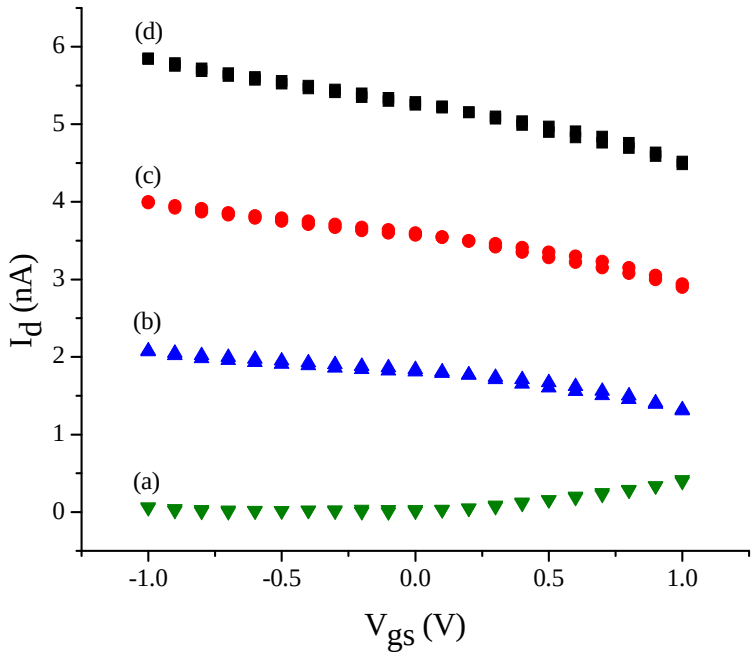

Figure 5.7 Transfer characteristics of the standard ISOFET (Cr/Au/P3HT/650 nm PMMA), varying V_{gs} between -1.0 and 1.0 V, W/L ratio = 40; using (a) V_{ds} 0. (b) V_{ds} -0.5. (c) V_{ds} -1.0. (d) V_{ds} -1.5 V.

Table 5.1 Transconductance values of the ISOFET coated with 650 nm PMMA

V_{ds} (V)	V_{gs} (V)	PMMA Thickenss (nm)	W/L ratio	g_m (nA V^{-1})
0	± 1.0	650	40	cut-off
-0.5	± 1.0	650	40	-0.25
-1.0	± 1.0	650	40	-0.41
-1.5	± 1.0	650	40	-0.57

The transconductance (g_m) of the device was obtained by equating the slopes of the transfer curves in Figure 5.7b, 5.7c and 5.7d. Table 5.1 shows the g_m values of the ISOFET with different V_{ds}. It is evident that the transconductance of the ISOFET increases when the magnitude of V_{ds} increases. The dependence of g_m on V_{ds} reveals that the transistor was operating in the accumulation regime [6]. By fixing V_{ds} below 0 V, the drain current of the device increased when increasing V_{gs}. The results show that the drain current of the ISOFETs depended on both V_{gs} and V_{ds}. It is evident that this device required a high voltage (V_{gs} > 1.0 V) to induce a field effect. Although the transconductance of the ISOFETs could be increased by increasing V_{ds}, the magnitude of V_{ds} was limited to avoid unwanted electrochemical reactions, both on the surface of the dielectric layer and at the dielectric/semiconductor interface. Therefore, the transconductance of the device with the 650 nm PMMA was low. This resulted in a low sensitivity to a change of V_{gs}. Since the change of ion concentration in the solution has a direct influence on V_{gs}, 650 nm of PMMA was not the best thickness for providing a high-sensitive device.

To improve the sensitivity of the devices requires a thinner dielectric layer and also higher applied voltages. As noted above, it is, however, necessary to keep the voltages below 1 V. Hence, the thickness of PMMA was reduced to 150 nm. The span of V_{gs} was kept below 1 V and V_{ds} was varied between 0 and -0.6 V. The transfer characteristics of the ISOFET with 150 nm PMMA are shown in Figure 5.8.

Compared to the data shown in Figure 5.7, the transfer graphs in Figure 5.8 show an improved field-effect response. Table 5.2 reveals that the devices with the thinner PMMA layer have the higher transconductance. The device has higher sensitivity to a change of V_{gs} because the thinner dielectric layer (PMMA) can produce a greater electric field at the dielectric/semiconductor interface. However, the leakage current was about the same order of magnitude compared to the transfer characteristics in Figure 5.7. This is because the devices with the 150 nm PMMA were operated at lower V_{gs} and V_{ds}. The semilogarithmic graphs in Figure 5.9 correspond to the data in Figures 5.8b, 5.8c and 5.8d. The curve for V_{ds} = -0.2 V shows the widest dynamic range of the drain current (two orders of magnitude).

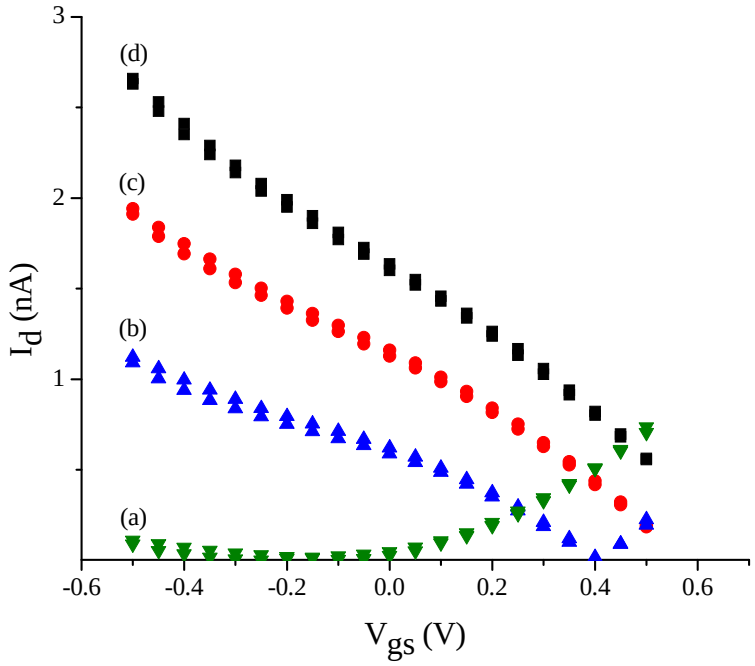

Figure 5.8 Transfer characteristics of the standard ISOFET (Cr/Au/P3HT/150 nm PMMA), varying V_{gs} between -0.5 and 0.5 V, W/L ratio = 40; using (a) V_{ds} 0. (b) V_{ds} -0.2. (c) V_{ds} -0.4. (d) V_{ds} -0.6 V.

Table 5.2 Transconductance values of the ISOFET coated with 150 nm PMMA

V_{ds} (V)	V_{gs} (V)	PMMA Thickenss (nm)	W/L ratio	g_m (nA V^{-1})
0	± 0.5	150	40	cut-off
-0.2	± 0.5	150	40	-0.98
-0.4	± 0.5	150	40	-1.55
-0.6	± 0.5	150	40	-2.05

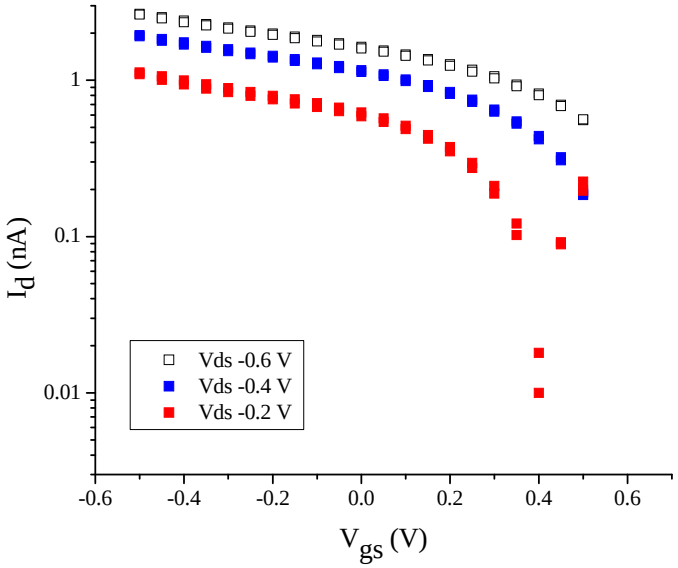

Figure 5.9 Semilogarithmic transfer graphs corresponding to the data in Figure 5.8b, 5.8c and 5.8d.

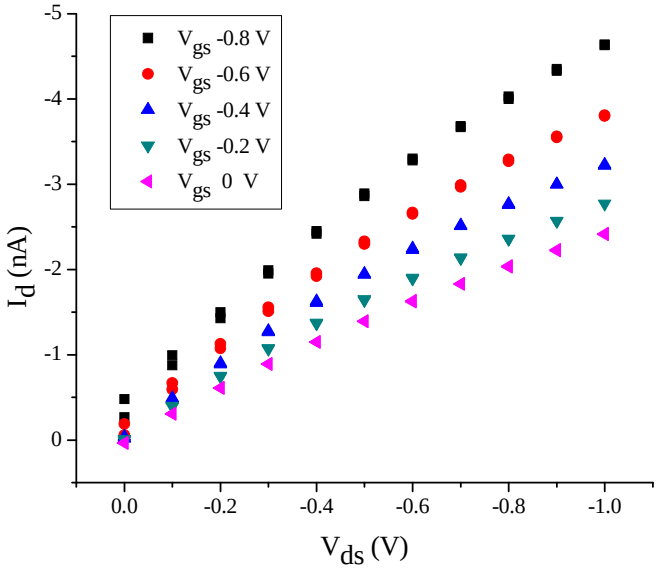

Figure 5.10 Output characteristics of the ISOFET with standard source-drain electrodes; scanning V_{ds} 0 V → -1 V → 0 V; V_{gs} = 0, -0.2, -0.4, -0.6, -0.8 V; W/L ratio = 40.

Output Characteristics

To obtain the output curves of the devices, V_{gs} was fixed while scanning V_{ds} 0 V $\rightarrow$ -1 V $\rightarrow$ 0 V. The output characteristics of the ISOFET, in DI water and using a Ag/AgCl reference electrode, are shown in Figure 5.10. A clear field effect is evident, although the magnitudes of the drain currents are low – in the nA range.

Figure 5.11 shows the typical hysteresis which occurred during scanning V_{ds} 0 V $\rightarrow$ -1 V $\rightarrow$ 0 V and fixing V_{gs} at -0.8 V. By defining I_a and I_b as shown in Figure 5.9, ΔI_d is the difference between the drain currents at V_{ds} 0 V. This value can be used to represent the width of the hysteresis of the drain current.

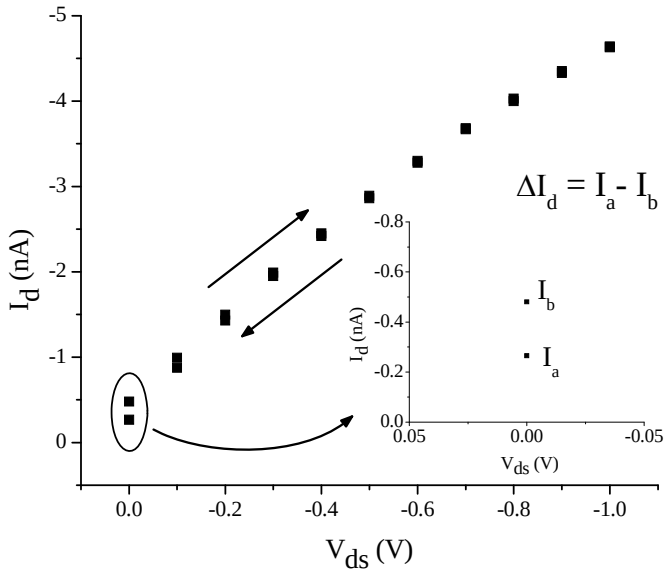

Figure 5.11 Output characteristics of the ISOFET with standard source-drain electrodes; scanning V_{ds} 0 V $\rightarrow$ -1 V $\rightarrow$ 0 V; V_{gs} = -0.8 V, in DI water.

Figure 5.12 shows the relation between ΔI_d and V_{gs} for V_{ds} = 0 V. It is evident that ΔI_d increases when the magnitude of V_{gs} increases. However, the increase in ΔI_d is not uniform, and can be divided into two regions. In the first region (solid line, $|V_{gs}| < 0.4$ V), the rise of V_{gs} leads to a slow increase in ΔI_d. In the second region (dashed line, $|V_{gs}| > 0.4$ V), the increase in V_{gs} gives rise to a rapid increase in ΔI_d. The slope in the second region is five times greater than that in the first region.

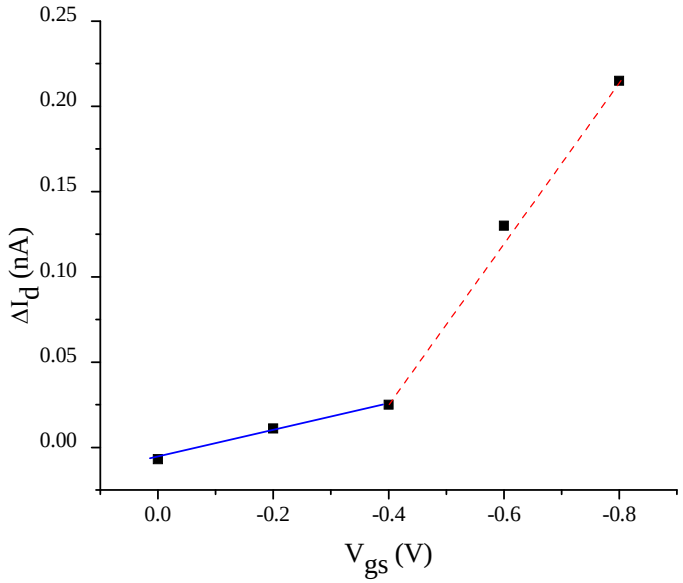

Figure 5.12 ΔI_d versus V_{gs}, V_{ds} = 0 V, the standard ISOFET, in DI water.

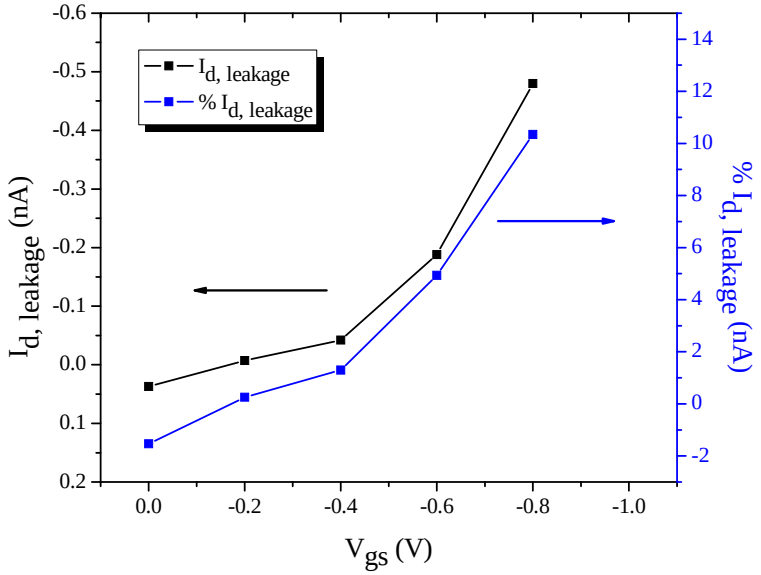

Figure 5.13 Leakage current, $I_{d,\ leakage}$, versus V_{gs}, V_{ds} = 0 V, the standard ISOFET, in DI water.

When using V_{ds} = 0 V, the drain current reflects the leakage current ($I_{d,\ leakage}$) from the gate to the drain electrode. By using the drain current at V_{ds} = -1 V as a reference value, the percentage of $I_{d,\ leakage}$ was then calculated. As shown in Figure 5.13, the leakage current is dependent on the gate voltage (V_{gs}). This curve has a similar shape to that shown in Figure 5.12, and can be divided into two regions ($|V_{gs}|$ < 0.4 V and $|V_{gs}|$ > 0.4 V). When $|V_{gs}|$ was set below 0.4 V, the leakage current is less than 0.1 nA or 2% of the maximum drain current ($I_{d,\ Vds\text{-}1V}$).

5.2.4 I–V Characteristics of Interdigitated ISOFETs in DI Water

Output Characteristics

The output characteristics of the ISOFET with the interdigitated source and drain electrodes, measured in DI water and using a Ag/AgCl reference electrode, are shown in Figure 5.14. In the same fashion as the previous section, V_{gs} was fixed while scanning V_{ds} over the range 0 V → -1 V → 0 V. The output curves reveal a field-effect response of the device, with the levels of I_d of the order of several tens of nanoamps, significantly higher than these reported in the previous section.

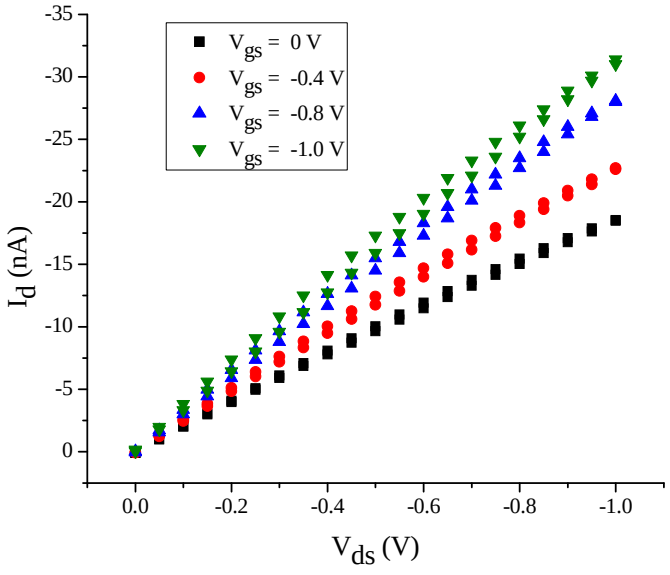

Figure 5.14 The output characteristics of the ISOFET with interdigitated source-drain electrodes; scanning V_{ds} 0 V → -1 V → 0 V, V_{gs} = 0, -0.4, -0.8, -1.0 V, in DI water, W/L ratio = 880.

Theoretically, the drain current is proportional to the W/L ratio of an ISOFET. This suggests that I_d of the interdigitated ISOFET in Figure 5.13 should be approximately 20 times higher than that of the standard ISOFET in Figure 5.9. In practice, the I_d of the interdigitated ISOFET is only about 5 times higher than that of the standard ISOFET. However, the drain current is only strictly proportional to the W/L ratio if the device is operated in its saturation mode. To avoid unwanted chemical reactions, the operating points of the devices described in this work were limited to the low voltage region, and hence, the ISOFETs were not in the saturation mode, but in the accumulation mode in the linear regime. This may be the reason why the drain currents of the devices are not directly proportional to the W/L ratio of the devices.

Figure 5.15 show the typical hysteresis which occurred during scanning V_{ds} 0 V $\rightarrow$ -1 V $\rightarrow$ 0 V and fixing V_{gs} at -1.0 V. By contrast to the previous section, I_a and I_b are defined at V_{ds} -0.5 V since this part of the output curve exhibits the largest hysteresis; ΔI_d is the difference between the drain currents at V_{ds} -0.5 V.

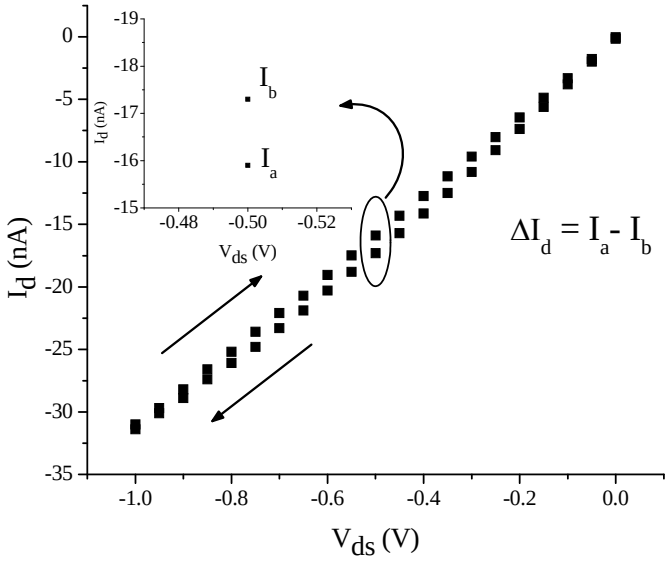

Figure 5.15 Output characteristics of the ISOFET with standard source-drain electrodes, scanning V_{ds} 0 V $\rightarrow$ -1 V $\rightarrow$ 0 V; V_{gs} = -1.0 V, in DI water.

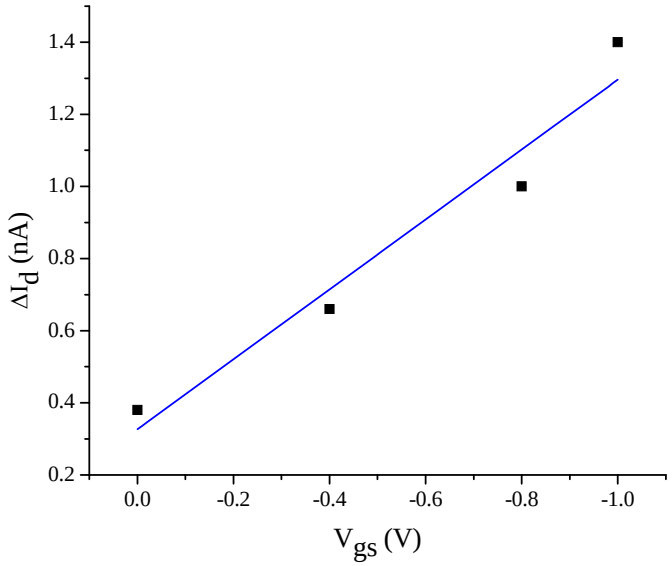

Figure 5.16 ΔI_d versus V_{gs}, V_{ds} = -0.5 V, the interdigitated ISOFET, in DI water.

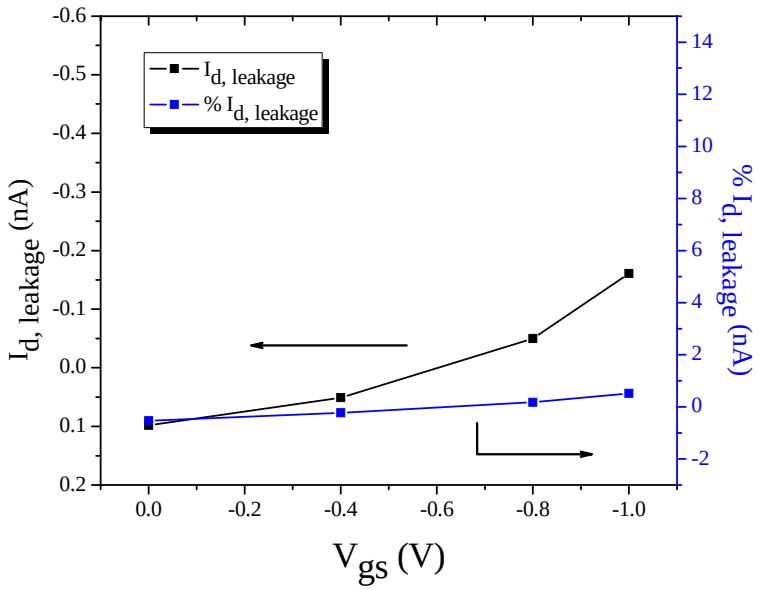

Figure 5.17 Leakage current, $I_{d,\ leakage}$ versus V_{gs}, V_{ds} = 0 V, the interdigitated ISOFET, in DI water.

In Figure 5.16, the curve shows the relation between ΔI_d and V_{gs} at V_{ds} -0.5 V. It is evident that ΔI_d increases as the magnitude of V_{gs} increases. Unlike the response of the standard ISOFET, the hysteresis of the drain current is linearly proportional to the gate voltage. The levels of the ΔI_d of the interdigitated ISOFETs reveal that the hysteresis of the device is higher than that of the standard device. In transferring more current through the source and drain electrodes, more electrons will be transported through the channel adjacent to the dielectric/semiconductor interface. As I_d increases, more electrons are therefore available for trapping in localised states at the interface. This may be the reason why the hysteresis of the interdigitated ISOFETs is larger than that of the standard device.

The leakage of the drain current was measured at different V_{gs} values by applying V_{ds} = 0 V. In the same manner as above, the percentage of $I_{d,\ leakage}$ was calculated by comparing with the maximum drain current ($I_{d,\ Vds\text{-}1V}$). As depicted in Figure 5.17, V_{gs} partly influences the leakage current. The interdigitated pattern of source and drain electrodes provides a large device area for transferring the charge. When considering the electrodes in Figure 5.2, the bulk area of the interdigitated electrodes, which is open to the solution, is much smaller than that of the standard electrodes. This probably reduces the leakage of the drain current when using the interdigitated source-drain electrodes.

5.2.5 Some Important Factors in Characterising ISOFETs

Light Effects

Since P3HT is a semiconductor with the band gap of 1.9 eV [10], the ISOFETs with P3HT as the active layer should be sensitive to light. Two 15-watt Kodak incandescent illuminators with a Kodak OC safelight filter were used to examine the light effects. The OC filter provides an amber light (dark yellow) with a peak emission at 590 nm [11]. The light sources were on the wall about 1 m above the ISOFET. The standard ISOFETs did not show any observable response to this light. This may be due to the small area for accumulating the free carriers generated by the photons. However, light exposure did become a crucial factor when characterising the devices using interdigitated source-drain electrodes.

To investigate the influence of light on the drain current, V_{ds} was scanned from 0 V to -1 V for six cycles while keeping V_{gs} constant at 0 V. The maximum I_d of each cycle at V_{ds} = -1 V was then selected. The results are shown in Figure 5.18. The drain current under illumination is about twice that of the same device examined in the dark. In Figure 5.18, under constant illumination, the drain current decreased with time, becoming stable after about 1000 s. In practice, it was difficult to keep the illumination constant during experiments. In addition, a small fluctuation of the light can lead to a large change of I_d. Experiments with ISOFETs were therefore all undertaken in the dark to avoid the unwanted change in the drain current.

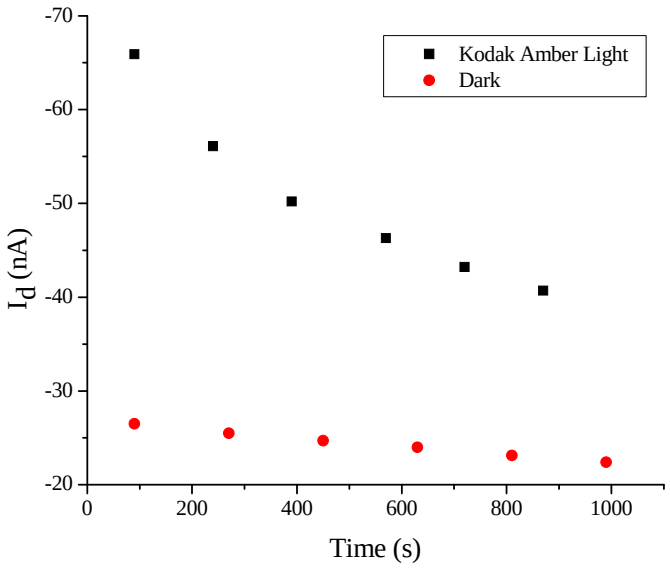

Figure 5.18 Typical responses of the interdigitated ISOFET under steady-state illumination, V_{gs} = 0 V, V_{ds} = -1 V, in DI water.

Period for Stabilising the Drain Current

To characterise the ISOFETs, V_{ds} was scanned from 0 V $\rightarrow$ -1 V $\rightarrow$ 0 V while keeping V_{gs} at a constant value. Following immersion in DI water, three consecutive measurements are shown in Figure 5.19a. The drain current drifted to lower values during scanning of V_{ds}. This drift is a significant factor when measuring the drain current immediately after immersing the device into the DI water.

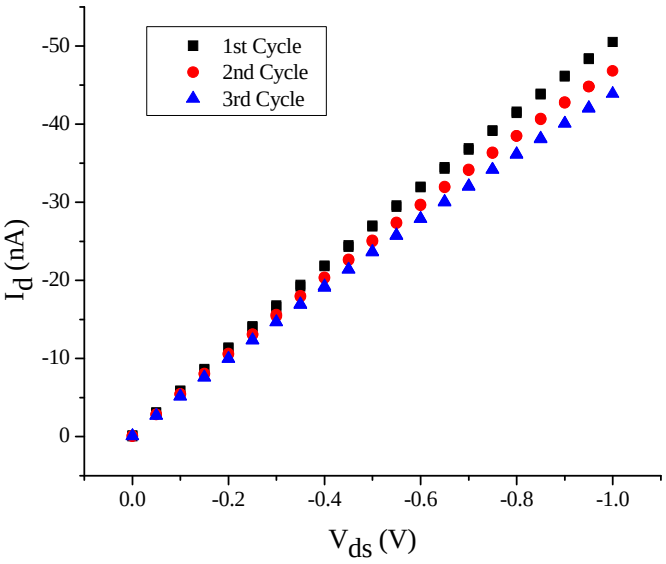

(a)

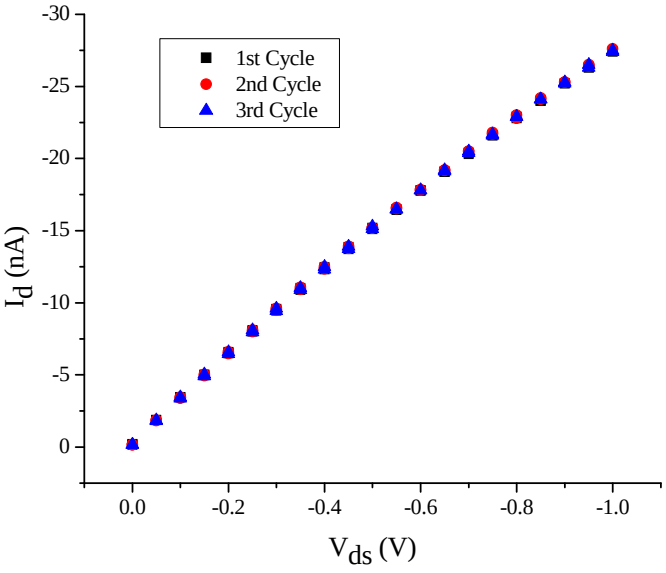

(b)

Figure 5.19 Comparison of the conditioning period using V_{gs} = 0 V, in DI water. (a) The ISOFET was left in DI water for 0 hr before the experiment. (b) The ISOFET was left in DI water for 2 hr before the experiment.

The drain current drifted about 24 % per hour (12 nA/hr) at V_{ds} = -1 V. This is lower than the 40 % per hour drift reported for a silicon-based ISFET with an aluminum oxide sensing layer, but higher than 6 % per hour for a device with a tantalum oxide sensing layer [12]. The relatively low stability of the aluminum oxide layer is due to the oxidisation of the oxide in an aqueous solution. However, tantalum oxide is not reactive to ions in solutions. The H^+ ions in DI water cannot oxidise the polymeric membrane. The PMMA layer should therefore be stable in DI water. However, the above experiments reveal that the PMMA layer was not stable immediately after immersing in DI water. Hydroxide ions can penetrate the dielectric and also the P3HT and interact with localised states near the valence band. This might hinder transition of the electrons from the valence band to localised states. This may explain why negative drifts were observed when leaving the ISOFETs in the DI water.

After the ISOFETs were left in the DI water 2 hr before the experiments, the responses of the device were more stable, as depicted in Figure 5.19b. In contrast to the responses in Figure 5.19a, there is virtually no drift during scanning three cycles of V_{ds}. After 2 hr in DI water, the active region of the ISOFET probably becomes completely hydrated and the interaction between the ions and the localised states has reached the equilibrium. In this work, the ISOFETs were left in DI water for about 2 hr before starting any measurement.

5.3 Conclusions

Ion sensitive organic field effect transistors have been fabricated successfully on hydrophobic glass using a top-gate structure. Standard source/drain electrodes were deposited using thermal evaporation. An interdigitated pattern of the source/drain electrodes was transferred on the substrates using photolithography. The P3HT and PMMA were deposited as the semiconductor and dielectric layers by spin-coating. Annealing after each step of spin coating was required to evaporate the residual solvent.

The ISOFETs exhibited a field effect and the response could be improved by using thinner PMMA layers. The results show that the ISOFETs were operated in accumulation mode. Interdigitated source/drain electrodes were used to increase the

drain current and sensitivity. A hysteresis of the drain current was observed, which depended on the gate voltage. Due to their lower operating voltages, the interdigitated ISOFETs showed lower leakage currents than for the standard devices. The devices were operated in the dark since light had a significant effect on the drain current. In addition, the results showed that the devices should be left in DI water for 2 hr in order for them to stabilise.

References

[1] H. Suzuki, H. Shiroishi, S. Sasaki and I. Karube. Microfabricated liquid junction Ag/AgCl reference electrode and its application to a one-chip potentiometric sensor. Anal. Chem., 71: 5069 – 5075, 1999.

[2] C. Bartic, A. Campitelli and S. Borghs. Field-effect detection of chemical species with hybrid organic/inorganic transistors. Appl. Phys. Lett., 82 (3): 475-477, 2003.

[3] Y. Yun, C. Pearson and M. C. Petty. Pentacene thin film transistors with a poly(methylmethacrylate) gate dielectric: Optimization of device performance. J. Appl. Phys. 105, 034508, 2009.

[4] J. E. Frommer. Conducting polymer solutions. Acc. Chem. Res., 19: 2-9, 1986.

[5] G. W. Heffner and D. S. Pearson. Molecular characterisation of poly(3-hexylthiophene). Macromolecules, 24: 6295-6299, 1991.

[6] C. D. Dimitrakopoulos and D. J. Mascaro. Organic thin-film transistors: a review of recent advances. IBM J. Res & Dev., 45 (1): 11-27, 2001.

[7] S. W. Kuo, H. C. Kao and F. C. Chang. Thermal behaviour and specific interaction in high glass transition temperature PMMA copolymer. Polymer, 44: 6873 – 6882, 2003.

[8] M. A. Zulfikar, A. W. Mohammad, A. A. Kadhum and N. Hilal. Synthesis and characterization of poly(methyl methacrylate)/SiO_2 hybrid membrane. Mat. Sci. Eng. A - Struct., 453 – 453: 422 – 426, 2007.

[9] T. S. Huang, Y. K. Su and P. C. Wang. Poly(methyl methacrylate) dielectric material applied in organic thin film transistors. Jpn. J. Appl. Phys., 47(4): 3185 – 3188, 2008.

[10] E. Bundgaard and F. C. Krebs. Low band gap polymers for organic photovoltaics. Sol. Energ. Mat. Sol. C., 91: 954 – 985, 2007.

[11] Eastman Kodak. Kodak Safelight filters. Technical information datasheet, 1999 [Revised Jul. 2002].

[12] C. G. Jakobson, U. Dinner, M. Feinsod and Y. Nemirovsky. Ion-sensitive field-effect transistors in standard CMOS fabricated by post processing. IEEE Sens. J., 2(4): 279-287, 2002.

Chapter 6
Hydrogen – Sensitive Sensors

6.1 Devices

In this chapter, the organic field effect transistor was used as a sensor to detect hydrogen ions (H^+) in an aqueous solution. The devices were fabricated and encapsulated as described in Chapter 5. Two types of ISOFETs were studied: uncoated and coated devices. Uncoated ISOFETs were used to investigate the responses to ions in solution by using a PMMA layer as the ion-sensitive membrane. The sensitivity of the devices was enhanced by depositing an LB membrane on top of the PMMA gate dielectric.

6.1.1 Uncoated Devices

As noted in Chapter 5, there were two types of an uncoated device based on the pattern of source and drain electrodes, namely a standard device and an interdigitated device. Poly(methyl methacrylate) was deposited as the dielectric layer on top of the poly(3-hexylthiophene) semiconductor. This insulator functioned as the active layer in monitoring the concentration of H^+ ions. The devices were stored in a desiccator before and after use in the experiments.

6.1.2 Coated Devices with LB membrane

Osa [1] reported that a stearic acid LB membrane could enhance significantly the sensitivity of Si-based ISFETs. Langmuir-Blodgett membranes were used in this study to improve not only the sensitivity but also the selectivity of the devices. With a similar molecular structure to stearic acid, arachidic acid was used to modify the dielectric surface of ISOFETs.

Apart from arachidic acid, valinomycin and a mixture of AA and val were also investigated. All these LB membranes were used as the H^+-sensitive layer in this chapter. Although the uncoated standard devices showed a field effect in

aqueous solutions, the response to a change of pH was relatively small compared to the interdigitated devices. Therefore, the study on the enhancement of the devices using LB membranes focused on only the devices with interdigitated source and drain electrodes.

Arachidic Acid

Arachidic acid was coated on the ISOFETs using the same procedure described in Section 4.3. The main objective of Chapter 4 was to investigate the deposition of a close-packed structure of arachidic acid. The floating layer was therefore transferred onto silicon substrates at 32 mN m^{-1} to ensure that the transferred layer was in the condensed phase before deposition. Although it was essential to coat dense LB films on the surface of ISOFETs, the ion-sensitive coatings were also required to have channels for H^+ ions. Instead of the highly dense membranes in the condensed phase, LB films with a 'looser' architecture were used in this Chapter. The AA monolayers were transferred onto substrates at 27 mN m^{-1}. This surface pressure is slightly below the boundary of phase transition into the AA condensed phase. Ten LB monolayers (Y-type deposition) were transferred onto the PMMA dielectric. After cleaning the surface of the subphase, 40 μl of AA of concentration of 1.17 mg ml^{-1} in chloroform ($CHCl_3$) was dispersed on the subphase surface using a micropipette. The AA was left on the subphase surface for 10 min in order to allow the chloroform to evaporate.

As shown in Figure 6.1a, the surface area of the fatty acid decreased abruptly when starting to control the surface pressure of the floating film at 27 mN m^{-1}. This led to a rapid increase of the surface pressure. After the pressure was approximately 27 mN m^{-1}, the area of the fatty acid film stabilised. At this pressure, the AA monolayer was left for 10 min before starting the LB deposition. In Figure 6.1a, there are small fluctuations while transferring the LB monolayer onto the ISOFET. The first and the second dips in the small frame of Figure 6.1a are enlarged in Figure 6.1b. The dipping speed was 0.08 mm s^{-1} and the drying period (between dips) was 5 min. The substrate started in air and was dipped in and out of the subphase five times. Ten Y-type LB monolayers of AA were deposited on the ISOFET.

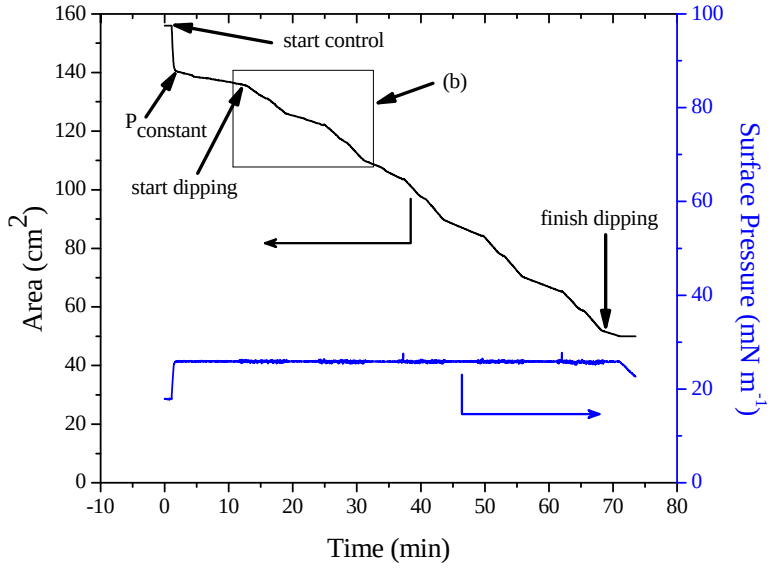

(a)

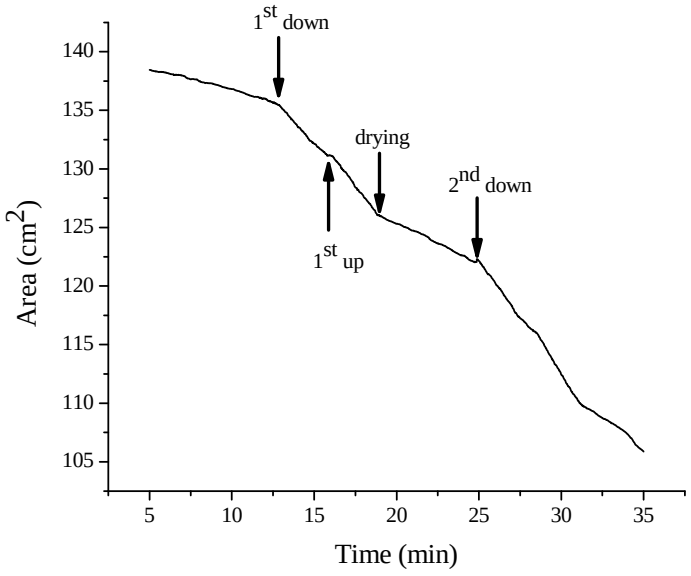

(b)

Figure 6.1 (a) Dipping profile of pure arachidic acid on an interdigitated ISOFET using DI water as the subphase; at a constant surface pressure of 27 mN m^{-1}. (b) Enlarged dipping profile (within the frame of Figure 6.1a).

Arachidic Acid-Valinomycin Mixtures

A mixture for the LB deposition was prepared by adding 5 mg valinomycin to 95 mg arachidic acid. This was mixed and then dissolved in 100 ml chloroform to prepare a solution at a concentration of 1 mg ml^{-1}. 40 μl of this solution was then dispersed on the subphase using a micropipette. By using the same method as described for depositing AA monolayers on ISOFETs, the floating film was left uncompressed for a further 10 min. The compressed film was left at a constant surface pressure of 27 mN m^{-1} for 10 min before deposition. The substrate was then dipped into the subphase to transfer 10 LB monolayers (Y-type deposition) onto the PMMA dielectric.

After starting to control the surface pressure of the mixed AA deposition, the area of the trough decreased rapidly to keep the pressure constant at 27 mN m^{-1}. The addition of the small amount of valinomycin (5% w/w) reduced the stability of the mixed LB film significantly compared to a pure AA film. This suggests that the molecules of valinomycin in the floating membrane disrupted the close packed arrangement of the AA molecules. In the aqueous ambient, proton (H^+)-valinomycin complexes can be formed more readily than the other monovalent cation-valinomycin complexes [2]. The reaction between H^+ ion and valinomycin is

$$\text{Valinomycin} + H^+ \leftrightarrow H^+\text{-Valinomycin Complex} \qquad (6.1)$$

Some molecules will interact with the protons and form proton-valinomycin complexes, while others remain uncomplexed. The AA/val monolayer would therefore consist of both uncomplexed and complexed molecules of valinomycin. However, at a fixed surface pressure, some complexed molecules might lose their H^+ ions to become uncomplexed (or vice versa). The molecules losing the H^+ ions would become larger while those capturing H^+ ions would be smaller. The complexed molecules could then move more easily throughout the membrane. Hence, the molecules in the floating monolayer may not be packed as well as those of the AA monolayer. This is one reason why only a small content of valinomycin was used in the mixture. Despite the decrease of the film stability on the subphase, the floating monolayer could be transferred successfully, as shown in Figure 6.2a and 6.2b.

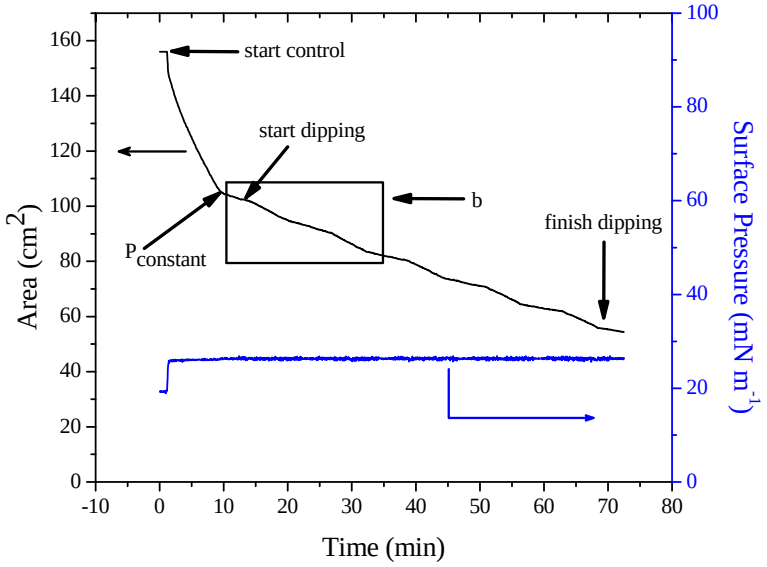

(a)

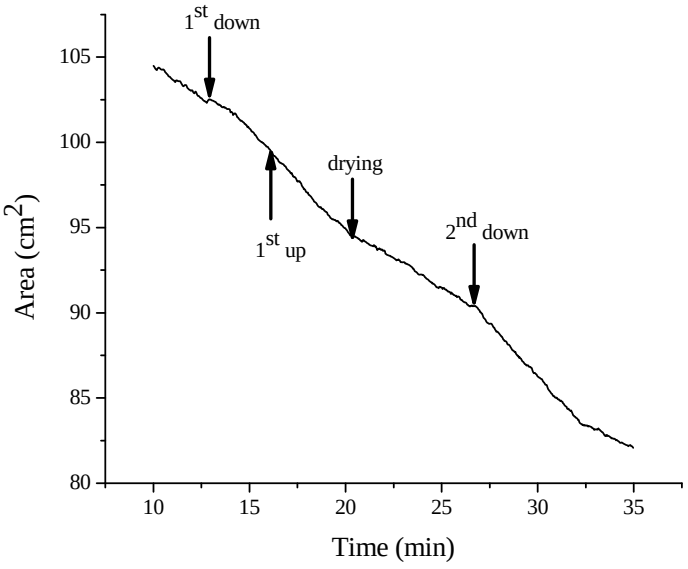

(b)

Figure 6.2 (a) Dipping profile of a mixture of arachidic acid and valinomycin (5% w/w) on an interdigitated ISOFET using DI water as the subphase; at a constant surface pressure of 27 mN m^{-1}. (b) Enlarged dipping profile (within the frame of Figure 6.2a).

Valinomycin

In Figure 6.3, the deposition profile is similar to the results in Section 4.3. It was found difficult to stabilise the surface pressure of the floating layer in order for the normal LB deposition process to be used [3]. The surface pressure decreased abruptly after starting to control the pressure at 15 mN m^{-1}. Although the pressure could be controlled at 14.00 ± 0.20 mN m^{-1}, the area at the floating film decreased significantly to maintain the constant surface pressure. After leaving valinomycin on the subphase to stabilise for 10 min, the deposition was undertaken as shown in Figure 6.3. Howarth et al reported the same deposition problem in a previous study [3].

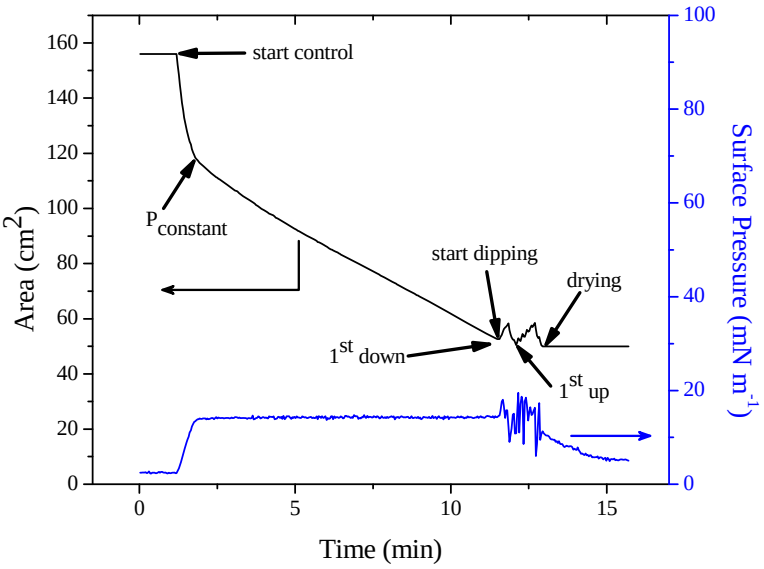

Figure 6.3 Dipping profile of pure valinomycin on an interdigitated ISOFET using DI water as the subphase; at the constant surface pressure of 15 mN m^{-1}.

As shown in Figure 6.3, the surface pressure of pure valinomycin cannot be stabilised on the subphase. Instead of establishing the close-packed structure on the subphase, the forces from the barriers may break the valinomycin floating layer during the pressure control. This probably leads to a significant decrease of the trough area before the first dip. With the instability of the valinomycin layer, numerous water molecules are probably incorporated in the floating film. The valinomycin that was deposited on the downwards movement simply came off the substrate during the upwards movement. Hence, the floating layer of valinomycin could not be built up as a multilayer film on the substrate.

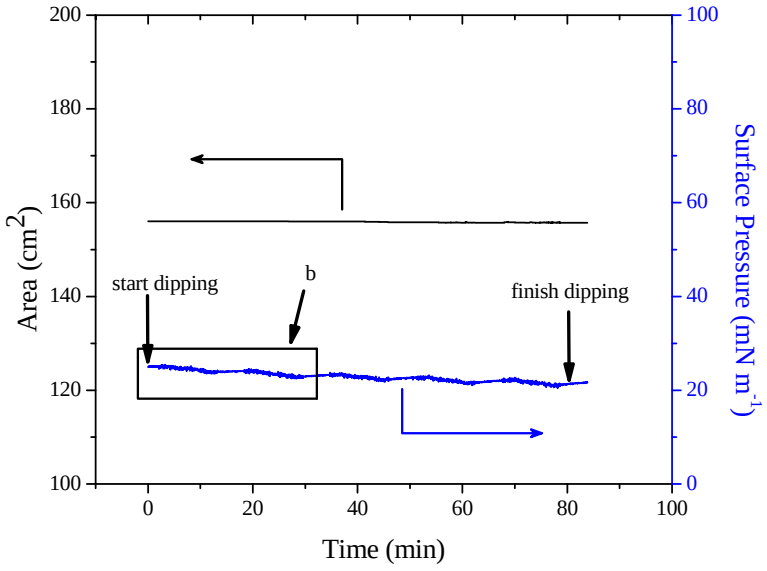

(a)

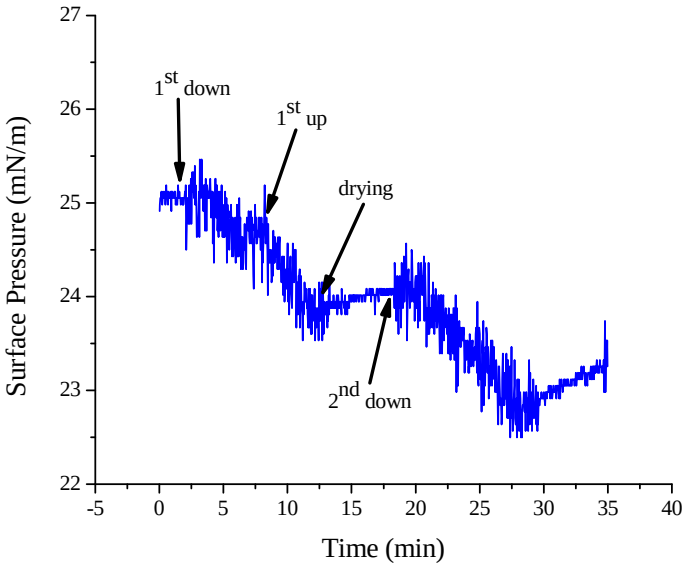

(b)

Figure 6.4 (a) Dipping profile of pure valinomycin on an interdigitated ISOFET using DI water as the subphase; without controlling the surface pressure. (b) Enlarged dipping profile (within the frame of Figure 6.4a).

To transfer the valinomycin monolayer successfully onto the ISOFET, an excess of valinomycin solution (approximately 20 μl of a chloroform solution with concentration 1 mg ml^{-1}) was dispersed over the subphase surface and left for 30 minutes. As noted above, the pressure was uncontrolled to avoid any damage to the valinomycin floating layer during film deposition. It was then found to be possible to transfer this floating layer (now significantly more than a monolayer in thickness) by raising and lowering the substrate through the floating valinomycin/air interface (Y-type deposition).

The dipping profile using this method is depicted in Figure 6.4a. By dispersing the relatively large amount of valinomycin on the subphase, a multimolecular layer would be formed on the subphase (i.e. instead of a monomolecular layer). The surface pressure was 25.00 ± 0.05 mN m^{-1} before the first dip and 21.60 ± 0.05 mN m^{-1} after the fifth last dip. As shown in Figure 6.4b, the pressure gradually decreased when lowering and raising the substrate through the valinomycin floating layer. The profile indicates that the surface pressure increased gradually during the drying period, instead of decreasing as in case of pressure-controlled deposition. When some molecules were deposited on the substrate, other molecules may be able to spread out to fill in the empty vacant area on the subphase. The floating layer was then stabilised at a new lower surface pressure.

6.2 Solution Preparation

A double junction Ag/AgCl reference electrode was used as the gate. The solution pH was kept below 7 to avoid the formation of silver hydroxide (AgOH), which can occur in basic solutions and affect the potential across the Ag/AgCl electrode. Furthermore, the pH of the solution was kept above 2 because the Araldite epoxy resin could be oxidised when in contact with a strong acid for a long period.

6.2.1 Buffer solutions

Two buffers, pH 4 and pH 7, were used to calibrate the pH meter before use. Buffer tablets, pH 4 (phthalate) and pH 7 (phosphate), were obtained from Fisher Scientific. After putting each tablet into a beaker with 100 ml DI water, the beaker

was covered with Parafilm M and left in the ultrasonic bath for two hours (until the tablet completely dissolved). The solutions were used without further filtering and kept at room temperature.

6.2.2 Test Solutions

All test solutions were based on non-chlorides to avoid an additional potential from the effect of chloride ions on the Ag/AgCl reference electrode. Only acetic acid was used to adjust the pH of the solution. This simple organic acid was added to the DI water to prepare non-buffered solutions, instead of buffer solutions which generally comprise various inorganic and organic ions. Therefore, interference from the other inorganic anions was minimised. After adjusting the pH, all the solutions were covered with parafilm M and left overnight at room temperature before use. As a result of the above precautions, the pH was stable during the experiments.

6.3 Experimental Methods

6.3.1 Electrical Measurements

Deionised water was used as the initial test solution in all the experiments. This was a reference to ensure the devices were stable before measuring the pH of the test solutions. The pH of DI water (always in the range 5.5 to 5.8) was measured before the experiment. Before use, the ion sensitive field effect transistor was rinsed with DI water to remove any contamination from its surface. As noted in Section 5.2.5, the ISOFET stabilisation was necessary for accurate measurements. The ISOFETs were therefore placed in a reference solution (DI water) for two hours.

The V_{ds} was scanned over the range 0 V $\rightarrow$ -0.2 V $\rightarrow$ 0 V. The period was approximately 90 seconds, as depicted in Figure 6.5. At the same time, V_{gs} was set at 0 V. I_d was then measured at V_{ds} = -0.2 V. Although the other conditions (such as V_{gs}, V_{ds} and pH of the solution) were fixed, the measured drain current at V_{gs} = -0.2 V would change significantly if the value of I_d at V_{gs} = 0 V was not stable. Therefore, before changing V_{gs} to -0.2 V, it was kept constant at 0 V until I_d was stable (approximately constant in each scanning cycle of V_{ds}; the difference of the I_d

in each cycle was less than 0.05 nA). For example, 6 cycles of V_{ds} were required to make the ISOFET stable as shown in Figure 6.5. In this Figure, I_d decreased exponentially to its final value as V_{ds} was scanned.

After the drain current of the devices was stable at V_{gs} = 0 V, V_{gs} was changed to -0.2 V. The increase in the magnitude of the drain current is shown in Figure 6.5. However, when V_{gs} returned to 0 V, I_d did not return to its previous value (before changing V_{gs} to -0.2 V). As shown in Figure 6.5, three cycles of V_{ds} (V_{gs} constant at 0 V) were required to return I_d to its initial value. This sequence of measurements was therefore repeated until obtaining 5 measurements of I_d at V_{gs} -0.2 V and V_{ds} -0.2 V were obtained.

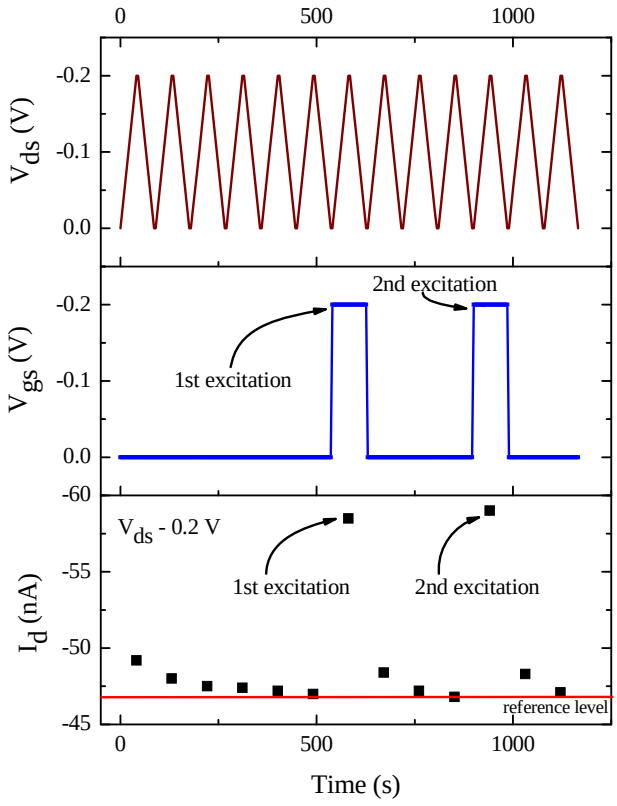

Figure 6.5 Typical responses of the ISOFET in DI water using sequence of the scan in V_{ds} over the range 0 V $\rightarrow$ -0.2 V $\rightarrow$ 0 V. The structure of the device: Cr/Au/P3HT/PMMA/10 AA. Measurement in the dark at room temperature.

6.3.2 pH Characterisation Procedure

In a similar method to that described in the previous section, V_{gs} was fixed at 0 V and V_{ds} was scanned from 0 V $\rightarrow$ -0.2 V $\rightarrow$ 0 V until I_d was stable (generally about 5 or 6 cycles of V_{ds}). V_{gs} was then changed to -0.2 V, and the drain current was measured. A second measurement was undertaken after I_d returned to its stable value. By repeating this measuring process, the average I_d at V_{gs} = -0.2 V and V_{ds} = -0.2 V was obtained using 5 measurements of I_d.

After the measurements, the Ag/AgCl reference electrode and the ISOFET were rinsed using DI water. The ISOFET was then immersed in a test solution with the highest pH, and 5 measurements of I_d were undertaken. The ISOFET and Ag/AgCl electrode were rinsed with DI water to remove any residual ions from the previous measurements. The test solution was changed to that with the lowest pH; then back to the second highest value and so on. The typical sequential responses of the ISOFET in the solutions with different pHs is shown in Figure 6.6. This measuring sequence was employed to obtain the 'real' responses (e.g. rather than an effect due to drift of the drain current with time).

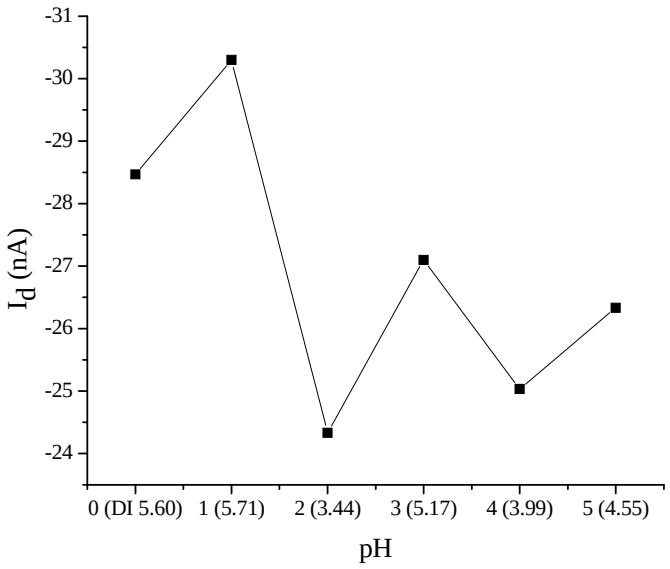

Figure 6.6 Typical sequential responses of the ISOFET in different pH solutions. The structure of the device : Cr/Au/P3HT/PMMA/10 monolayers of 95%AA + 5%val. Measurement in the dark at room temperature.

6.4 pH Responses

6.4.1 Uncoated ISOFETs

The responses of the uncoated ISOFETs with the standard (non-interdigitated) pattern of source and drain electrodes were measured using the measuring sequence as described in the previous section. The devices had a W/L ratio of about 40. The drain current was measured at V_{ds} = -0.2 V and V_{gs} = -0.6 V. A typical pH response of the uncoated standard devices is shown in Figure 6.7. When increasing the solution pH, the drain current increased. However, this response to the H^+ concentration was small with a sensitivity of 0.18 ± 0.1 nA pH^{-1} (or nA dec^{-1})

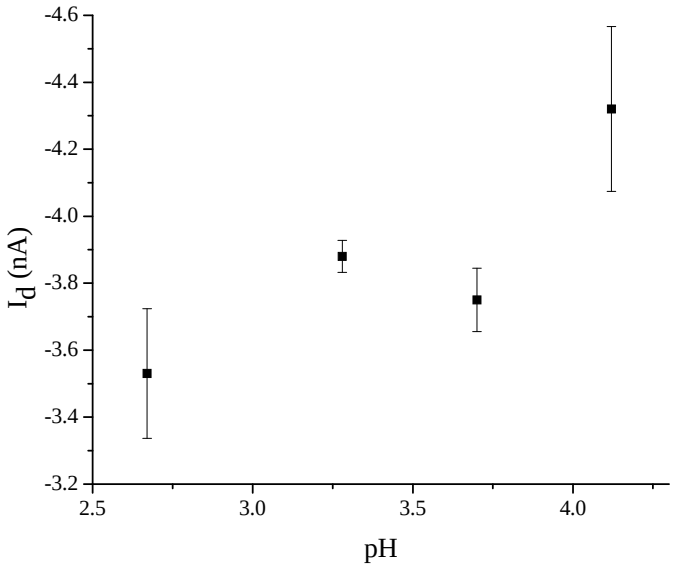

Figure 6.7 The pH response of an uncoated standard ISOFET (W/L ratio = 40) at room temperature. V_{ds} = -0.2 V and V_{gs} = -0.6 V.

As noted in Section 5.1.3, in the case of the interdigitated ISOFETs, the distance between the source and drain was 25 μm. This was half the distance between the electrodes in case of the standard devices. For V_{ds} = -0.6 V, the electric field of the interdigitated ISOFETs was increased. Additionally, their W/L ratio was increased to 880. These factors made the carrier accumulation between the electrodes increase significantly. Consequently, more than ten cycles of V_{ds} were required to return I_d to the stable state, and hence the period to measure the ISOFET

response in each solution was more than two hours. However, such a period might lead to a change in the hydrogen ion concentration due to water evaporation. As the evaporation rate of water in still air is approximately 84.4 g m^{-2} hr^{-1} [4], the 2 hr period can result in approximately 0.34 g water evaporating from a 100 ml beaker (5 cm diameter). To keep this water evaporation below 0.1 g, the measuring period was limited to 30 min; in essence, V_{gs} was reduced from -0.6 V to -0.2 V when characterising the pH responses of the interdigitated ISOFETs.

The pH response of the interdigitated ISOFET shown in Figure 6.8 is similar to that of the standard ISOFET; the magnitude of I_d increases with the solution pH. The sensitivity of the uncoated interdigitated device is 0.5 ± 0.1 nA pH^{-1}, significantly greater than the standard ISOFET.

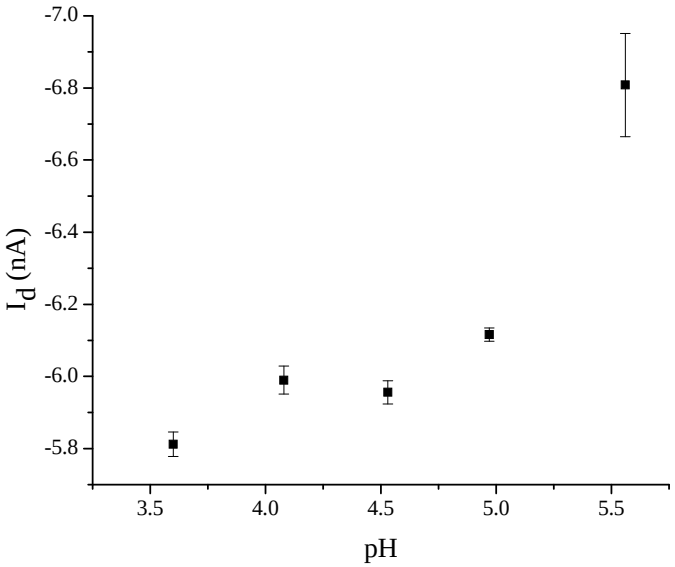

Figure 6.8 The pH response of the uncoated interdigitated ISOFET (W/L ratio = 880) at room temperature. V_{ds} = -0.2 V and V_{gs} = -0.2 V.

The results for both uncoated standard and interdigitated ISOFETs are consistent with the result reported previously by Bartic et al. [5]. This may be because the oxygen atoms, negatively charged in the PMMA, can attract H^+ ions (positive) in the solutions. Since the adsorbed ions are positive charges, they prevent hole accumulation at the interface between the semiconductor and insulator. An increase in the pH (i.e. to a more basic solution) will decrease the positive charge (H^+ ions) density in the solution. Fewer H^+ ions are therefore adsorbed on the PMMA

surface. This leads to an increase in the density of holes in the accumulation layer of the P3HT [6]. As the result, the magnitude of the drain current increased when the pH of the solution increased.

6.4.2 LB-Coated ISOFETs

Pure arachidic acid (AA), pure valinomycin (val) and a mixture of 95%AA + 5%val were deposited on top of the interdigitated ISOFETs using the LB technique. Their pH responses were measured using the same method as described in section 6.4.1. The pH response of the interdigitated ISOFET coated with 10 LB layers of pure AA is shown in Figure 6.9. As before, the magnitude of the drain current increased when increasing the pH.

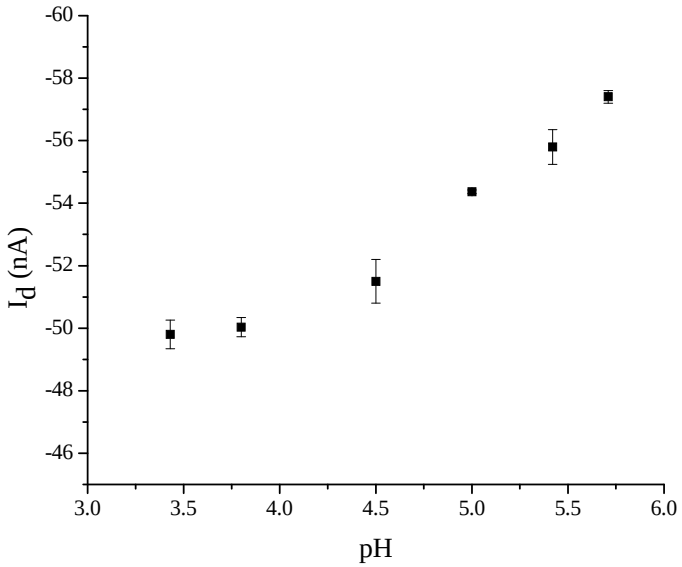

Figure 6.9 The pH response of the interdigitated ISOFET coated with 10 LB layers of pure AA, at room temperature, V_{ds} = -0.2 V and V_{gs} = -0.2 V.

Figure 6.10 shows the pH response of the ISOFET coated with 10 layers of 95%AA + 5% val. The pH response of the ISOFET coated with multilayer valinomycin is shown in Figure 6.11. Both responses are similar to that of the AA-coating ISOFET in Figure 6.9; the magnitude of the drain current increased when the pH increased.

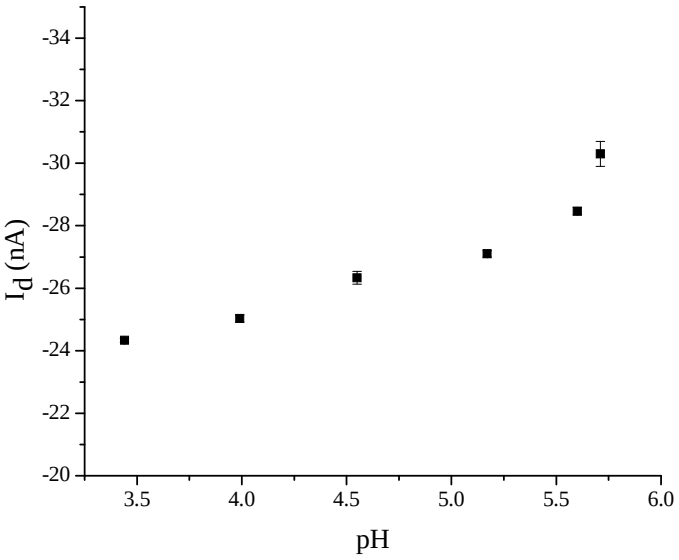

Figure 6.10 The pH response of the interdigitated ISOFET coated with 10 LB layers of 95%AA + 5 %val; at room temperature; V_{ds} = -0.2 V and V_{gs} = -0.2 V.

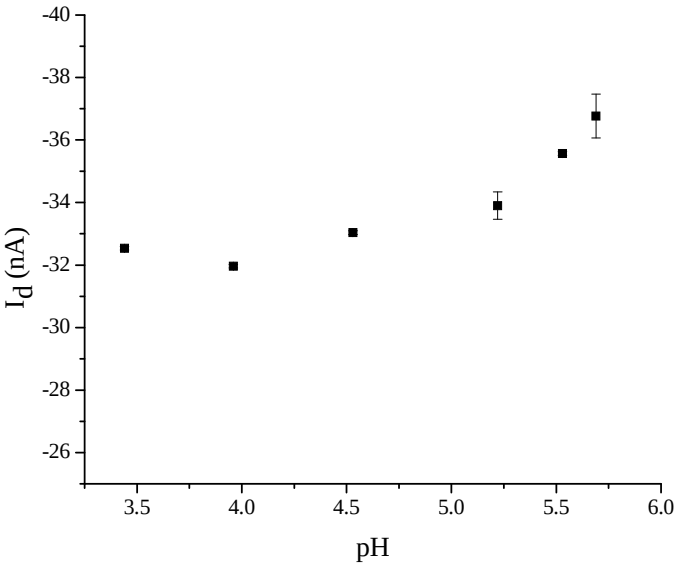

Figure 6.11 The pH response of the interdigitated ISOFET coated with multilayer valinomycin; at room temperature; V_{ds} = -0.2 V and V_{gs} = -0.2 V.

Table 6.1 compares the sensitivities of the uncoated and coated ISOFETs with the interdigitated source-drain pattern. The sensitivity of the ISOFET coated with pure AA membrane was approximately 3.4 ± 0.1 nA pH^{-1}, almost an order of magnitude greater than the corresponding uncoated device.

Table 6.1 The pH sensitivities of the ISOFETs with interdigitated source-drain pattern.

Device	Sensitivity
Uncoated ISOFET	0.5 ± 0.1 nA pH^{-1}
ISOFET/10 LB AA	3.4 ± 0.1 nA pH^{-1}
ISOFET/10 LB 5%val+95% AA	2.3 ± 0.1 nA pH^{-1}
ISOFET/10 LB val	1.8 ± 0.1 nA pH^{-1}

Figure 6.12 shows a schematic diagram of the 10-layer arachidic acid membrane. Thermodynamically, the hydrated H^+ and water molecules are small and hence able to move freely through the LB membrane. When the LB membrane was submerged into water, the carboxylic head groups (-COOH) ionised and formed negative charge layers within the membrane.

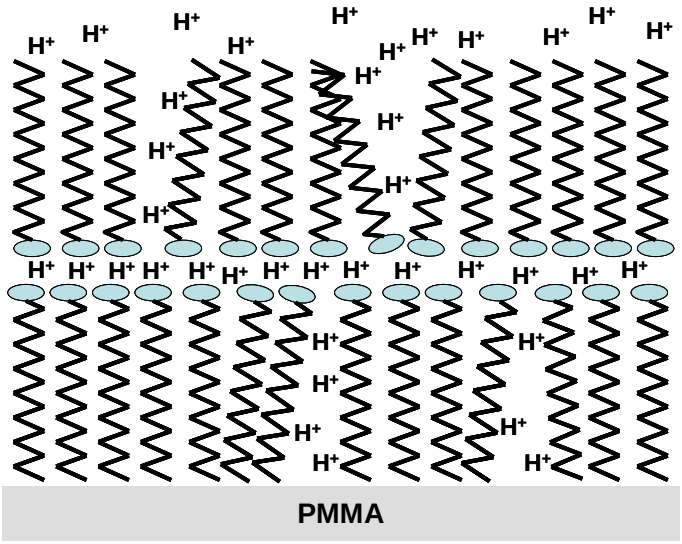

Figure 6.12 Schematic diagram of the 10-layer AA membrane when exposed to the acid solutions.

The H^+ ions from the –COOH groups were not bound to the LB membrane, but able to diffuse out of the carboxylic acid layers. As some H^+ ions were lost from the membrane following ionisation, the negatively charged layer might exert a strong

attractive force on the holes compared to the weak forces from the negative polarity of the PMMA molecules. This led to the accumulation of the large number of holes at the P3HT/PMMA interface of the AA-coated ISOFETs.

Apart from attracting holes in the semiconductor layer, the ionised layers of carboxylic acid also generate a strong attractive force to trap positive ions. When decreasing the pH of the solution, the ionised carboxylic acid layers trapped significantly more H^+ ions than the PMMA surface. This would give a difference in the net negative charge on the ISOFET surface, and hence lead to a change of Nernst potential as shown in Figure 2.10. Therefore, the number of the holes accumulated at the semiconductor/insulator interface also changed. As the result, the ISOFET coated with AA membrane was more sensitive to the variation of pH than the uncoated devices.

In Figure 6.9, saturation of the drain current is evident when the pH is below 4. However, the magnitude of the saturated drain current is much higher than that of the uncoated device in Figure 6.8. This suggests that only a few outer ionised carboxylic acid layers interacted with the H^+ ions in solution, while the inner layers might possess a net negative charge. With a decrease in the pH, more H^+ ions were available in the solution. However, the device showed a response to an increase in the number of H^+ ions if the pH was above 4. This probably reveals that the ionised outer layers may be fully recombined with H^+ ions at pH 4. Hence, the outer layers could not respond to the increase in the H^+ concentration when the pH was reduced below 4. Meanwhile, the large number of H^+ ions in solution was probably unable to increase the H^+ penetration into the inner carboxylic acid layers. This may be because the inner layers of 20-carbon alkyl groups of the AA membrane prevented the H^+ penetrating the inner carboxylic acid layers. Therefore, the total number of H^+ ions trapped in the AA layers was constant. This would lead to a constant net charge on the surface of the ISOFET. As a consequence, the ISOFET was not sensitive to a change of H^+ ions when the pH was below 4.

From Table 6.1, the sensitivity of the ISOFET coated with AA/val mixture was approximately 2.3 ± 0.1 nA pH^{-1}. A schematic diagram of the 10-layer membrane of 95%AA + 5 %val is given in Figure 6.13. As the sizes of valinomycin and arachidic acid molecules are different, the layers of arachidic acid, the major constituent, are disrupted considerably by the valinomycin molecules. As a result,

the layers of carboxylic acid head groups are not as close-packed as those in the pure AA membrane. The electric field generated from the negative charge of the AA/val membrane was therefore weaker than that produced from the pure AA membrane. However, the force generated from the ionised AA/val membrane was significantly stronger than that from the uncoated surface (i.e. PMMA molecules). Consequently, the number of holes accumulating at the P3HT/PMMA interface of the AA/val-coated ISOFET was less than that at the semiconductor/insulator interface of the AA-coated ISOFET. These accumulating holes were, however, greater in number than those gathering at the P3HT/PMMA interface of the uncoated ISOFETs.

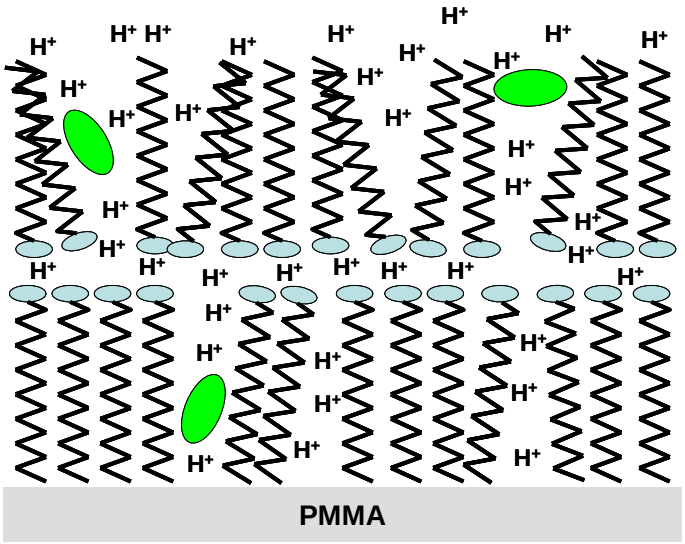

Figure 6.13 Schematic diagram of the 10-layer membrane of 95%AA + 5 %val when exposed to the acid solutions.

As the molecular organisation of the AA/val membrane was disrupted, more H^+ ions were able to penetrate the membrane when compared to the pure AA membrane. However, the sensitivity of the ISOFET coated with AA/val mixture was lower than that of the AA-coated ISOFETs. This may be because the disruption from the valinomycin molecules provides pinholes in the AA/val layers. Some of the trapped H^+ ions may leak from the membrane through these pinholes, and lower the Nernst potential, as a result. Therefore, fewer holes were trapped in the ionised carboxylic acid layers. With the same change in pH, the change in I_d of the AA/val ISOFETs was therefore smaller than that occurred in the AA-coated ISOFETs. This led to the lower sensitivity of the AA/val ISOFETs.

The pH response in Figure 6.10 does not show any saturation region. Instead of complete recombination, the H^+ leakage due to the disruption of the valinomycin molecules probably makes the layers of the ionised carboxylic acid head groups partially recombine with the H^+ ions at pH below 4. In addition, the pinholes may lead to the penetration of more H^+ into the inner carboxylic acid layers. Some free ionised carboxylic head groups therefore remained in the AA/val film. These free negative sites can then trap more H^+ ions when the pH decreases below 4.

Table 6.1 shows that the sensitivity of the ISOFET coated with the pure valinomycin was approximately 1.8 ± 0.1 nA pH^{-1}. Although valinomycin molecules do not ionise in water, the presence of twelve peptide bonds in valinomycin provides a stronger negative polarity than that from the ester groups of PMMA molecules. As a result, the attractive force generated from the peptide bonds is significantly greater and able to accumulate more holes when compared to the uncoated ISOFETs. The magnitude of I_d therefore increased significantly for the valinomycin membrane on the ISOFETs.

Theoretically, a peptide bond has less negative polarity than an ionised carboxylic acid head group. This is a reason why the drain current magnitude of the AA/val-coated ISOFETs was lower than that of the pure AA-coated ISOFETs. However, the result in Figure 6.11 shows a higher drain current of the valinomycin-coated ISOFET than the AA/val-coated ISOFET. This is probably because arachidic acid molecules are not ionised completely in low-pH solutions since arachidic acid is a weak acid (its dissociation constant, pK_a, > 4.7 [7]).

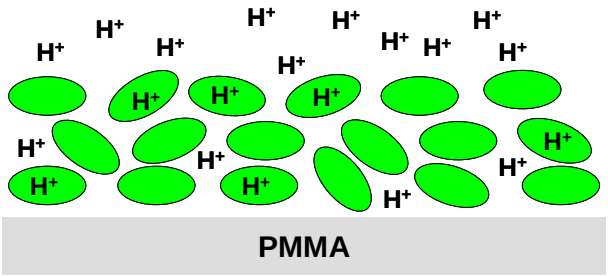

Figure 6.14 Schematic diagram of the multilayer valinomycin when exposed to the acid solutions.

Multilayers of valinomycin, rather than monolayers, were deposited onto the ISOFETs using the method described in Section 6.1.2. More valinomycin molecules

were deposited on the ISOFET than those expected from the 10-monolayer valinomycin film. These led to the greater attractive force than that produced from the disrupted membrane of the AA/val mixture.

The sensitivity of the ISOFET coated with pure valinomycin is the lowest among all coated ISOFETs in this study - but higher than that of the uncoated devices. As shown in Figure 6.14, the pure valinomycin membrane probably does not possess a close-packed architecture. As a result, the surface area for trapping H^+ ions in the valinomycin membrane is significantly larger than that of uncoated PMMA surface. This reveals that the Nernst potential across the valinomycin layer is larger than that on the PMMA surface. When the pH decreased, more H^+ ions may be trapped in the valinomycin membrane. This would lead to an increase of the ISOFET sensitivity when the device was coated with pure valinomycin membrane. However, when compared to the ionised carboxylic head groups, the attractive forces from the valinomycin film were weak and hence bound fewer H^+ ions. In case of the valinomycin-coated device, the change of the number of H^+ ions trapped in the valinomycin membrane was smaller than those occurred in the other ISOFETs coated with the pure AA or the AA/val mixture, when the pH of the solution was changed. The valinomycin-coated ISOFET therefore became less sensitive to H^+ than the other coated ISOFETs.

With a SiO_2 ion sensitive layer, Bartic et al [5] reported that the sensitivity of the organic-based transistor to H^+ ions was 12.5 nA pH^{-1} at V_{gs} = -2 V and V_{ds} = -2 V; however, the sensitivity increased significantly to 62.5 nA pH^{-1} when V_{gs} = -2 V and V_{ds} = -10 V. By using Ti_2O_5 [6], the sensitivity of the ion sensitive FET could be increased to approximately 160 nA pH^{-1} at V_{gs} = -0.5 V and V_{ds} = -0.2 V. These results show that the ISOFET sensitivity could be enhanced by using a high dielectric constant material as an ion sensitive membrane. Additionally, Vogel et al [8] showed that the sensitivity of Si-based ISFET was improved by coating the LB membrane on top of the gate dielectric. However, the sensitivities of the coated devices in this study were significantly lower compared to those of the devices with inorganic active insulators, such as SiO_2 (> 50 nA pH^{-1}) or Ti_2O_5 (> 150 nA pH^{-1}). This is probably because dielectric constants of organic LB films are lower than those of inorganic membranes.

6.5 Conclusions

Organic field effect transistors can detect hydrogen ions in aqueous solutions. Uncoated ISOFETs showed a response to H^+ ions, although their sensitivity was small. The sensitivity of the devices was improved significantly by coating the gate dielectric (PMMA) with an LB film, which functioned as an ion-sensitive membrane. In this research, LB films of AA, AA/val and pure val were all investigated.

It was found that the ISOFETs coated with the LB membranes of AA, AA/val or pure val have significantly higher sensitivities than that of the uncoated device. The devices with the AA membrane exhibited the highest sensitivity to H^+ ions. This may be because a number of H^+ ions are trapped in the compact ionised layers of carboxylic head groups. However, a small amount of valinomycin will probably disrupt the compact molecular architecture of the LB membrane. This could lead to leakage of H^+ ions from the ionised carboxylic acid layers. Therefore, the sensitivity of devices with an AA/val film was slightly less than those with a pure AA membrane.

In case of valinomycin membranes, the presence of twelve ester groups in valinomycin molecules provides a stronger ionic force to attract H^+ ions than the single ester group in PMMA molecules. Its porosity may also increase the active area for H^+ trapping in the membrane. As a consequence, devices with valinomycin membranes have higher sensitivity to H^+ than the uncoated devices. However, their sensitivity was found to be lower than those with AA or AA/val membranes. It is suggested that the ionic force from the ester groups is weaker than that from the carboxylic head groups.

References

[1] T. Osa. Potentiometric response of lipid modified ISFET. Appl. Biochem. Biotech., 41: 35 – 40, 1993.

[2] J. W. Nichols and D. W. Deamer. Net proton-hydroxyl permeability of large unilamellar liposomes measured by an acid-base titration technique. Proc. Natl. Acad. Sci., 77(4): 2038 – 2042, 1980.

[3] V. A. Howarth, M. C. Petty, G. H. Davies and J. Yarwood. The deposition and characterisation of multilayers of the ionophore valinomycin. Thin Solid Films, 160: 485 – 489, 1988.

[4] L. M. K. Boelter, H. S. Gordon and J. R. Griffin. Free evaporation into air of water from a free horizontal quiet surface. Ind. Eng. Chem., 38(6): 596 – 600, 1946.

[5] C. Bartic, B. Palan, A. Campitelli and G. Borghs. Monitoring pH with organic-based field-effect transistors. Sens. Act. B., 83: 115 – 122, 2002.

[6] C. Bartic, A. Campitelli and S. Borghs. Field-effect detection of chemical species with hybrid organic/inorganic transistors. Appl. Phys. Lett., 82: 475 – 477, 2003.

[7] C. O. da Silva, E. C. da Silva and M. A. C. Nascimento. Ab initio calculations of absolute pK_a values in aqueous solution I : Carboxylic acids. J. Phys. Chem. A, 103: 11194 – 11199, 1999.

[8] A. Vogel, B. Hoffmann, S. Schwiegk and G. Wegner. Novel Langmuir-Blodgett membranes for silicon-based ion sensors. Sens. Act. B., 4: 65 – 71, 1991.

Chapter 7

Potassium – Sensitive Sensors

7.1 Experimental Procedure

In this research, sulphate salts were used to avoid any interference from chloride ions. Both sodium sulphate and potassium sulphate (anhydrous, ACS reagents, ≥ 99.0%) were dissolved in DI water to concentrations of 0.5, 1, 5, 10, 50 mg ml^{-1}. The concentrations of the test solutions were limited to 50 mg ml^{-1} to prevent any precipitation of the salt during the experiments. The pH can vary with concentration of the solution. However, with the use of very low K_2SO_4 concentration, the pH was found to be approximately constant in all the test solutions.

As the standard (non-interdigitated) ISOFETs exhibited lower sensitivity to H^+ ions in Chapter 6, only interdigitated devices were used in this chapter. The ISOFET was conditioned in DI water for two hours, as described in Chapter 6. The experiments started with DI water (as a reference solution). Following this, the device was tested in one of the K_2SO_4 solutions. Before testing in the next solution, the device was rinsed with DI water. The solution was changed alternately between high-concentration solutions (> 5 mg ml^{-1}) and low-concentration solutions (< 5 mg ml^{-1}). In some cases, the device was tested in solutions with the addition of Na^+, thereby investigating the selectivity of valinomycin.

To maintain the stability of the pH during the measurements, the solutions were covered by parafilm and left overnight at room temperature before use in the experiments. As noted in Chapter 6, all electrical measurements were undertaken in the dark at room temperature. V_{ds} and V_{gs} were scanned and changed as described in Section 6.3.1. Five measurements were undertaken in the same solution. The average of the drain current was calculated at V_{ds} = -0.2 V and V_{gs} = -0.2 V. The graphs were then plotted to show the pK or pNa responses of the devices versus the average of I_d.

7.2 pK Responses

The pK response of the uncoated interdigitated device is shown in Figure 7.1. The magnitude of the drain current became smaller on increasing the concentration of K^+ ions. On applying a negative voltage to the gate electrode, the accumulated charges near the PMMA surface would ideally be only hydroxide ions (OH^-), while those around the gate would be H^+. It is, however, impractical to separate the positive ions from the negative ions completely by applying a small negative voltage. The concentration of K^+ ions would therefore decrease at a distance from the reference electrode. The concentration of hydroxide ions would be low around the reference electrode but higher near the surface of the dielectric. Therefore, the majority of the ions are negative on the PMMA surface with a small number of positive ions. Around the gate electrode, the majority ions are, in contrast, positive with small number of OH^- ions. The net negative charge on the PMMA surface leads to an effective potential across the ISOFET insulator. This potential produces the electric field which accumulates holes at the insulator/dielectric interface.

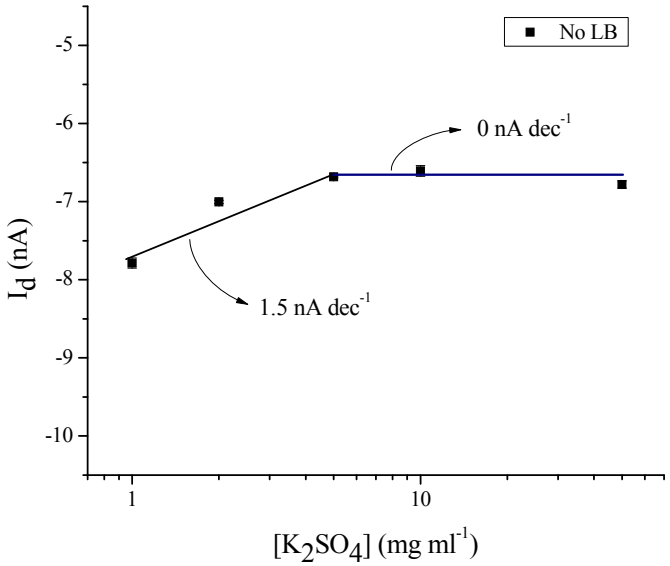

Figure 7.1 pK response of an uncoated interdigitated ISOFET.

At low concentrations (below 5 mg ml^{-1}) of K^+, the magnitude of the drain current decreases with an increase in the potassium concentration. The result suggests that fewer holes are accumulated at the P3HT/PMMA interface when increasing the concentration of K^+ ions.

From the atomic perspective, a potassium ion has one proton more than the number of electrons. In contrast, a hydrogen ion (H^+) does not have any electrons, but one proton. After the first ionisation, there is no electron cloud surrounding a hydrogen nucleus, while there are 3 electron shells (18 electrons) surrounding a potassium nucleus. As a result, negative ions can come closer to a hydrogen ion than a potassium ion, and hence hydrogen ions exert a stronger Coulombic force to negative ions than potassium ions. However, the sensitivity of the uncoated device to K^+ ions is about 1.5 nA dec^{-1} (at low concentrations, < 5 mg ml^{-1}), as shown in Figure 7.1. This is significantly higher than the sensitivity to H^+ ions, approximately 0.5 nA dec^{-1}, as shown in Figure 6.8. Consequently, K^+ ions were able to accumulate on the PMMA surface more effectively than H^+ ions. This suggests that the attractive force for the ions is Van der Waals force in nature, rather than a Coulombic force between the ions and the ester group of PMMA. For example, ions with greater mass would be able to adsorb on PMMA more readily than those with light mass.

Van der Waals forces are a sum of attractive and repulsive forces between molecules. In this research, the relevant forces are those between hydrated ions and a planar dielectric surface that is assumed to be infinite. The Van der Waals force (F_w) between a spherical mass and an infinite wall can be written [1]

$$F_w = \frac{2\pi^2 n^2 \lambda R^3}{3d^2 (d+2R)^2} \qquad (7.1)$$

where n is the number of molecules per cm^3, λ is the London-Van der Waals constant, which is proportional to the molecular weight of the particle [2], R is the radius of the molecules, and d is the distance between the wall and the edge of the molecule.

In case of adsorbed ions on ISOFETs, the n and d parameters are approximately constant in all the experiments. In solution, ions will be in the form of

hydrated ions, surrounded by water molecules. The water molecules will dominate the molecular size of any hydrated ion. If ions have the same charge, their molecular radii can approximately be constant. As reported by Nightingale [3], the molecular radius of hydrated H^+ is about 0.28 nm, while those of hydrated K^+ and hydrated Na^+ are 0.33 nm and 0.35 nm, respectively. In Equation 7.1, the Van der Waals force therefore depends on the molecular weight (via the λ term).

In this study, the hydration number, which is the number of water molecules surrounding an ion in the solution, may be used to explain the experimental results. The hydration number for H^+ is 4 [4], while that of K^+ ions is approximately 6 [5]. The molecular weight of hydrated K^+ ions is about 147, which is significantly more than that of hydrated H^+ ions, about 73. Therefore, the Van der Waals force of K^+ ions would be more than that of H^+ ions. This may be the explanation of why the devices respond to K^+ ions better than H^+ ions at low concentrations.

In Figure 7.1, the drain current becomes saturated for potassium concentrations greater than about 5 mg ml^{-1}. This indicates that the effective potential across the PMMA becomes constant when the ionic concentration is increased. Hence, the accumulated charge on the PMMA surface remains constant, although the concentration of K^+ ions is increased. The accumulated K^+ ions form a space charge on the PMMA surface and also produce a repulsive force. This Coulombic force then prevents other K^+ ions from aggregating on the PMMA.

Figure 7.2 shows the potassium response of the ISOFET with an AA LB membrane. In a similar fashion to Figure 7.1, the magnitude of I_d is inversely proportional to the concentration of potassium ions, and saturates for potassium concentrations greater than about 5 mg ml^{-1}. However, the magnitude of the drain current in Figure 7.2 has increased significantly, approximately five times higher than that of the uncoated device in Figure 7.1. This suggests that the effective potential across the dielectric layer of the device coated with AA membrane was greater compared to that of the uncoated ISOFET. This is probably due to the fact that the LB membrane can ionise, forming a negative plane of carboxylic acid groups when the device was submerged in the solution, as shown in Figure 7.3. These dense negative charges can induce a larger Nernst potential, and hence generate a significantly stronger electric field across the dielectric. More holes were then accumulated at the P3HT/PMMA interface.

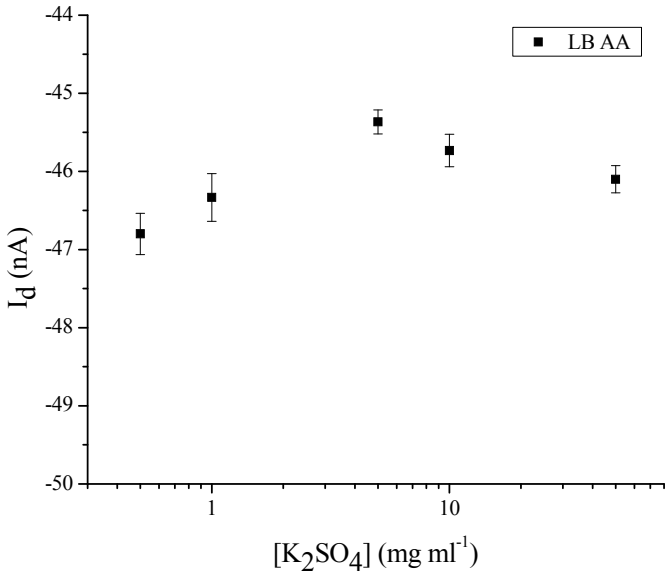

Figure 7.2 pK response of an interdigitated ISOFET with 10 LB monolayers of pure AA.

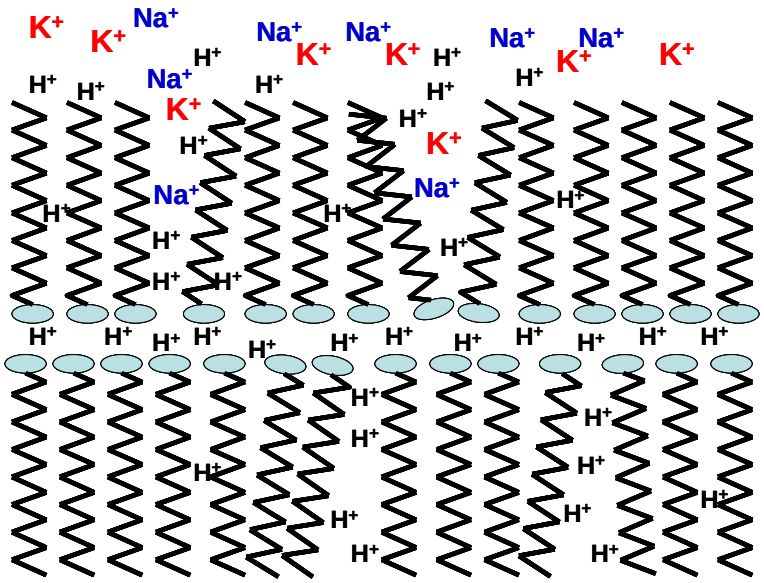

Figure 7.3 Schematic diagram of the ISOFETs coated by 10 LB monolayers of AA when exposed to the aqueous solutions.

The K^+ response of the ISOFET device coated with 95% AA+5% val is shown in Figure 7.4. As the main constituent of the LB membrane is arachidic acid, the K^+ response of this device is similar to that of the AA-coated device, as depicted in Figure 7.2.

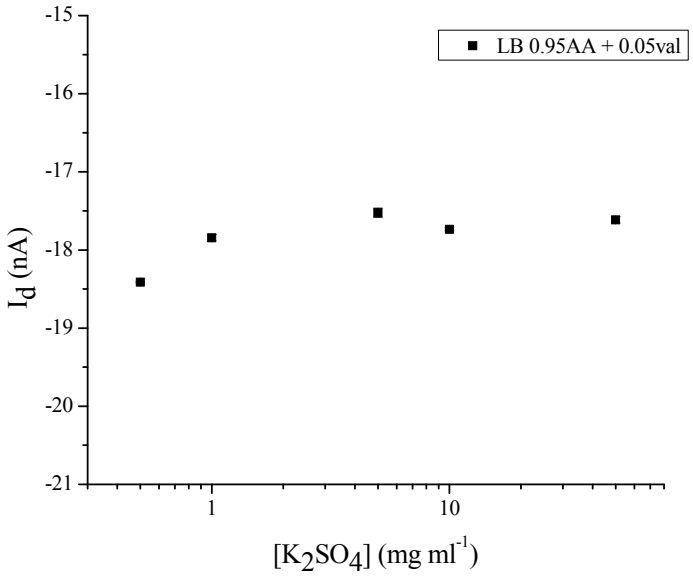

Figure 7.4 pK response of an interdigitated ISOFET with 10 LB monolayers of 95%AA + 5%val.

Transistor devices which were coated with layers of pure valinomycin were then tested. A larger response to K^+ ions (compared to the other coated devices) is evident in Figure 7.5. This shows that more K^+ ions could be accumulated in the valinomycin-coated membrane than in the other LB membranes studied.

Table 7.1 shows the sensitivities of both uncoated and coated ISOFETs to potassium ions. The sensitivity of the AA-coated device is less than 0.5 nA dec^{-1}, which is similar to that of the uncoated devices. This indicates that LB layers did not have any influence on the ISOFET sensitivity. As noted above, the carboxylic acid groups of the AA molecules form a charged plane inside the LB membrane when hydrolysed in water. However, the membrane has a Y-type structure with its hydrophobic outer surface in contact with the solution. This prevents hydrated K^+ ions penetrating the membrane. Only small molecules, such as hydrated H^+ ions, can penetrate and be trapped at the hydrolysed carboxylic planes. Larger K^+ ions would be adsorbed on the surface of the AA membrane by Van der Waals forces. Therefore, the sensitivity of the ISOFET is similar to that of the uncoated device.

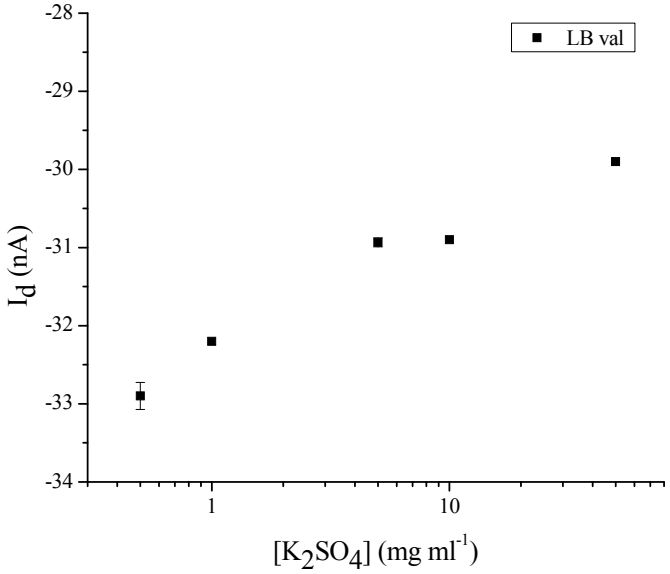

Figure 7.5 pK response of an interdigitated ISOFET with 10 LB monolayers of pure valinomycin.

Table 7.1 The sensitivities of the interdigitated ISOFETs to potassium ions.

Device	Sensitivity
Uncoated ISOFET	0.5 ± 0.1 nA dec^{-1}
ISOFET/10 LB AA	< 0.5 nA dec^{-1}
ISOFET/10 LB 5%val+95% AA	0.9 ± 0.1 nA dec^{-1}
ISOFET/10 LB val	1.5 ± 0.1 nA dec^{-1}

As shown in Table 7.1, the average sensitivity of the ISOFET coated with 10 LB monolayers of 95%AA + 5%val is about 1 nA dec^{-1}, significantly higher than the responses measured to hydrogen ions, as described in Chapter 6. The magnitude of I_d is much higher than that of the uncoated device but significantly lower than that of the AA-coated device. Based on the model in Figure 2.10, the Nernst potential of the AA/val coated device is expected to be lower than that of the AA-coated device. This may be because the net negative charge becomes smaller. Hence, more K^+ ions would be able to penetrate into the LB membrane and become trapped at the carboxylic acid groups. As shown in Figure 7.6, the presence of valinomycin is likely to disrupt the close packing of fatty acid molecules, leading to a leakage of K^+ ions into the membrane.

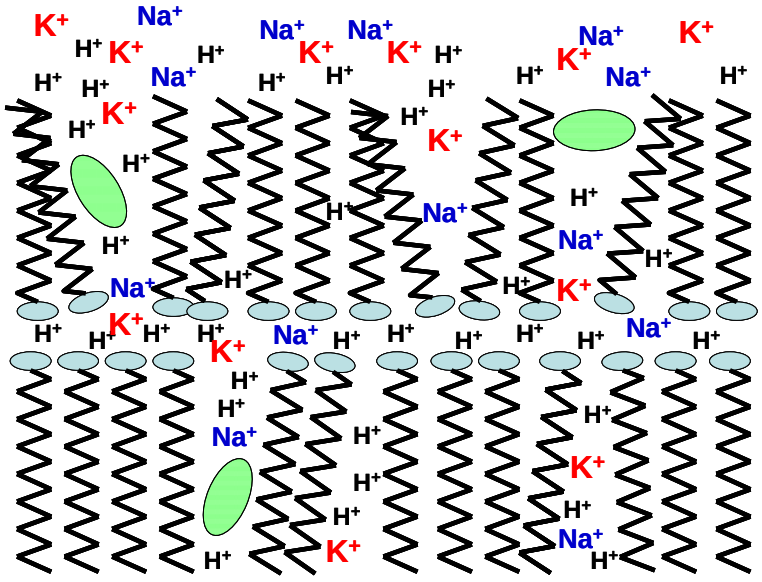

Figure 7.6 Schematic diagram of the ISOFETs coated by 10 LB monolayers of 5%val + 95%AA when exposed to the aqueous solutions.

Table 7.1 shows that the average sensitivity of the ISOFET coated with pure valinomycin is approximately 1.5 nA dec^{-1}. In comparison with the other coated devices, this valinomycin-coated ISOFET has the highest sensitivity to K^+ ions. When compared to the model in Figure 2.10, the valinomycin membrane induced the highest potential among the coated devices. This may be because the valinomycin molecules trap a K^+ ion within their cavity, as depicted in Figure 7.7. The valinomycin then shields the repulsive force of the trapped K^+ ions. In this way, more K^+ ions could be accumulated in the membrane.

Valinomycin generally requires a fatty-acid host matrix to form a favourable membrane structure to complex with K^+ ions [6-8]. The fatty acid is essential to transport the ions across the LB membrane. In fact, valinomycin can interact with K^+ and form the complex although the response of the pure valinomycin membrane to K^+ is lower than that of the valinomycin/fatty acid films [9]. In this work, the molecules of valinomycin were used to trap potassium ions within the membrane, instead of transporting the ions across the LB layer in their complexed form. The pK sensitivity in Figure 7.5 may therefore originate from the formation of K^+-valinomycin complexes.

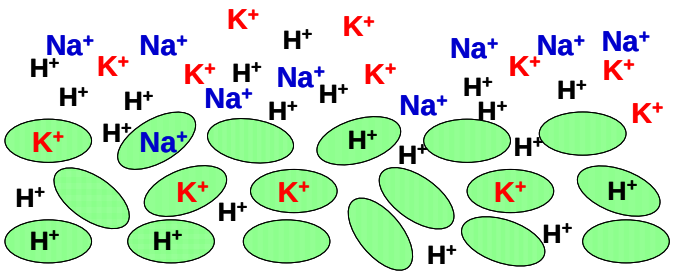

Figure 7.7 Schematic diagram of the ISOFETs coated by multimolecular layers of pure valinomycin.

To form the complex, a valinomycin molecule needs to change its conformation, as shown in Figure 7.8. The experimental results suggest that valinomycin may form a complex with K^+ ions in aqueous ambient although there is no fatty acid in the LB membrane. This is probably because the valinomycin molecules are not closely packed in the LB film. Therefore, the molecules are able to deform on interaction with K^+, forming the complex.

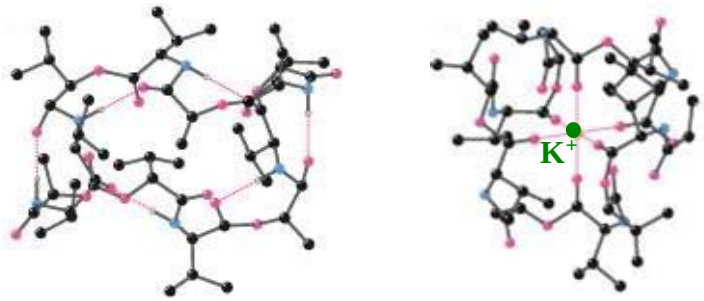

(a) (b)

Figure 7.8 Schematic diagrams of molecular structures. (a) Uncomplexed valinomycin. (b) Valinomycin - K^+ complex.

7.3 pNa Responses

Figure 7.9 shows the sodium response of the uncoated ISOFET. This is similar to the pK response in Figure 7.1. The magnitude of I_d decreases when the concentration of Na^+ ions increases. When the number of Na^+ in the solution increases, more Na^+ ions were adsorbed on the PMMA surface. As a result, fewer holes were accumulated at the semiconductor/insulator interface.

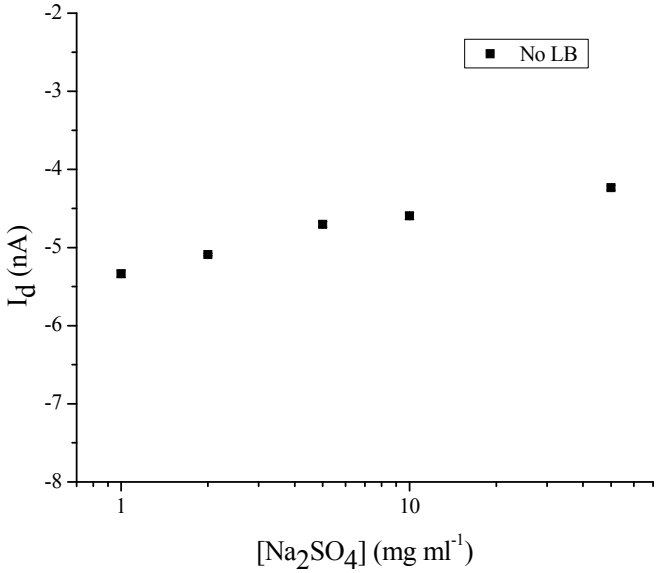

Figure 7.9 pNa response of an uncoated interdigitated ISOFET.

The Na^+ response of the ISOFET device coated with 95% AA+5% val is shown in Fig. 7.10. The ISOFET coated with AA/val mixture has the similar response as that of the uncoated devices. The magnitude of the drain current decreased when increasing the concentration of Na^+ ions. In comparison with the pK response, the Na^+ response of the ISOFET coated with pure valinomycin is shown in Figure 7.11. The magnitude of the drain current is much higher than that of the uncoated device in Figure 7.9. This reveals that more holes were accumulated at the P3HT/PMMA interface. This is because more negative charges were accumulated in valinomycin film than on the uncoated surface, which may be due to the presence of peptide bonds in valinomycin molecules. These bonds have greater positive polarity than ester groups in PMMA. Therefore, more hydroxide ions can be trapped in the valinomycin membrane than on the PMMA surface. As a consequence, a larger Nernst potential was induced to trap more holes.

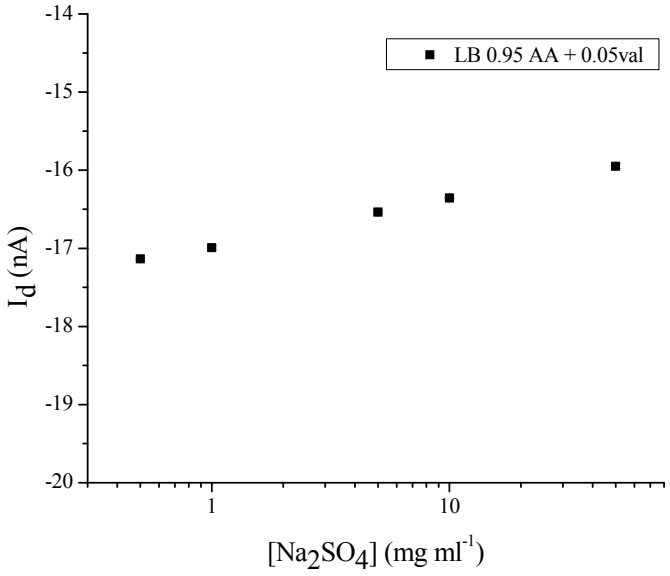

Figure 7.10 pNa response of an interdigitated ISOFET with 10 LB monolayers of 95%AA + 5%val.

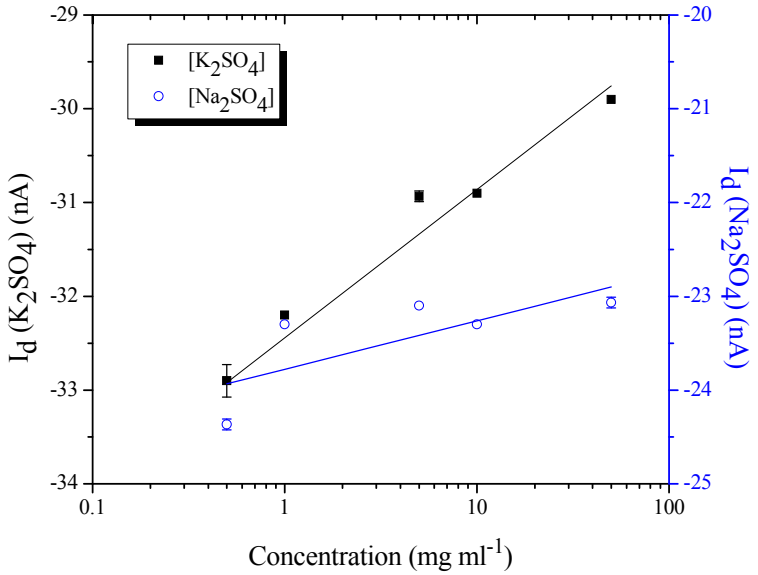

Figure 7.11 pK and pNa responses of an interdigitated ISOFET with 10 LB monolayers of pure val.

Table 7.2 summarises the sensitivities of both uncoated and coated ISOFETs to H^+, K^+ and Na^+ ions. The sensitivity of the uncoated ISOFET to Na^+ ions is about 0.5 nA dec^{-1}, similar to that of its pH response. However, in contrast to the response to K^+ ions, the results do not reveal any saturation at high ionic concentrations. This is probably because the Van der Waals force, F_W, between Na^+ ions and the PMMA surface depends on the inner water shell of Na^+. The hydration number of the inner shell for a Na^+ ion is 3 – 4 [10]. The hydrated Na^+ ions therefore have a molecular weight less than 95. As described in Section 7.2, hydrated Na^+ ions have a similar molecular weight to hydrated H^+, but are much lighter than hydrated K^+. This lower weight of the hydrated Na^+ ions leads to a smaller Van der Waals force than that from hydrated K^+ ions. At the same concentration as K^+ ions, a smaller number of Na^+ ions are therefore adsorbed at the PMMA surface. These will produce weaker repulsive force compared to that from the K^+ ions. Therefore, on increasing the concentration, more Na^+ ions could be accumulated at the PMMA surface without any saturation.

Table 7.2 Sensitivities of the ISOFETs to H^+, K^+ and Na^+.

Device	Sensitivity		
	pH	$[K^+]$	$[Na^+]$
ISOFET	0.5 ± 0.1 nA pH^{-1}	0.5 ± 0.1 nA dec^{-1}	0.6 ± 0.1 nA dec^{-1}
ISOFET/10 LB AA	3.4 ± 0.1 nA pH^{-1}	< 0.5 nA dec^{-1}	-
ISOFET/10 LB 5%val+95% AA	2.3 ± 0.1 nA pH^{-1}	0.9 ± 0.1 nA dec^{-1}	1.0 ± 0.1 nA dec^{-1}
ISOFET/10 LB val	1.8 ± 0.1 nA pH^{-1}	1.5 ± 0.1 nA dec^{-1}	0.5 ± 0.1 nA dec^{-1}

The result in Figure 7.9 reveals that the device did not reach its detection limit. The uncoated ISOFET has a wider measuring range for Na^+ than that for K^+ ions. However, the uncoated device with the PMMA surface does not have selectivity to any particular ion, but is able to detect H^+, K^+ and Na^+. Since ester groups do not have any selectivity to different negative ions, the PMMA surface can interact with any cation in an aqueous solution. This is similar to inorganic surfaces, such as Si_3N_4 [11] or Ta_2O_5 [12]. These surfaces show responses to both H^+ and other alkali-metal ions [13].

As shown in Table 7.2, the sensitivity of the ISOFET coated with AA/val film is approximately 1 nA dec^{-1}. Valinomycin in general does not form complexes with Na^+ [14]. However, the device with 5% w/w valinomycin in the coated membrane has a similar sensitivity to Na^+ ions as to K^+ ions. This suggests that neither K^+ nor Na^+ forms a valinomycin complex inside the LB membrane. Instead, both Na^+ and K^+ ions were probably trapped in the ionised carboxylic acid layers. This may be the reason why the LB film of the AA/val mixture does not function as a K^+-selective coating.

The sensitivity of this AA/val-coated device to Na^+ is higher than that of the uncoated ISOFET. This suggests that the attractive force to Na^+ ions is stronger than the Van der Waals force of the PMMA surface. This may be because the valinomycin molecules disrupt the membrane and allow Na^+ ions to leak into the LB film. The ionised carboxylic acid layers in the AA/val membrane generate a stronger Coulombic force than the dipole and Van der Waals forces from the PMMA surface. As a result, more Na^+ ions may be trapped at the carboxylic acid layer in the AA/val membrane more than those adsorbed on the PMMA surface. Moreover, the ionised carboxylic acid layers generate a stronger electric field than the dipoles of the ester groups in the PMMA layer, and thereby accumulate more holes at the semiconductor/dielectric interface. This may be an explanation of the large drain current of the ISOFET with the AA/val membrane in Figure 7.10.

As shown in Figure 7.11, the drain current of the valinomycin-coated ISOFET seems to become constant when the Na_2SO_4 concentration is higher than 1 mg ml^{-1}. This device can show a small response to Na^+ ions, approximately 0.5 nA dec^{-1}. In this case, the outer shell of hydrated ions may be the key factor in the complexation between valinomycin and ions (instead of the inner shell). As reported by Andreoli et al [14], the size of the pore in the centre of the valinomycin molecule (around 0.6 nm) can accommodate an outer shell of hydrated K^+ ions (less than 0.5 nm) but it is too small to fit an outer shell of hydrated Na^+ ions (about 0.65 nm). Hence, hydrated Na^+ cannot move through the valinomycin membrane, but may accumulate at the surface. As a result, Na^+ ions may be adsorbed on the surface of valinomycin film.

The peptide bonds in valinomycin molecules probably produce strong attractive forces and thereby trap Na^+ ions effectively. With the small number of Na^+ ions, the surface of the valinomycin membrane may be covered with hydrated Na^+

ions. Therefore, an increase of the Na^+ concentration cannot produce further adsorption on the valinomycin membrane. As a result, the induced Nernst potential will then become constant.

For clinical application, the device is required to detect potassium ions in the concentration range between 2 and 10 mEq L^{-1} (or milliequivalent molar) [15] and to detect sodium ions in the range between 0 and 200 mEq L^{-1} [16]. However, the potassium concentration in human serum is in the range of 3.5 – 5 mEq L^{-1} [17, 18] while the sodium concentration is in the range of 135 – 150 mEq L^{-1} [17, 18]. In this study, the devices were tested in potassium solutions in the range of 0.5 – 50 mg ml^{-1} (or 2.9 – 296.9 mEq L^{-1}) and sodium solutions in the range of 0.5 - 50 mg ml^{-1} (or 3.5 – 352.0 mEq L^{-1}). It is evident that the ISOFETs in this study have potential for clinical use.

7.4 Conclusions

Uncoated ISOFETs show a small response to both K^+ and Na^+ ions since the ester group in PMMA molecules does not have the selectivity to any monovalent ion while producing a weak ionic force to attract the ions. The ISOFETs with the AA membrane do not show any enhancement in the response to monovalent ions. However, the devices coated with the LB film of the AA/val mixture have shown improvements in the sensitivity to both K^+ and Na^+. Although the ion-sensitive membrane of this device contains valinomycin, it does not show any selectivity to K^+ ions over Na^+ ions. By depositing the pure valinomycin membrane, the response of the ISOFETs has been improved, with both an increase in sensitivity and selectivity to K^+ ions.

References

[1] J. T. Feddema, P. Xavier and R. Brown. Micro-assembly planning with Van der Waals force. Proceedings of the 1999 IEEE International Symposium on Assembly and Task Planning : 32 – 38, 1999.

[2] R. L. Desautels. Theory of Van der Waals forces as applied to particlate materials. Educ. Reso. for Part. Techn., 051Q-Lee: 1 – 8, 2005.

[3] E. R. Nightingale. Phenomenological theory of ion solvation: Effective radii of hydrated ions. J. Phys. Chem., 63 (9): 1381 – 1387, 1959.

[4] H. L. Clever. The hydrated hydronium ion. J. Chem. Educ., 40 (12): 637 – 641, 1963.

[5] A. K. Soper and K. Weckstrom. Ion solvation and water structure in potassium halide aqueous solutions. Biophys. Chem., 124: 180 – 191, 2006.

[6] S. Varma, D. Sabo and S. B. Rempe. K^+/Na^+ selectivity in K channels and valinomycin: over-coordination versus cavity-size constraints. J. Mol. Biol., 376: 13 – 22, 2008.

[7] S. Pathirana, W. C. Neely, L. J. Myers and V. Vodyanoy. Interaction of valinomycin and stearic acid in monolayers. Langmuir, 8: 1984 – 1987, 1992.

[8] V. A. Howarth, M. C. Petty, G. H. Davies and J. Yarwood. Infrared studies of valinomycin-containing Langmuir-Blodgett films. Langmuir, 5: 330 – 332, 1989.

[9] X. L. Yang, P. Dutta, G. K. Wong and J. B. Ketterson. Surface plasmon resonance as a probe of the complexing process of valinomycin Langmuir-Blodgett films by potassium ions. Thin Solid Films, 219: 210 – 214, 1992.

[10] A. L. Van Geet. Hydration number of sodium ions determined by sodium magnetic resonance. J. Am. Chem. Soc., 94 (16): 5583 – 5587, 1972.

[11] B. D. Liu, Y. K. Su and S. C. Chen. Ion-sensitive field-effect transistor with silicon nitride gate for pH sensing. Int. J. Electron., 67(1): 59 – 63, 1989.

[12] C. Bartic, A. Campitelli and S. Borghs. Field-effect detection of chemical species with hybrid organic/inorganic transistors. Appl. Phys. Lett., 82: 475 – 477, 2003.

[13] G. Eisenman. Cation selective glass electrodes and their mode of operation. J Biophys, 2 (2): 259 – 323, 1962.

[14] T. E. Andreoli, M. Tiefenberg and D. C. Tosteson. The effect of valinomycin on the ionic permeability of thin lipid membranes. J. Gen. Physiol., 50: 2527 – 2545, (1967).

[15] H. He, M. A. Mortellaro, M. J. P. Leiner, R. J. Fraatz and J. K. Tusa. A fluorescent sensor with high selectivity and sensitivity for potassium in water. J. Am. Chem. Soc., 125: 1468 – 1469, 2003.

[16] J. S. Benco, H. A. Nieaber and W. G. McGimpsey. A sodium ion sensor based on a covalently-linked aminorhodamine B-calix[4]arene chromoionophore. Sensor. Actuat. B-Chem. 85: 126 – 130, 2002.

[17] W. Simon, D. Ammann, P. Anker and U. Oesch. Ion-selective electrodes and their clinical application in the continuous ion monitoring. Ann. NY Acad. Sci., 428(1): 279 – 285, 1984.

[18] W. J. Marshall and S. K. Bangert. Clinical chemistry, 6th edition. Mosby Elsevier, London, 2008.

Chapter 8

A Preliminary Study into the Behaviour of LB Films Deposited onto Porous Supports

In living cells, cell membranes have significantly higher selectivity to K^+ ions over Na^+ ions. The mechanism is based on the transfer of the ions across the membrane, instead of trapping them on/in the membrane. By adapting this mechanism to the ISOFET, the performance of the device may be enhanced. Therefore, the main objective of this chapter is to investigate a measurement system mimicking the semi-permeable membrane found in living cells. This work focuses on a preliminary study of porous membranes with and without LB films coated on their surfaces.

8.1 Membrane Preparation

8.1.1 Porous Membranes

Lipid bilayer membranes are, in practice, very fragile. With small forces, the membranes can be damaged easily. In living cells, a microfilament, based on a protein network, is used as the structural scaffolding for the cell membrane, which has a similar structure to a lipid bilayer. This protein filament generally increases the mechanical strength of the membrane and makes it sustainable in the natural environment.

Since Langmuir-Blodgett membranes are fragile, appropriate physical supports are necessary to provide robust artificial membranes. To imitate the transportation mechanism across cell membranes in living cells, porous substrates are therefore used as a support for an artificial membrane. Millipore porous membranes were selected for supporting the LB film in this study. These membranes are made up from nylon 6,6, generically known as a polyamide. Nylon 6,6 is made of hexamethylenediamine and adipic acid, as shown in Figure 8.1.

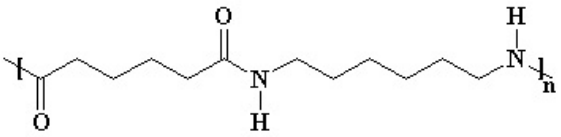

(a)

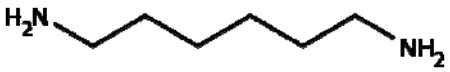

(b)

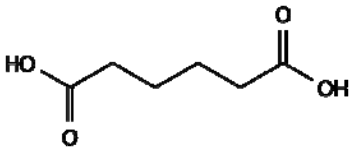

(c)

Figure 8.1 (a) Nylon 6,6. (b) Hexamethylenediamine. (c) Adipic acid.

(a)

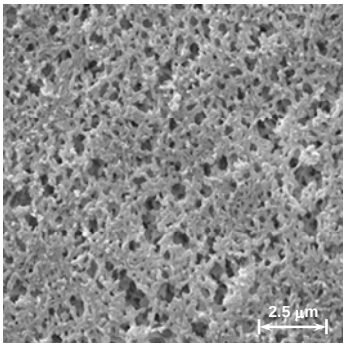

(b)

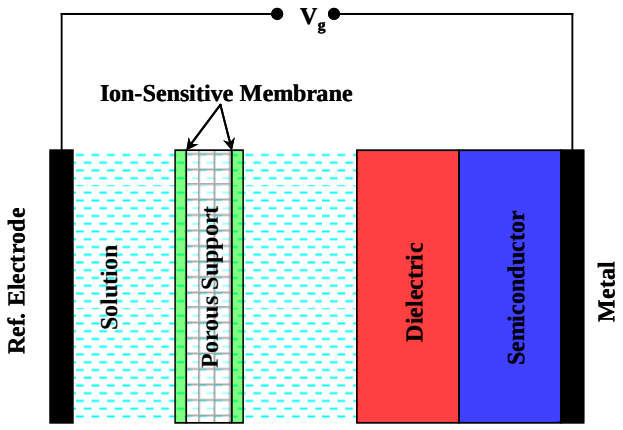

(c)

Figure 8.2 A porous membrane. (a) Millipore membrane with 0.45 µm pore size. (b) Image from the scanning electron microscope. (c) Schematic diagram of the ISOFET with the porous support coated with ion-sensitive membranes.

The Millipore membranes are hydrophilic and are not reactive to most acids, bases, or electrolytes. However, the membranes can be degraded by very strong acids. They can provide a high flow rate on application of an adequate pressure. Figure 8.2a shows a typical circular membrane with a diameter of 2.5 cm. Figure 8.2b shows an image from a scanning electron microscope. The membrane has pore sizes ranging from 0.2 to 1.2 μm. The average pore size is approximately 0.45 μm, and the membrane thickness is about 170 μm.

Millipore membranes swell following immersion in DI water. A change in size of membranes can lead to damage of the LB films. Therefore, it was essential to leave these nylon membranes in DI water for 48 hr to avoid any swelling during LB film deposition. After deposition of an LB film, the coated membranes were kept in DI water at room temperature until use in the experiment. Figure 8.2c shows a typical schematic diagram of the ISOFET with the porous support coated with ion-sensitive membranes.

Figure 8.3 A porous membrane with the holder, used for LB film deposition.

The nylon membranes were not rigid; therefore, it was impractical to dip these into an aqueous subphase without some support. As shown in Figure 8.3, the membrane was clamped in a custom-made holder. The area on each side of the nylon membranes available for LB deposition was approximately 3.5 cm^2.

8.1.2 LB Film Deposition

Monolayers of arachidic acid/valinomycin mixtures and valinomycin were deposited onto the porous membranes using the Langmuir-Blodgett method, as described in Chapter 4.

Arachidic Acid/Valinomycin Mixture

As noted in section 4.3.4, pure valinomycin does not form a stable monolayer on the surface of an aqueous subphase. Pathirana and Neely have suggested that interactions between a fatty acid and valinomycin may promote complex formation of valinomycin molecules with potassium ions [1]. A mixture of arachidic acid and valinomycin, with a 9:1 weight ratio, was deposited onto the nylon membrane. Monolayers of arachidic acid/valinomycin mixture were successfully transferred onto the porous support by using the substrate holder shown in Figure 8.2. The dipping profile in Figure 8.4 shows two dip cycles. The results reveal a reduction in the monolayer area during dipping with a transfer ratio of 0.97 ± 0.02.

Figure 8.4 shows that a monolayer was transferred to the substrate when the substrate was first moved downwards into the subphase. This is expected for a hydrophobic substrate and suggests that the surface of these nylon membranes is partly hydrophobic. This is probably related to the 6-carbon alkyl (hexyl) groups in the nylon molecules, as shown in Figure 8.1a. By starting and ending the deposition in air, the LB films on porous membranes should have a Y-type structure, as shown in Figure 3.10b. As described in Section 6.2.1, the small decrease of the trough area during the drying period may result from the complexation between H^+ ions and valinomycin molecules in the floating layer.

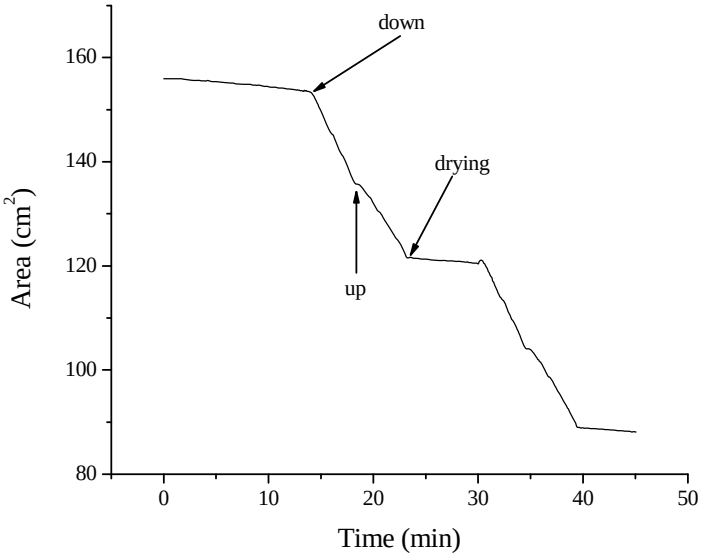

Figure 8.4 Dipping profile of the mixture of arachidic acid and valinomycin (9:1 weight ratio) on the Millipore 0.45 μm porous membrane.

Valinomycin

To transfer the LB film of valinomycin onto porous substrates, a large monolayer area was required due to the large area of the substrate. In this study, 50 μl of 0.2 mg ml^{-1} valinomycin solution in chloroform was spread on DI water. The film was left on the surface of the subphase for 60 min to stabilise the valinomycin molecules. As shown in Figure 4.15, a floating layer of pure valinomycin could not be stabilised on the LB trough surface while keeping the surface pressure constant at about 15 mN m^{-1}. By contrast with the film deposition of pure arachidic acid, when the surface pressure reached 15 mN m^{-1}, the floating layer was not stabilised on the subphase before deposition. However, the film was deposited immediately onto the porous substrate at a dipping speed of 0.08 mm s^{-1}.

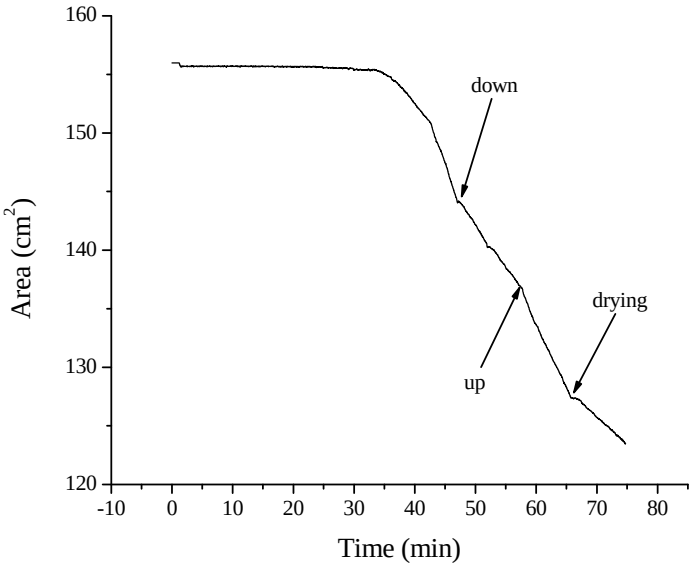

Figure 8.5 Dipping profile of valinomycin on the Millipore 0.45 μm porous membrane.

The dipping profile of pure valinomycin on the Millipore membrane is shown in Figure 8.5. By contrast with the unsuccessful deposition of pure valinomycin onto the silicon surface in Section 4.3, the valinomycin film was transferred successfully onto the porous membrane with the transfer ratio of 0.86 ± 0.02. This is probably because the valinomycin molecules could anchor themselves in the holes of the porous membrane. This may prevent the transferred layer from peeling off during the next dip.

8.2 Electrical Characteristics

A schematic diagram of the measuring system is shown in Figure 8.6. This was used to measure the built-in potential across a membrane. In this figure, two compartments contain saline solution with an insertion 'slot' for the membrane. The compartments were made from polytetrafluoroethylene (PTFE) to render them inert to chemicals. The potential was measured using a high-impedance voltmeter. In this study, Ag/AgCl reference electrodes were used as the electrodes in the measurement compartments. This high-impedance system can couple significant noise. Therefore, an aluminum Faraday cage was used for electrical isolation.

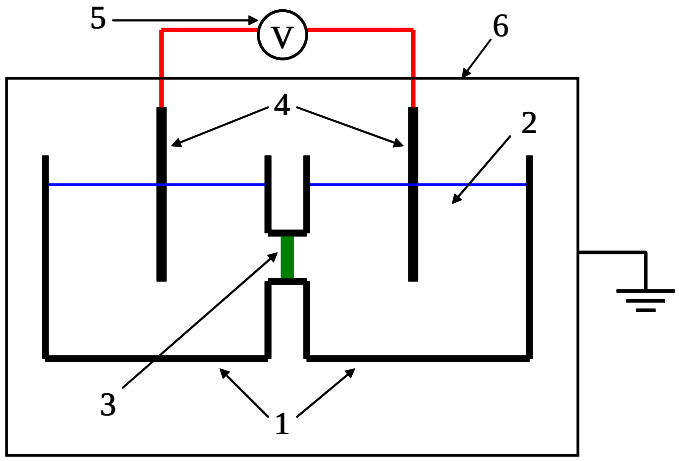

Figure 8.6 Schematic diagram of the measuring system. 1) PTFT compartments. 2) Solutions. 3) Membrane. 4) Electrodes. 5) Voltmeter. 6) Faraday cage.

8.2.1 Uncoated Porous Membranes

With the uncoated 0.45 μm porous membrane, the measured potential responses are shown in Figure 8.7. There is no significant change during measuring the voltages across the reference electrodes. In case of DI water, KCl solution and NaCl solution, the responses fluctuated around mean values of -5.0, 0.5 and -2.5 mV. In this work, both double junction Ag/AgCl electrodes were filled with 3M NaCl solution. With the same concentration in both compartments, the built-in potentials between the electrodes and the solution are almost identical. In theory, the potential

across the electrodes should be zero. In practice, porous frits in reference electrodes which are used as a salt bridge are not perfectly identical. Small differences between these frits probably accounts for the non-zero potentials measured in these experiments. The differences of the average values of the responses may result from an extra interface between the inner solutions of the electrodes and the test solution. This will provide an extra liquid junction potential in the measuring system.

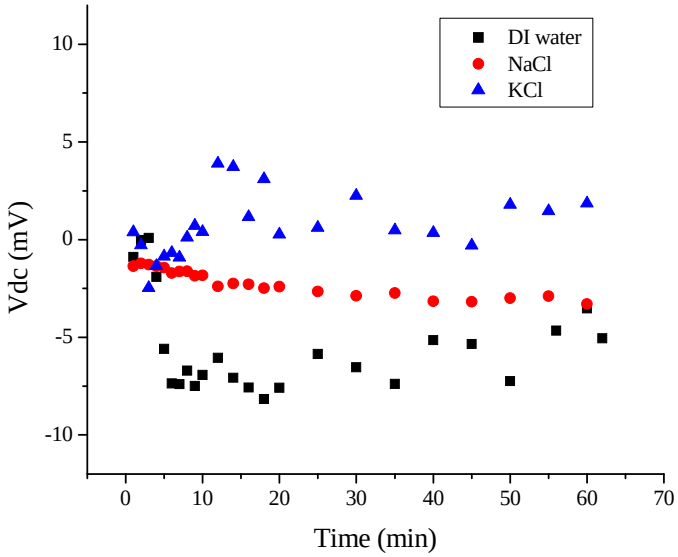

Figure 8.7 Potentials across 0.45 μm porous membrane; the same concentration in both compartments, DI water, KCl (0.01M) and NaCl (0.01M).

When the KCl concentration in the left compartment is 10 times higher than that in the right compartment, the potential (red) across the Ag/AgCl electrodes decreases with time, as shown in Figure 8.8. The gradual change reveals that the difference in concentration between the compartments becomes smaller. This indicates that both K^+ and Cl^- ions can diffuse through the porous membrane. The response seems to converge to the potential across the solutions with the same concentration. To some extent, the partly hydrophobic property may hinder the ion diffusion across the Millipore membrane. This may account for the 60 min period over which the measured potential charges.

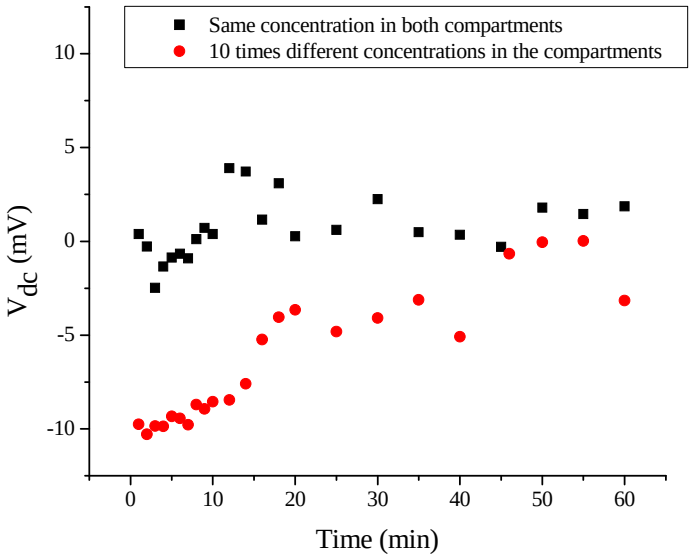

Figure 8.8 Potentials across the uncoated 0.45 μm porous membrane; the same concentration in both compartment (0.01M:0.01M) and 10 times different concentrations (0.01M:0.001M).

8.2.2 Coated Porous Membranes

Mixture of Arachidic Acid and Valinomycin

With the LB film of the arachidic acid/valinomycin mixture, the potentials across the electrodes in KCl solutions are shown in Figure 8.9. In case of the same concentration in both compartments, the measured potential fluctuated around the average value, 2.5 mV. When using the 10-time difference in concentrations as in Figure 8.9, the signal varies with time.

During the first few minutes of the measurement, the potential across the electrodes in the different concentration solutions (KCl 0.01M : KCl 0.001M) was significantly higher than the response of the same concentration solutions (KCl 0.01M : KCl 0.01M) in both compartments. These results indicate that the LB membrane of the arachidic acid/valinomycin mixture does not form a barrier to the ions. Similar to the results of the uncoated membrane in Figure 8.8; the change of the potentials during the measurements may come from the diffusion of the ions

across the coated membrane. Despite the fact that the transfer ratio is approximately unity, the LB film may not be well organised on these Millipore substrates. The surface is probably too rough to allow arachidic acid and valinomycin molecules to form a compact film. Additionally, the molecules of valinomycin may disrupt the LB membrane. These probably provide diffusion channels for the ions.

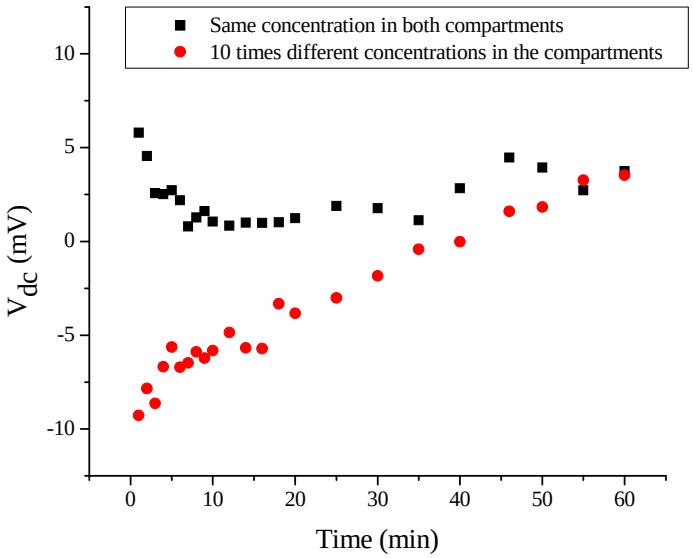

Figure 8.9 Potentials across the 0.45 μm porous membrane coated with 4 LB layers of 95%AA+5%valinomycin; KCl (0.01M) : KCl (0.01M) and KCl (0.01M) : KCl (0.001M).

Valinomycin

The measured potentials across a membrane coated with a pure valinomycin film are illustrated in Figure 8.10. The response is approximately constant when using the solutions with the same concentration. However, a variation in potential was evident when the solutions have 10-times difference in their concentrations. These responses are similar to those for AA/val mixture. The valinomycin molecules on the porous membrane might not form a compact monolayer. Instead, there may be holes in the valinomycin film on the porous membrane. The ions may thus leak through the membrane via these holes.

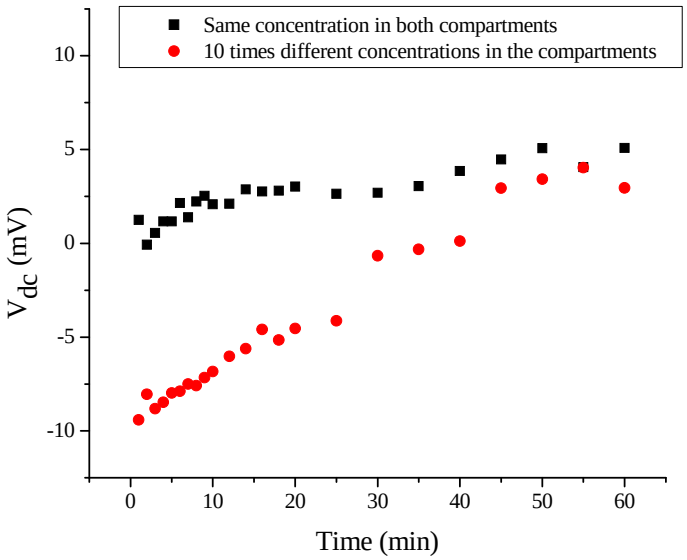

Figure 8.10 Potentials across the 0.45 μm porous membrane coated with 2 LB layers of pure valinomycin; KCl (0.01M) : KCl (0.01M) and (0.01M) : KCl (0.001M).

Artificial membranes coated on porous membranes have a similar architecture to cell membranes in living cells. Sato et al [2] reported that bilipid layer membranes containing valinomycin could show a selective response to K^+ ions. This suggests that artificial membranes will exhibit the semi-permeable characteristics if highly packed LB membranes are deposited successfully on porous membranes. In this work, the LB films coated on the porous substrates are supposed to be semi-permeable. Only K^+ ions, but not Cl^- ions, should pass through the membranes because of the presence of valinomycin molecules. In this way, a potential across the membrane obeys the Nernst equation, as described in Chapter 2. With a 10-times difference in concentration, a potential should be approximately 59 mV. However, the results of both coated membranes are significantly less than that theoretical value. Moreover, they are similar to the responses of the uncoated membrane. These suggest that the artificial membranes in this study did not exhibit any semi-permeable characteristics due to the ion leakage through the holes in the LB membranes.

8.3 Conclusions

Monolayers of arachidic acid/valinomycin mixture and valinomycin were successfully deposited on the 0.45 μm porous membrane. However, the films of arachidic acid/valinomycin mixture and valinomycin cannot fully insulate the porous membrane. In addition, the responses of coated membranes are similar to that of the uncoated membranes. These responses are approximately constant when the concentrations in both compartments are the same. The potentials across the membranes, however, tend to decrease gradually when the concentrations between the two compartments were 10-times different. This gradual change probably comes from ion leakage through the holes in the LB membrane.

References

[1] S. Pathirana and W. C. Neely. Interaction of valinomycin and stearic acid in monolayers. Langmuir, 8(8): 1984 – 1987, 1992.

[2] H. Sato, H. Hakamada, Y. Yamazaki, M. Uto, M. Sugawara and Y. Umezawa. Ionophore incorporated bilayer lipid membranes that selectively respond to metal ions and induce membrane permeability changes. Biosens. Bioelectron., 13: 1035 – 1046, 1998.

Chapter 9
Conclusions and Suggestions for Further Work

9.1 Conclusions

The main objectives of this research were to characterise ion sensitive organic field-effect transistors (ISOFET), to examine the effects of organic Langmuir-Blodgett membranes on the ISOFET devices and to investigate the behaviour of Langmuir-Blodgett films on porous supports.

In this study, organic materials were used to fabricate thin film transistors because they are cheap and require low-cost manufacturing process compared to inorganic materials [1]. A metal-oxide-semiconductor field effect transistor architecture was employed to fabricate the ISOFET. To use the transistors as an ion-sensitive device, the gate electrode was, however, removed to expose the dielectric layer to a solution [2]. In operating this device, a silver/silver chloride double-junction reference electrode was used as the gate. The LB films were coated on top of the dielectric of some transistors. In this way, these transistors were modified to specify to particular ions.

To fabricate source and drain electrodes, thermal vapour deposition was used to deposit 20 nm chromium and 20 nm gold layers on glass substrates. Two patterns of source/drain electrodes, namely standard and interdigitated patterns, were used in this research. The standard pattern was transferred onto the substrates using the shadow mask technique, while the photolithographic method was employed to transfer the interdigitated pattern.

By using spin-coating, poly (3-hexylthiophene) (P3HT) and poly(methyl methacrylate) (PMMA) were coated on substrates as semiconductor and dielectric layers, respectively. It was found that a 55 nm P3HT layer was deposited using spin-coating at a spin speed of 5000 rpm for 45 s. In the case of PMMA deposition, a two-step process was employed by spinning at 500 rpm for 10 s followed by 3000 rpm for 50 s. Two separate PMMA layers were coated to avoid any pin-holes in the gate dielectric. Before depositing the subsequent layer, the samples were annealed in

vacuum to remove any residual solvent. The total thickness of both PMMA layers was approximately 130 nm.

By mimicking membranes in living cells, Langmuir-Blodgett films were used as ion-sensitive membranes. These LB coatings were used to enhance the sensitivity and selectivity of the ion-sensitive field effect transistors. Arachidic acid (AA), 1,2-dipalmitoyl-sn-glycero-2-phosphatidic acid (DPPA), valinomycin (val) and the arachidic acid/valinomycin mixture were investigated. The results show that AA, DPPA and AA/val mixture could form a compact floating layer on the DI water, while valinomycin formed a loosely packed architecture on the subphase. AA and AA/val films were transferred successfully onto the substrate. However, it was not possible to coat DPPA and pure val films on a substrate with a high transfer ratio. Instead of using a constant-pressure deposition process, a constant-trough-area deposition method was used to transfer the pure-valinomycin floating layer onto an ISOFET. Since an excess of valinomycin was dispersed on the subphase, the surface pressure was approximately constant during the film deposition; hence, the thickness of each valinomycin layer was approximately uniform.

Reference FETs were characterised in air by depositing an aluminum gate electrode on top of the PMMA layer. The results show that the threshold voltage (V_T) was approximately 10 V and the field-effect mobility was approximately 4.5 x 10^{-3} cm^2 V^{-1} s^{-1}. In the case of the ISOFETs, by using Ag/AgCl reference electrode as the gate, the device was biased at very low operating voltages (below 1 V) to avoid any unwanted electrochemical reaction.

Due to the fact that P3HT has the band gap of 1.9 eV [3], the P3HT devices are generally sensitive to light. Therefore, the ISOFET devices were operated in the dark to avoid any unwanted effect on the drain current. In addition, the results showed that it was essential to leave the ISOFETs in DI water for 2 hr in order for them to stabilise before use.

All the experiments were undertaken in DI water and aqueous solutions. The results show that the ISOFETs were operated in the accumulation mode and the interdigitated devices possessed the high sensitivity over the standard FETs. Moreover, the hysteresis of the drain current depended on the gate voltage. Since the interdigitated ISOFETs were operated at the lower gate voltages, they showed lower leakage currents than for the standard devices.

To measure a pH response, the devices were tested in acidic solutions to prevent the presence of silver hydroxide (AgOH) in the reference electrode. Additionally, acetic acid was used to prepare test solutions to avoid interference from chloride ions. The uncoated ISOFETs showed a small pH response, with the sensitivity of about 0.5 ± 0.1 nA pH^{-1}. By coating some LB membranes on top of the gate dielectric (PMMA), the ISOFETs showed a significantly higher sensitivity to the H^+ ions. The ISOFET coated with a pure AA had a pH sensitivity of approximately 3.4 ± 0.1 nA pH^{-1}, while that coated with an AA/val film had the sensitivity of about 2.3 ± 0.1 nA pH^{-1}. These results suggest that the compact ionised layers of carboxylic head groups may lead to an improvement in the pH sensitivity of the ISOFETs. However, the valinomycin molecules may disrupt the membrane architecture of the AA/val film, and hence the sensitivity of the devices with the AA/val film was slightly less than those with the pure AA membrane. In the case of the valinomycin-coated ISOFET, its sensitivity to H^+ ions was about 1.8 ± 0.1 nA pH^{-1}. This is probably due to the fact that the twelve peptide bonds [4] in valinomycin molecules can generate a stronger force to attract H^+ ions than the single ester group in PMMA molecules. Moreover, the porous structure of the valinomycin film may increase the active area for H^+ trapping in the membrane. This provides the valinomycin-coated devices with a greater sensitivity to H^+ ions than the uncoated devices.

To investigate pK and pNa responses, sulphate salts (K_2SO_4 and Na_2SO_4) were used to prepared test solutions to avoid the interference from chloride ions. It was found that the uncoated ISOFETs had a small response to both K^+ and Na^+ ions. This is because the ester groups in PMMA molecules do not have selectivity to any monovalent ion but produce a weak ionic force to attract any ions in solution. In the case of the ISOFET coated with a pure AA membrane, the coated devices had the same selectivity to K^+ ions as to Na^+ ions. This indicates that the ionised carboxylic acid layers in the AA film do not have selectivity to any particular monovalent ion. In the case of the ISOFETs coated with an AA/val film, the sensitivity to both K^+ and Na^+ improved significantly but the devices did not show any selectivity to K^+ ions over Na^+ ions. However, the valinomycin-coated ISOFET has shown enhancements in both sensitivity and selectivity to K^+ ions.

Langmuir-Blodgett membranes coated on top of the dielectric have a similar structure to the membranes in living cell. However, the valinomycin trapped target ions within the membrane, instead of transporting the ions through the membrane. To study the facilitated movement of potassium ions across the membrane, LB membranes of arachidic acid/valinomycin mixture and valinomycin were coated on a 0.45 μm porous nylon membrane. It was found that the responses of both AA/val-coated and valinomycin-coated membranes were similar to that of the uncoated membrane. This may reveal that the coated films did not fully insulate the membrane. This led to the gradual decrease of the potentials across the membranes when the concentrations between two compartments were 10-times difference. In addition, this may indicate that the collapse of the LB membrane due to the water removal after film deposition probably provides the leakage channels across the membrane.

9.2 Suggestions for Further Work

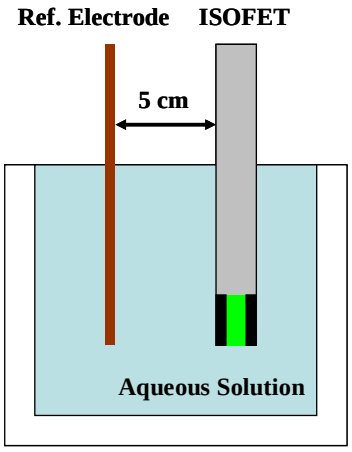

Figure 9.1 Schematic diagram of the measurement configuration using a reference electrode.

Apart from thickness of the dielectric, distance between the gate and the device is likely to be a key factor to obtain a good response. Therefore, the further study is required to optimise an arrangement of a gate electrode. Figure 9.1 shows a schematic diagram of the measurement configuration with a reference electrode as the gate. With this configuration, the organic thin-film transistors have exhibited

field-effect characteristics. However, the magnitude of the drain current was small and hence led to the small sensitivity to monovalent ions. Since the ISOFET is operated in solution, it is impractical to enhance the ISOFET response by increasing the operating voltages over 1 V.

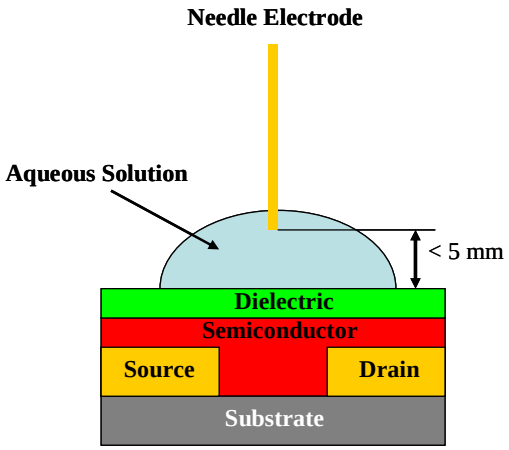

Figure 9.2 Schematic diagram of the measurement configuration using a needle electrode [5,6].

The distance between the gate (reference electrode) and the ISOFET was relatively large, approximately 5 cm. It is evident that the reduction of this gap can strengthen an electric field exerting on the ISOFET. Additionally, a Ag/AgCl reference electrode has some measurement limitations, such as the interference from chloride ions. Therefore, a metal needle (such as Au or Pt) may be an appropriate gate electrode. Figure 9.2 shows a schematic diagram of the measurement configuration using a metal needle as the gate electrode [5,6]. In this way, the gap between the gate and the ISOFET can be reduced to less than 5 mm; hence the strength of the electric field should increase more than 10 times over that generated from the measurement configuration in Figure 9.1. In addition, with a gold or platinum needle, the ISOFET device can be operated in acid solutions, basic solutions and chloride-salt solutions.

References

[1] C. D. Dimitrakopoulos and P. R. L. Malenfant. Organic thin film transistors for large area electronics. Adv. Mater., 14(2): 99 – 117, 2002.

[2] C. Bartic and G. Borghs. Organic thin-film transistors as transducers for (bio)analytical applications. Ana. Bioanal. Chem., 384: 354 – 365, 2006.

[3] E. Bundgaard and F. C. Krebs. Low band gap polymers for organic photovoltaics. Sol. Energ. Mat. Sol. C., 91: 954 – 985, 2007.

[4] M. Pinkerton, L. K. Steinrauf and P. Dawkins. The molecular structure and some transport properties of valinomycin. Biochem. Bioph. Res. Co., 35(4): 512 – 518, 1969.

[5] L. Kergoat, L. Herlogsson, D. Braga, B. Piro, M. C. Pham, X. Crispin, M. Berggren and G. Horowitz. A water-gate organic field-effect transistor. Adv. Mater., 22: 2565 – 2569, 2010.

[6] L. Kergoat, N. Battaglini, L. Miozzo, B. Piro, M. C. Pham, A. Yassar and G. Horowitz. Use of poly(3-hexylthiophene)/poly(methyl methacrylate) (P3HT/PMMA) blends to improve the performance of water-gated organic field-effect transistors. Org. Electron., 12: 1253 – 1257, 2011.

Publications and International Conferences

Publications

S. Ritjareonwattu, Y. Yun, C. Pearson and M. C. Petty. Enhanced sensitivity of an organic field-effect transistor pH sensor using a fatty acid Langmuir-Blodgett film. Org. Electron., 11(11): 1792 – 1795, 2010.

S. Ritjareonwattu, Y. Yun, C. Pearson and M. C. Petty. An ion sensitive organic field-effect transistor incorporating the ionophore valinomycin. IEEE Sens. J., in press.

International Conferences

S. Ritjareonwattu, Y. Yun, C. Pearson and M. C. Petty. An organic ion-sensitive thin-film transistor. 5th International Conference on Organic Electronics, Liverpool (United Kingdom), June 15 – 17, 2009.

S. Ritjareonwattu, Y. Yun, C. Pearson and M. C. Petty. Improved sensitivity of an organic field-effect transistor pH sensor using Langmuir-Blodgett film. 6th International Conference on Organic Electronics, Paris (France), June 22 – 25, 2010.